Modulación de la exportación nuclear de transcritos durante la respuesta a nitrato en *Arabidopsis thaliana*

Tesis entregada a la Pontificia Universidad Católica de Chile en cumplimiento parcial de los requisitos para optar al Grado de Doctor en Ciencias Biológicas con mención en Genética Molecular y Microbiología

Por

ALEJANDRO ALFREDO FONSECA CÁRDENAS

Director de tesis: Dr. Rodrigo A. Gutiérrez

Enero, 2021

AGRADECIMIENTOS

Este trabajo fue financiado por el Centro de Regulación del Genoma (CRG) (15090007) del Fondo de Desarrollo de Áreas Prioritarias (FONDAP), el núcleo Milenio de Biología integrativa (iBIO) (ANID - Programa Iniciativa Científica Milenio - ICN17_022) y el Fondo Nacional de Desarrollo Científico y Tecnológico (FONDECYT) (1180759) atribuidos al Dr. Rodrigo Gutiérrez. Mis estudios de doctorado fueron financiados por la Agencia Nacional de Investigación y Desarrollo (ANID), a través de la beca de doctorado nacional (21161516), beca de pasantía internacional (752190026) y beca de asistencia a eventos para estudiantes de doctorado (81180499).

Durante el desarrollo de esta tesis he recibido un tremendo apoyo y asistencia por lo cual expreso mis sinceros agradecimientos a las siguientes personas:

- A mi director de tesis, el Dr. Rodrigo Gutiérrez (PUC).
- A los miembros de la comisión evaluadora: Dra. Loreto Holuigue (PUC), Dra. Francisca Blanco (UNAB) y Dr. Marcelo López-Lastra (PUC).
- Al Dr. Tomás Moyano (PUC), por ayudarme, enseñarme, y discutir todo lo respectivo al análisis de datos.
- A la Dra. Stefanie Rosa (Swedish University of Agricultural Sciences), por aceptar mi pasantía en su laboratorio, y además enseñarme y discutir lo respectivo al RNA smFISH.
- Al Dr. Luis Mercado (PUC), por su orientación en el análisis estadístico de los datos.

- A todos los miembros que han pasado por el Laboratorio de Biología de Sistemas Vegetales (PSBL) (PUC) en el periodo 2016-2020, por todo el feedback, discusiones, ayuda con experimentos y ambiente laboral.
- A Karem Tamayo y Melissa Aguilar por el apoyo técnico y logístico para la ejecución del proyecto en el laboratorio.
- A mis compañeros de laboratorio Francisca Díaz, Andrea Vega, Laura Delgado, Jonathan Morales y Tomás Moyano por sus correcciones del escrito.
- A mis amigos y compañeros de doctorado (GMM 2016): Verónica Del Rio, Bárbara Schultz, Luisa Duarte, Aldo Barrera, Kevin Simpson, Pablo Vergara y Miguel Ibeas por su apoyo con los ramos y discusión del proyecto.
- A Aldo Seguel y Ariel Herrera por su apoyo con la discusión del proyecto y resultados.
- A mis amigos y a mi familia por todo el apoyo incondicional que siempre me dan.

CONTENT INDEX

FIGURE INDEX

CHAPTER 1

CHAPTER 2

TABLE INDEX

CHAPTER 1

CHAPTER 2

LIST OF ABBREVIATIONS

ABRC: Arabidopsis biological research center

AGI: Arabidopsis genome initiative ID

AIC: Akaike information criterion

ANOVA: Analysis of variance

CA: Cytoplasmic accumulation

cDNA: Complementary DNA

CDS: Coding sequence

ChIP: Chromatin immunoprecipitation

Col-0: Columbia-0

CR: Cytoplasmic reduction

D: Delayed-cytoplasmic accumulation

DAPI: 4′,6-diamidino-2-phenylindole

DAP-seq: DNA affinity purification sequencing

DLT: Differentially localized transcript

DNA: Deoxyribonucleic acid

GC: Guanine-Cytosine

GFF: Generic feature format

GNR: Gene regulatory networks

GO: Gene ontology

HSP: Heat shock protein

KCl: Potassium chloride

k_{decay}: Decay constant

KEGG: Kyoto encyclopedia of genes and genomes

KNO_3: Potassium nitrate

LB: Left border

log2: Binary logarithm

mRBP: mRNA binding protein

mRNA: Messenger RNA

MS: Murashige & Skoog

NA: Nuclear accumulation

NO^{-3}: Nitrate

NPC: Nuclear pore complex

NR: Nuclear reduction

PCR: Polymerase chain reaction

qPCR: Quantitative polymerase chain reaction

RBP: RNA binding protein

RNA: Ribonucleic acid

RNPII: RNA polymerase II

RQN: RNA quality number

RSA: Root system architecture

RT: Retro transcriptase

Seq: Sequencing

SJD: Splicing junction density

smFISH: Single-molecule fluorescence in situ hybridization

T: Treatment

T0: Time zero

$t_{1/2}$: Half-life

TA: Total accumulation

TCA: Tricarboxylic acid cycle

T-DNA: Transfer-DNA

TF: Transcription factor

Ti: Time

TPM: Transcripts per million

TR: Total reduction

TREX: Transcription-export complex

TSS: Transcription start site

TTS: Transcription termination site

UTR: Untranslated region

WT: Wild type

ΔNC: Subtraction between nuclear and cytoplasmic RNA levels

RESUMEN

El nitrógeno es un macronutriente esencial para el crecimiento, desarrollo y productividad agrícola de las plantas. El nitrato, la principal fuente de nitrógeno en los suelos agrícolas, es una importante molécula señalizadora que regula la expresión génica en organismos vegetales. La respuesta a nitrato se ha caracterizado principalmente a nivel del transcriptoma utilizando ARN de células completas y muchas veces pasando por alto eventos de regulación postranscripcional. La exportación nuclear de ARN mensajeros (ARNm) se destaca como un paso crucial en la modulación de la expresión génica al conectar los procesos de transcripción y traducción. En un esfuerzo por dilucidar la función de la exportación nuclear de ARNm en la respuesta a nitrato, se analizó la dinámica de la acumulación nucleocitoplasmática de transcritos en raíces de *Arabidopsis thaliana* tratadas con nitrato, utilizando una estrategia de fraccionamiento celular y secuenciación de ARN. Se identificaron 402 genes con transcritos diferencialmente localizados (DLT) en respuesta al nutriente. Cinco patrones de localización de ARNm fueron observados en respuesta a nitrato: Reducción nuclear, reducción citoplasmática, acumulación nuclear, acumulación citoplasmática y acumulación citoplasmática retrasada. Las transcritos con diferentes patrones de localización mostraron diferencias en su longitud, contenido GC y densidad de sitios de corte y empalme. Además, se identificaron diferencias en los cambios inducidos por nitrato en la ocupancia de la ARN polimerasa II y de la vida media entre DLTs, destacándose a *NITRATE REDUCTASE 1* (*NIA1*) como el gen con el transcrito con mayores cambios en síntesis y degradación. Mediante

detección *in situ* de molécula única para *NIA1*, se mostró que su acumulación nuclear temprana ocurre principalmente en los sitios de síntesis. Además, el análisis de los perfiles de decaimiento del ARN de *NIA1* en diferentes tiempos del tratamiento mostró una vida media más alta en su fase nuclear que en la citoplasmática, lo que sugiere que el retraso en la acumulación citoplasmática podría ser una estrategia para regular la concentración de ARN en el citoplasma. debido a sus altas tasas de transcripción y degradación.

Además, con el fin de dilucidar los efectos fisiológicos que podría generar la localización diferencial de los transcritos en la respuesta a nitrato, se realizó una red génica, seguida de un análisis de genética reversa. Se identificaron seis factores de transcripción con ARNm diferencialmente localizados como nodos principales de genes de respuesta a nitrato. BZIP3 y VRN1 destacaron por ser reguladores de genes involucrados en el transporte de nitrato, asimilación de nitrato y procesos de desarrollo. Análisis preliminares de la raíz de mutantes insercionales para los genes *BZIP3* y *VRN1* mostraron diferencias en la longitud de la raíz primaria y la emergencia de raíces laterales en respuesta a nitrato. Además, se observaron ligeras diferencias en la inducción de los niveles de ARNm para los genes que codifican para reductasas y transportadores de nitrato.

De esta manera, esta tesis describe la dinámica de la distribución nucleocitoplasmática de transcritos en respuesta a nitrato, controlando la expresión de genes esenciales para procesos metabólicos y de regulación. Estos resultados sugieren que la exportación nuclear de ARNm cumple un papel de ajuste de la expresión génica para adaptar la fisiología vegetal a un estímulo nutricional.

ABSTRACT

Nitrogen is an essential macronutrient for plant growth, development, and agricultural productivity. Nitrate, the primary source of nitrogen in agricultural soils, is an important signaling molecule that regulates global gene expression in plants. The nitrate response has been mainly characterized at the transcriptome level using RNA from complete cells and overlooking post-transcriptional regulation events. mRNA nuclear export highlights as a crucial step in modulating gene expression by connecting the transcription and translation processes. In an effort to elucidate the role of nuclear mRNA export in the nitrate response, the nucleocytoplasmic dynamics for transcript accumulation were analyzed in nitrate-treated *Arabidopsis thaliana* roots through a cell-fractionation/RNA-seq strategy. We identified 402 genes with differentially localized transcripts (DLTs) in response to the nutrient. Five mRNA-localization patterns were identified: nuclear reduction, cytoplasmic reduction, nuclear accumulation, cytoplasmic accumulation, or delayed-cytoplasmic accumulation. Transcripts with different localization patterns showed differences in their transcript length, GC-content, and splicing junction density. In addition, we identified differences in nitrate-induced changes in RNA polymerase II occupancy and half-lives among DLTs. *NITRATE REDUCTASE 1* (*NIA1*) stood out as the gene with the greatest changes in RNA synthesis and decay features. RNA single-molecule FISH showed that *NIA1* transcript early nuclear accumulation mainly occurs in the synthesis loci. Analysis at different times of RNA decay profiles for *NIA1* showed a higher half-life in its nuclear phase when compared with its cytoplasmic one, suggesting that

the delay in the cytoplasmic accumulation could be a strategy for buffering the cytoplasmic levels of transcripts due to its high transcription and decay rates.

Furthermore, to elucidate the physiological effects that the differential localization of transcripts in response to nitrate could have, we constructed a gene network and performed a reverse genetic strategy. We identified six transcription factors with differentially localized mRNAs as the main hubs of nitrate-responsive genes. BZIP3 and VRN1 emerged as regulators of gene-targets involved in nitrate transport, nitrate assimilation, and developmental processes. Preliminary analyses for nitrate root-elicited-changes in insertional mutants of *BZIP3* and *VRN1* genes showed differences in primary root length and lateral root emergence. Besides, we observed slight differences in the induction of mRNA levels for genes that codify nitrate reductases and transporters.

This work shows the dynamics of mRNA nucleocytoplasmic distribution in response to nitrate regulates many essential genes for metabolic and regulatory processes. These results suggest a role of mRNA nuclear export in the fine-tuning of gene expression to adapt plant physiology to a nutritional stimulus.

INTRODUCTION

In eukaryotic cells, the nuclear envelope adds complexity to the gene expression regulation since the mRNA synthesis and processing usually occur in the nucleus and the translation in the cytoplasm (Martin and Koonin, 2006). Therefore, particular nucleocytoplasmic distributions of transcripts are found inside the cell. Genome-wide studies that analyzed RNA nucleocytoplasmic levels have shown that asymmetry in RNA distribution is a feature observed in animals (Barthelson et al., 2007; Djebali et al., 2012; Solnestam et al., 2012; Bahar Halpern et al., 2015; Battich et al., 2015; Chen and Van Steensel, 2017; Kim et al., 2017; Benoit Bouvrette et al., 2018), protists (Pastro et al., 2017), and plants (Reynoso et al., 2018; Lee and Bailey-Serres, 2019; Palovaara and Weijers, 2019).

The mRNA nuclear export directly connects nuclear and cytoplasmic transcript levels (Bahar Halpern et al., 2015; Hansen et al., 2018). This process is highly regulated to tune the gene expression according to cell requirements (Wickramasinghe et al., 2014; Parry, 2015; Chen and Van Steensel, 2017). The mRNA export in response to an environmental stimulus is regulated by changes in the composition of the nuclear pore complex (NPC) and the export ribonucleoprotein (RNP) complexes. For example, in yeast exposed to heat stress, the selective binding of stress-responsive mRNAs (e.g., those that codify for Heat Shock Protein (HSP)) to nuclear export proteins prioritizes their delivery into the cytoplasm over transcripts with other functions (Saavedra et al., 1996; Hieronymus and Silver, 2003; Zander et al., 2016). Similar

evidence has been reported in animal cells during proliferation (Chakraborty et al., 2008), differentiation (Mancini et al., 2010; Wang et al., 2013), and DNA repair (Wickramasinghe et al., 2013).

Studies focused on understanding the mRNA nucleocytoplasmic dynamic regulation have been mostly performed in animal cell models (Stewart, 2019). Nevertheless, plants are organisms with complex molecular adaptation strategies due to their sessile lifestyle and the diversity of colonized environments (Raza et al., 2020). Despite that the plant nuclear export components have high structural similarities to those described for other organisms (Tamura et al., 2010; Yelina et al., 2010), the lack or the diversification of some components suggest that the mRNA nuclear export process could be different in plants (Ehrnsberger and Grasser, 2019; Tamura, 2020). However, only a pair of works have described nucleocytoplasmic dynamics at genome-wide level, focusing on the flooding stress response (Lee and Bailey-Serres, 2019; Reynoso et al., 2019).

Plant response to a nutritional stimulus generates a strong gene-reprogramming to control plant growth and development (Schachtman and Shin, 2007). For instance, nitrate, the primary source of nitrogen in agricultural soils, acts as a signaling molecule that controls a sophisticated regulatory network involving the expression of thousands of genes (Sakakibara et al., 1997; Ho et al., 2009; Canales et al., 2014; Vidal et al., 2020), having an impact on growth, root development, leaf development, seed dormancy, and flowering time (Fredes et al., 2019; Vidal et al., 2020). Although many nitrate response elements have been identified by transcriptomic analysis (Vidal and Gutierrez, 2008; Gutiérrez, 2013; Canales et al., 2014; Varala et al., 2018; Brooks et al., 2019), not many post-transcriptional studies have been conducted.

Consequently, how nucleocytoplasmic dynamics change in response to nitrate and the mRNA nuclear export role under a nutritional stimulus are still unknown.

In this thesis, we proposed to evaluate the role of mRNA nuclear export during the *Arabidopsis thaliana*'s nitrate response by analyzing the genome-wide nucleocytoplasmic dynamics in response to nitrate treatments. Furthermore, we identified and functionally evaluated potential regulators with favored cytoplasmic accumulation. In this way, insights into the effect of nucleocytoplasmic transport during a nutritional event are reported for the first time in plants.

The hypothesis and aims of this work are explained below. This thesis is structured into two chapters. The first chapter, titled "Changes in mRNA nucleocytoplasmic distribution in response to nitrate treatments in *Arabidopsis thaliana* roots", shows the activities regarding specific aims 1 and 2. The second chapter, titled "Functional characterization of transcription factors with a differential mRNA localization in response to nitrate treatments", describes the preliminary results obtained for the specific aim 3.

Hypothesis

The nuclear export of transcripts involved in the nitrate response is regulated during a nutritional stimulus in *Arabidopsis thaliana* roots.

Main aim:

To identify and characterize transcripts with potential regulation in their nuclear export in response to nitrate treatments in *Arabidopsis thaliana* roots.

Specific aims:

1.- To analyze the effect of nitrate on the nucleocytoplasmic distribution of transcripts at a genome-wide level.

2.- To characterize structure, synthesis, and decay features for transcripts with a differential nucleocytoplasmic distribution in response to nitrate treatments.

3.- To evaluate the role of transcription factors whose mRNAs are differentially localized in response to nitrate treatments.

CHAPTER 1: Changes in mRNA nucleocytoplasmic distribution in response to nitrate treatments in *Arabidopsis thaliana* roots

Changes in mRNA nucleocytoplasmic distribution in response to nitrate treatments in *Arabidopsis thaliana* roots

Alejandro Fonseca[1,2,3], Tomás C. Moyano[1,2,3], Stefanie Rosa[4], Rodrigo A. Gutiérrez[1,2,3]

Affiliations

[1] ANID–Millennium Science Initiative Program-Millennium Institute for Integrative Biology (iBio), Santiago, Chile

[2] Departamento de Genética Molecular y Microbiología, Facultad de Ciencias Biológicas, Pontificia Universidad Católica de Chile, Santiago, Chile

[3] FONDAP Center for Genome Regulation, Santiago, Chile

[4] Department of Plant Biology, Swedish University of Agricultural Sciences (SLU), Uppsala, Sweden

*Corresponding author: email: rgutierrez@bio.puc.cl, Rodrigo A. Gutiérrez

ABSTRACT

Nitrate (NO^{-3}), the primary source of nitrogen in agricultural soils, is an important signaling molecule that regulates global gene expression in plants. The nitrate response has been extensively characterized at the transcriptome level using RNA from complete organisms, organs or cells. However, we know very little about the subcellular localization of mRNA or its impact on gene expression. To understand the nucleocytoplasmic dynamics of transcripts during the nitrate response, we isolated mRNA from the nucleus, cytoplasm, and whole-cells from nitrate-treated *Arabidopsis thaliana* roots and performed RNA-seq analysis. We identified 402 differentially localized transcripts (DLTs) in response to nitrate, which included enriched GO-terms for nitrogen and carbohydrate metabolism, response to stimulus, and transport. These genes showed five distinctive localization patterns during the treatment: nuclear reduction, cytoplasmic reduction, nuclear accumulation, cytoplasmic accumulation, or delayed-cytoplasmic accumulation in response to nitrate. We found structural differences in genes with different localization patterns: a higher splicing-junction density in the nuclear-accumulated transcripts; a lower GC content in the cytoplasmic-accumulated group; and shorter exonic regions and lower splicing sites in genes with changes in cytoplasmic RNA levels. DLTs also exhibited differential changes induced by nitrate in mRNA turnover rates and RNA polymerase II (RNPII) occupancy of cognate genes. The *NITRATE REDUCTASE 1* (*NIA1*) transcript exhibited the largest changes in synthesis and decay. Single-molecule RNA FISH experiments against *NIA1* showed that early-RNA nuclear accumulation occurs mainly in the synthesis loci. In addition, analysis of decay profiles for *NIA1* at different treatment times showed a higher half-life when the transcript accumulated more in the nucleus than in the cytoplasm. We hypothesize that the cytoplasmic accumulation delay could be a strategy for buffering

cytoplasmic transcript levels due to its high transcription and decay rates. These results show a dynamic mRNA nucleocytoplasmic distribution in response to nitrate and suggest a relevant role for mRNA nuclear export in the plant's adaptive response to nitrogen nutrient signals.

INTRODUCTION

Nitrogen (N) is an essential macronutrient whose availability limits growth and development in plants (Andrews et al., 2013; Gutiérrez, 2013; Fredes et al., 2019; Vidal et al., 2020). Nitrate is the most abundant source of N in agricultural soils (Owen and Jones, 2001). Nitrate acts as a signaling molecule (Scheible et al., 1997; Wang et al., 2004) that initiates a signal transduction cascade (Undurraga et al., 2017; Vidal et al., 2020). Nitrate is sensed by the dual-affinity transceptor NPF6.3/NRT1.1 in root cells (Ho et al., 2009). Different regulators, at the local and systemic level, orchestrate downstream responses affecting nutrient metabolism and a series of developmental processes associated with root development (Forde and Walch-liu, 2009; Vidal et al., 2010; Gruber et al., 2013; Alvarez et al., 2014; Bouguyon et al., 2016; Canales et al., 2017), shoot development (Rahayu et al., 2005; Landrein et al., 2018; Poitout et al., 2018; Moreno et al., 2020), seed dormancy (Alboresi et al., 2005; Yan et al., 2016), and flowering time (Castro Marín et al., 2011; Gras et al., 2018). In addition to the NRT1.1 transceptor, key components in the nitrate signaling pathway include CIPK23 kinase (Liu and Tsay, 2003), calcium as a second messenger (Riveras et al., 2015), and a myriad of transcription factors controlling transcriptional responses such as NLP7 (Marchive et al., 2013), TGA1 and TGA4 (Alvarez et al., 2014), NAC4 (Vidal et al., 2013b), SPL9 (Krouk et al., 2010), HRS1 and HHO1 (Medici et al., 2015; Maeda et al., 2018), NRG2 (Xu et al., 2016), TCP20 (Guan et al., 2017), and CRF4 (Varala et al., 2018).

In eukaryotic cells mRNA synthesis and processing occur in the nucleus and translation mostly in the cytoplasm (Martin and Koonin, 2006). This compartmentalization of mRNA processes allows for a more sophisticated regulation of gene expression (Wickramasinghe and

Laskey, 2015). The nucleocytoplasmic dynamic of transcripts is mainly determined by synthesis, export, and decay factors (Bahar Halpern et al., 2015; Hansen et al., 2018). The kinetic rates of some of these processes have been quantified at the genome-wide level in yeast (Miller et al., 2011; Sun et al., 2012; Eser et al., 2014), mouse (Schwanhäusser et al., 2011; Tippmann et al., 2012; Rabani et al., 2014; Jovanovic et al., 2015), and *Drosophila* cells (Chen and Van Steensel, 2017). These results indicate that synthesis and decay rates contribute to mRNA steady-state levels in a species-specific manner. The sequencing of RNA from cellular fractions of different eukaryotic species showed that transcripts are asymmetrically distributed between the nucleus and cytoplasm (Barthelson et al., 2007; Djebali et al., 2012; Solnestam et al., 2012; Bahar Halpern et al., 2015; Battich et al., 2015; Chen and Van Steensel, 2017; Pastro et al., 2017; Benoit Bouvrette et al., 2018; Reynoso et al., 2018; Lee and Bailey-Serres, 2019; Palovaara and Weijers, 2019). Controlling mRNA nuclear export to change the availability of transcripts for translation allows the cell to fine-tune gene expression according to environmental and cellular requirements (Wickramasinghe et al., 2014; Parry, 2015; Chen and Van Steensel, 2017; Yang et al., 2017b; Lee and Bailey-Serres, 2019).

In plants, the export-machinery components are more diverse than in yeast or animals (Yelina et al., 2010; Pfaff et al., 2018), which suggests that their ability to regulate export in response to a stimulus is more versatile (Ehrnsberger and Grasser, 2019). Some studies have shown that subsets of mRNAs display particular nucleocytoplasmic distributions during different plant processes, such as cell cycle control (Yang et al., 2017a), ethylene signaling (Chen et al., 2019), RNA-directed DNA methylation (Choudury et al., 2019), and stress response (Yeap et al., 2019). However, the mRNA nucleocytoplasmic dynamic at the genome-wide level has only been described in response to flooding stress (Lee and Bailey-Serres, 2019;

Reynoso et al., 2019). Genome-wide changes in gene expression in response to nitrate treatments have been thoroughly characterized in a number of studies (Wang et al., 2003; Wang et al., 2004; Gutiérrez et al., 2007; Wang et al., 2007; Gifford et al., 2008; Hu et al., 2009; Krouk et al., 2009; Krouk et al., 2010; Patterson et al., 2010; Ruffel et al., 2011; Vidal et al., 2013a; Alvarez et al., 2014; Walker et al., 2017; Gaudinier et al., 2018; Varala et al., 2018; Alvarez et al., 2019; Moreno et al., 2020; Swift et al., 2020). However, we currently lack understanding of the importance of mRNA nucleocytoplasmic dynamics in the nitrate response.

In this work, we aimed to understand the nucleocytoplasmic dynamics of mRNAs in response to nitrate signal. We used RNA-seq analysis from nuclear, cytoplasmic, and total fractions to identify differentially localized transcripts (DLTs) in response to nitrate treatments. Transcripts with different localization profiles showed distinct sequence features and nitrate-induced changes for RNA polymerase II occupancy and half-lives. Integrated analysis of our genome-wide data sets allowed us to describe nucleocytoplasmic dynamics and propose a role for mRNA nuclear export in regulating gene expression that is critical for the plants' ability to adapt to nutritional changes.

RESULTS

Identification of differentially expressed genes in response to nitrate in subcellular fractions

To analyze the mRNA levels in response to nitrate in cellular fractions, RNA was obtained from nuclear, cytoplasmic, and total fractions. RNA samples were prepared from *Arabidopsis* roots 0, 20, 60, and 120 min after nitrate or control treatments. As a control experiment, we quantified RNA levels for selected transcripts using RT-qPCR. As shown in Supplemental Figure 1, we observed enrichment of unprocessed transcripts in the nuclear fraction, and a significant reduction in the cytoplasmic fraction as compared to total RNA. The material obtained from cellular fractions was used for RNA-seq analysis. Supplemental Table 1 summarizes quality parameters for all libraries. We performed three independent biological replicates for each condition (separate plant material). We found high reproducibility among replicate experiments with a mean Pearson correlation of 0.985 ± 0.003 (Supplemental Table 1). Sequence data was mapped to Araport11 Arabidopsis genome and counts were normalized as detailed in Materials and Methods.

To identify genes with changes in their mRNA levels in response to the treatments, we performed two-way analyses of variance (ANOVA) for total or each cellular fraction separately. Our ANOVA model evaluated the effect of treatments (KCl and KNO_3), time (20, 60, 120 min) or their interactions (Supplemental Figure 2A-C). We selected significant models with a p-value < 0.01 after FDR correction. We found 6,006 genes whose mRNA levels depended on the treatment or interactions in the total fractions. Using gene ontology (GO) over-representation analysis, we identified expected biological processes for the nitrate treatment, such as nitrate response, nitrate transport, nitrate assimilation, development, response to hormones, amino

acids, nucleotide metabolism, carbon metabolism, among others (Supplemental Figure 3A). We identified 2,634, and 3,473 differentially expressed genes in the nuclear or cytoplasmic fractions, respectively (Supplemental Figure 2B-C), representing a total of 4,445 regulated genes. However, we found that only 1,652 (37.1%) of these genes were shared between both compartments (Supplemental Figure 3B). GO term analysis identified over-represented biological processes in the nuclear, cytoplasmic or in both fractions. For instance, nitrate transport (also its parent term 'anion transport') was found over-represented only in the nuclear fraction (Supplemental Figure 3A). On the other hand, cellular amino acid catabolic process and lateral root development GO terms were found over-represented only in the cytoplasmic fraction. Other processes, such as nitrate response, nitrate assimilation, and nitrate transport, were found over-represented in both fractions. However, these biological processes can have similar or different dynamics of mRNA accumulation of cognate genes (Supplemental Figure 3A). For instance, nitrate assimilation is found over-represented earlier in the nucleus, while amine transport is found over-represented earlier in the cytoplasm (Supplemental Figure 3A).

When we compared all regulated genes (Supplemental Figure 3A) we found 1,183 genes that are regulated in the subcellular fractions but did not show significant changes in the total fraction (Supplemental Figure 3B-C). These results indicate that the analysis of the nitrate-response from subcellular fractions provides complementary information to the analysis of total RNA, identifying genes whose mRNA accumulate specifically in one fraction and that cannot be easily detected in total RNA. Importantly, despite extensive transcriptome analysis of the nitrate response in *Arabidopsis*, we identified 445 genes that had not been identified in previous studies (Supplemental Figure 4). These genes code for proteins involved in growth and development (e.g., *AUXIN RESISTANT 1, GROWTH-REGULATING FACTOR 2* and

BRASSINOSTEROID-INSENSITIVE 2), cell cycle (e.g., *INCREASED LEVEL OF POLYPLOIDY1-1D*), signaling (e.g., *CBL-INTERACTING PROTEIN KINASE 19* and *MAP KINASE 7*), protein modification (e.g., *SUMO-ACTIVATING ENZYME 2* and *UBIQUITIN PROTEIN LIGASE 6*), nitrogen compound metabolism (e.g., *METHIONINE OVER-ACCUMULATOR 2* and *NICOTINAMIDASE 1*), response to stress (e.g., *ANKYRIN REPEAT-CONTAINING PROTEIN 2* and *C-REPEAT/DRE BINDING FACTOR 1*), among other functions. Furthermore, uncharacterized long non-coding RNAs (*AT1G06103, AT1G08697, AT2G09525, AT3G05055, AT4G06085, AT4G06935, AT4G06945, AT5G06585, AT5G09125*) and antisense long non-coding RNAs (*AT1G34844, AT1G67328, AT2G07275, AT3G01205, AT3G09575, AT4G05015, AT4G22233, AT5G01375, AT5G08235, AT5G09595*) were also regulated in response to nitrate in the subcellular fractions. These genes represent new components of the nitrate response and contribute important functions to the plant adaptation to changes in N availability.

Differentially localized transcripts in response to nitrate

In order to identify genes that change their distribution between nuclear-cytoplasmic fractions in response to nitrate, we calculated the delta between normalized counts in nuclear and cytoplasmic fractions (ΔNC). These ΔNC values were used for two-way ANOVA analysis to evaluate the effect of the treatment, time, or their interactions. We selected significant models with a p-value<0.01 after FDR correction. Differentially localized transcripts (DLTs) in response to nitrate were defined as transcripts whose ΔNC depend on the treatment or the treatment-time interactions (p-value<0.01). Using this approach, we identified 402 DLTs in

response to nitrate treatments in *Arabidopsis* roots (Supplemental Figure 2D). mRNA-levels for DLTs in the total fraction should be a combination of the levels we measured in each individual fraction. To confirm this assumption, we estimated a 'reconstituted cell' count for each DLT by simply adding nuclear and cytoplasmic normalized counts (Figure 1A). A high correlation (Pearson correlation value of 0.99) was observed when reconstituted cell counts (i.e., Nuclear+Cytoplasmic levels) was compared with mRNA levels obtained in the total fraction, validating our experimental approach and data analysis procedure (Figure 1B).

Interestingly, 21.6% of the 402 DLTs in response to nitrate were not identified as regulated in the total RNA fraction (Supplemental Figure 5). Some of these genes code for transcriptional regulators (e.g., *ERF1*, *ERF105*, and *AFP3*), nutrient metabolism (e.g., *CYANASE – CYN* - and *SERINE ACETYLTRANSFERASE 2;1* - *SERAT2;1*), auxin response (*SAUR-59*), and root development (e.g., *POPCORN*).

To understand the nitrate response dynamics of mRNA levels in the different fractions, we performed hierarchical clustering analysis for the 402 DLTs. We obtained 13 clusters with 5 or more genes which included a total of 389 DLTs (Figure 1A). As shown in Figure 2 and Supplemental Figure 6, these 13 clusters correspond to five different localization patterns: Nuclear reduction (NR), containing 81 genes with decreasing RNA levels in the nucleus; Cytoplasmic reduction (CR), with 125 genes with decreasing RNA levels in the cytoplasm; Nuclear accumulation (NA), containing 76 genes with increasing levels in the nucleus; Cytoplasmic accumulation (CA), with 72 genes with increasing levels in the cytoplasm; and Delayed-cytoplasmic accumulation (D), containing 33 genes which showed nuclear enrichment at 20 min of treatment and cytoplasm enrichment at later times (Figure 2).

Significantly over-represented Gene Ontology (GO) and Kyoto Encyclopedia of Genes and Genome (KEGG) terms in DLTs include metabolic processes (cofactor, nitrogen compound, carbohydrate, glycerolipid, energy metabolism), localization (anion, amine, and organic acid transport) and response to stimulus functions (Figure 3). In the nuclear accumulation pattern, we identified anion transport, histidine biosynthesis, and nucleotide biosynthesis. In the cytoplasmic accumulation pattern, we found nicotianamine biosynthesis, regulation of organic acid and amino acid export, and sulfur metabolism pathways over-represented. In addition, we found that the following biological processes were over-represented among the DLTs with delayed-cytoplasmic accumulation pattern: carbohydrate metabolism (specifically glycolysis/gluconeogenesis and TCA cycle), nitrogen compound metabolism, cofactor metabolic process, and cellular amino acid biosynthesis. In the cytoplasmic reduction pattern, we found response to stimulus and glycerolipid metabolism functions. We did not observe over-represented terms for the nuclear reduction pattern, and just 'response to stimulus' and 'glycerolipid metabolism' were found in the cytoplasmic reduction pattern (Figure 3). These results demonstrate that relevant functions for the nitrate response are differentially modulated in the cellular fractions.

We selected two representative genes from each localization pattern validation of the RNA-seq data. We measured RNA levels by RT-qPCR in the time-point where the biggest differences are observed between cellular fractions (Supplemental Figure 7). The selected genes were: *MPK9* and *SDR2* for the nuclear reduction pattern; *SUFE2* and *RCAR1* for the cytoplasmic reduction pattern; *NRT2.2* and *BCA4* for the nuclear accumulation pattern; *BZIP3* and *AT1G49230* for the cytoplasmic accumulation pattern; and *NIA1* and *IDH1* for the delayed-

cytoplasmic accumulation pattern. In all cases, we were able to validate the differential mRNA localization pattern (Supplemental Figure 7), confirming the RNA-seq results.

Our cell-fractionation/RNA-seq strategy allowed us to identify transcripts with differential localization in the nucleus and cytoplasm in response to nitrate. The corresponding genes have relevant functions for the nitrate response. Moreover, more than 20% of these genes have not been previously characterized in the plant's response to N nutrients.

DLT localization patterns show differences in their RNA sequence features

In order to evaluate whether specific sequence features could be associated to the differential mRNA localization, we evaluated features described to associate with nucleocytoplasmic levels in other species (Palazzo and Lee, 2018). For instance, sequence features are related to RNA binding protein recognition leading to different RNA destinies (Chen and Van Steensel, 2017; Benoit Bouvrette et al., 2018; Dedow and Bailey-Serres, 2019), also the time transcripts are retained in the nucleus is associated to RNA length and splicing events (Mordstein et al., 2020). We found differences in length, guanine-cytosine (GC) content, and splicing junction density in DLTs as compared to transcripts without differences in nucleocytoplasmic localization in response to nitrate treatments (Figure 4 and Supplemental Figures 8 and 9). Cytoplasmic accumulated transcripts showed shorter RNAs and lower GC content in their exonic regions as compared to transcripts that are induced in response to nitrate but are not differentially localized (Figure 4A-B). These differences are mainly due to shorter CDS regions and lower GC content in the UTRs (Supplemental Figure 8A-F). Cytoplasmic reduced transcripts also showed shorter exonic regions as compared to transcripts that are

repressed in response to nitrate but are not differentially localized (Figure 4A-B, Supplemental Figure 8A-B). In order to evaluate whether these sequence features could be associated with differences in RNA secondary structure formation, we predicted RNA folding energy *in silico* using the RNAfold software (Materials and Methods). DLTs with cytoplasmic accumulation or reduction patterns exhibited less stable mRNA structures as compared to RNAs that respond to the treatment in the total fraction (induction or repression, respectively) (Supplemental Figure 8G). These differences are also observed in the cytoplasmic accumulation pattern when only the UTRs sequences were analyzed (Supplemental Figure 8H-I). In addition, we observed differences in splicing junction density in DLTs as compared to transcripts without differences in nucleocytoplasmic localization in response to nitrate treatments (Figure 4C). Transcripts in the cytoplasmic reduction pattern showed lower splicing junction density than repressed transcripts in the total fraction. Moreover, transcripts in the nuclear accumulation and delayed-cytoplasmic accumulation patterns also showed higher splicing junction density as compared to induced transcripts in the total fraction. On the other hand, transcripts in the cytoplasmic accumulation pattern showed the lowest splicing junction density values among DLTs (Figure 4C).

These results show that transcripts with differential localization in response to nitrate have characteristic sequence features. These sequence features have been associated to modulation of nucleocytoplasmic distribution in yeast and animal systems. Our results suggest similar mechanisms may be implicated in the differential localization of plant transcripts.

Increased RNA polymerase II occupancy is associated to induced DLT genes.

Synthesis and decay have been described as the most critical processes that determine nucleocytoplasmic mRNA levels inside the cell (Bahar Halpern et al., 2015; Hansen et al., 2018). Therefore, we mined published data from our group obtained under comparable experimental conditions to evaluate whether DLTs exhibit specific changes in these features during the nitrate treatment (Figure 5A) (Alvarez *et al*., 2019). We analyzed changes in the RNPII occupancy 12 min after nitrate treatments (Figure 5A). Most of the repressed genes in response to the nitrate treatment did not exhibit changes in RNPII occupancy. We did not observe differences between transcripts with nuclear reduction or cytoplasmic reduction as compared to repressed genes in the total fraction. On the contrary, induced genes by the nitrate treatments also exhibited increased RNPII occupancy. Transcripts with nuclear accumulation, cytoplasmic accumulation, and delayed-cytoplasmic accumulation showed higher values than transcripts of induced genes in response to nitrate that are not differentially localized.

These results indicate that an increase in mRNA synthesis rate leads to nuclear accumulation. Interestingly, DLTs with cytoplasmic accumulation, which also have significant increased RNPII occupancy, should require other regulation levels for explaining its nucleocytoplasmic distribution.

Negative correlation between mRNA decay rates and mRNA accumulation for DLTs

We measured global mRNA decay-rates and estimated half-lives using RNA-seq of rRNA-depleted samples. We extracted total RNA from nitrate or control treated roots in the presence of cordycepin. Sequence data was mapped to Araport11 Arabidopsis genome, and counts were normalized to analyze mRNA decay profiles (Materials and Methods)

(Supplemental Figure 10). Normalized counts were used for modeling decay rates by means of an exponential adjustment for RNA levels as a function of time (Materials and Methods). Figure 5B shows changes in mRNA half-lives for each DLT pattern as well as for nitrate-responsive transcripts that are not differentially localized in the total fraction. Most repressed genes did not change half-lives of cognate mRNAs in response to the treatments. In contrast, transcripts in the delayed-cytoplasmic accumulation, nuclear accumulation, and cytoplasmic accumulation patterns showed significantly faster turnover rates in response to the nitrate treatments (Figure 5B). Moreover, transcripts with delayed-cytoplasmic accumulation showed significantly higher destabilization as compared with those from nuclear accumulation pattern, indicating the cytoplasmic accumulation leads to faster turnover rates of these transcripts in response to the nitrate treatments.

Interestingly, we found a significant negative correlation when we compared changes in RNPII occupancy and half-lives (Figure 5C) for all nitrate-response genes (Pearson correlation = -0.36, $p < 0.001$). We found an even stronger negative correlation when only DLTs were included in the comparison (Pearson correlation = -0.48, $p < 0.0001$). We calculated the mean rank for RNPII occupancy and half-lives changes and found the top 5% were DLTs primarily in the delayed-cytoplasmic accumulation pattern (green dots in the top left quadrant in Figure 5C and Supplemental Table 2). Among these, the mRNA that encodes the nitrate reduction enzyme NIA1 stood out as the transcript with the biggest differences (red arrow in Figure 5C).

These results indicate that synthesis and decay rates and nucleocytoplasmic distribution of DLTs in response to nitrate are connected processes. The negative correlation between RNPII occupancy and half-lives indicate that induced DLTs are molecules with a rapid replacement in

response to the nitrate treatment. This suggests a role for nucleocytoplasmic dynamics in controlling gene expression, especially for those from the delayed-cytoplasmic accumulation pattern (e.g., *NIA1*).

NIA1 delayed-cytoplasmic accumulation allows to extend the mRNA half-life after a strong transcriptional activation

We selected the *NIA1* transcript for validation and further characterization of extreme DLT patterns in order to obtain insights into the role of nucleocytoplasmic dynamics during the nitrate treatments. We selected this transcript for three main reasons: (1) the importance of the *NIA1* gene for the nitrate response, (2) the nitrate-induced changes in mRNA synthesis and decay described in the previous section, and (3) its delayed-cytoplasmic accumulation, which allow us to study its nuclear (20 min of treatment) and then its cytoplasmic (60-120 min of treatment) accumulation phases (Figure 6A). *NIA1* mRNA localization at the subcellular level was evaluated by RNA single-molecule FISH (smFISH) in root tips, using a mix of specific fluorescent probes (Materials and Methods). The number of nuclear, cytoplasmic and total mRNA molecules were calculated using the FISHquant software as detailed in the Material and Methods section. As shown in Figure 6B, probe signal showed two different patterns: (1) small fluorescent dots, corresponding to single-molecule RNAs distributed throughout the whole cell and (2) big fluorescent foci located in the nucleus, which correspond to active transcription sites where nascent RNAs accumulate. These foci disappear with cordycepin treatments (Supplemental Figure 11A). We calculated the number of transcripts for entire cells considering single molecule counts and the estimated number of molecules in transcription sites. As expected, we observed higher number of RNA molecules per cell area in the nitrate- as

compared to the control-treated roots, with higher RNA numbers at 120 min than at 20 min of treatments (Figure 6C). We found that the estimated number of molecules was higher in the nucleus at 20 min but was higher in the cytoplasm at 120 min (Figure 6D-E), which is consistent with the delayed-cytoplasmic accumulation DLT pattern described for this transcript. This result validates the differential localization pattern for *NIA1* mRNA observed in the RNA-seq data at a cellular level. We did not observe differences in the number of nuclear transcripts from single-molecule signals in the nitrate-treated roots between times (Figure 6F). However, we observed a higher number of nuclear transcripts in transcription sites at 20 min as compared to 120 min after the nitrate treatment (Figure 6G). This result indicates that differences in mRNA nuclear levels for *NIA1* are due to mRNAs accumulating in synthesis loci. Moreover, this may be related to the activation of more synthesis loci since we observed a higher number of active transcription-sites per cell at 20 min as compared to the 120 min after nitrate treatments (Supplemental Figure 11B), but no differences in the intensity of these loci (Supplemental Figure 11C). These results indicate that early nuclear accumulation of *NIA1* is associated with a strong transcriptional activation. After some minutes, nuclear accumulation diminishes, and transcripts accumulate in the cytoplasm presumably due to increased export rates.

Furthermore, to evaluate the relationship between decay and the nuclear or cytoplasmic accumulation phases, we measured mRNA levels by RT-qPCR after cordycepin treatments and compared differences in *NIA1* decay rates at 20 min and 120 min of nitrate treatments (Figure 6H-I). In its nuclear-accumulation phase, *NIA1* transcript showed a half-life 12.7 times greater than in its cytoplasmic-accumulation phase. Similar results were obtained for *VRN1*, another gene with a similar localization profile (Supplemental Figure 12A), that showed a 2.11-fold higher half-life at 20 min as compared to 120 min (Supplemental Figure 12B-C). This analysis

provide evidence for a relationship between differential subcellular localization and stability control for these nitrate-responsive genes. These results also suggest a role for nucleocytoplasmic dynamics in controlling transcript levels of rapidly replaced mRNAs. In the case of delayed-cytoplasmic transcripts (particularly *NIA1*), regulation of mRNA nuclear export could explain the lag in cytoplasmic accumulation. This strategy could avoid big quantities of newly synthetized mRNA (in the first minutes after the perception of nitrate) to overwhelm translation machinery. It could also play a role in coordination of expression of multiple genes that are required for specific biological processes to operate.

mRNA transcription and export machinery are differentially expressed in the cytoplasm in response to nitrate treatments.

mRNA export is considered the primary biological process that connects nuclear and cytoplasmic levels of transcripts. We sought to elucidate a mechanism that could explain differential mRNA accumulation by evaluating the expression of different components involved in mRNA synthesis, processing, export and decay in our data set using GO annotations (Supplemental Figure 13). Interestingly, only 'mRNA transcription' and 'RNA export from the nucleus' were over-represented among all mRNA processes analyzed for the nitrate-regulated genes identified in this study. Transcripts from the mRNA-transcription machinery showed enrichment at 20 and 60 min in cytoplasmic and total fractions. In contrast, transcripts from the mRNA-export machinery were enriched at 120 min after nitrate treatments only in the cytoplasmic fraction (Supplemental Figure 13). These results highlight the importance of RNA transcription and export during the nitrate response and suggest temporal coordination between

these processes for the maintenance of the cellular machinery involved in nitrate-responsive gene expression.

DISCUSSION

In this study, we described the nucleocytoplasmic dynamics of mRNA in response to nitrate treatments in *Arabidopsis thaliana* roots. We identified new nitrate-response genes using nuclear and cytoplasmic transcriptome data. Differentially localized transcripts (DLTs) during the nitrate response showed differences in sequence, synthesis, and decay features. These results suggest a role for mRNA nuclear export in controlling the distribution and availability of transcripts with relevant functions in the response to nitrate treatments. In this way, the expression of genes whose mRNAs are rapidly replaced can be tuned. These findings highlight the relevance of modulating nucleocytoplasmic distribution for the control of gene expression in the plant's adaptive response to nitrogen nutrient signals.

mRNA nucleocytoplasmic dynamics for the regulation of relevant genes in the plant's nitrate response

Particular nucleocytoplasmic distributions of mRNA have been observed in different eukaryotic species under a variety of cellular conditions. This mechanism is known to be an essential strategy for the control of gene expression in eukaryotes (Barthelson et al., 2007; Djebali et al., 2012; Solnestam et al., 2012; Bahar Halpern et al., 2015; Battich et al., 2015; Chen and Van Steensel, 2017; Kim et al., 2017; Pastro et al., 2017; Benoit Bouvrette et al., 2018; Reynoso et al., 2018; Lee and Bailey-Serres, 2019; Palovaara and Weijers, 2019). However, most of this research has been performed in animal cells under constant conditions. Our work addresses the relevance of this process in plants in response to an environmental stimulus.

Using cell-fractionation and RNA-seq analysis we obtained a high-resolution subcellular transcriptome in response to nitrate treatments in *Arabidopsis thaliana* roots. Thousands of genes have been previously reported as differentially expressed in response to nitrate treatments under various experimental conditions (Wang et al., 2004; Krouk et al., 2010; Canales et al., 2014; Varala et al., 2018; Alvarez et al., 2019; Swift et al., 2020), and several layers of regulation of gene expression have been described (Vidal et al., 2020). Notwithstanding, in this work we identified 1,183 genes regulated in the subcellular fractions that are not detected as regulated in the total fraction (Supplemental Figure 3B). A large proportion of these genes (445 out of 1,183) has not been reported in prior studies of the root transcriptome (Supplemental Figure 4). This result indicate that our approach gives new information about mRNA accumulation in the response to nitrate treatments, not only describing the mRNA levels in subcellular compartments, but also identifying new genes that have not been characterized in the *Arabidopsis thaliana* response to nitrate.

The nitrate-response is a dynamic process. For instance, transcripts involved in nitrogen uptake and assimilation are enriched among regulated genes at early time points (5-15 minutes), while other metabolic and developmental processes are regulated at later time points (after the first hour) (for example see Varala et al., 2018). In this work, we describe the temporal dynamic of mRNA accumulation in subcellular fractions and show that transcripts with different functions accumulate at different time points in the nucleus or cytoplasm (Supplemental Figure 3A). Furthermore, we identified a group of genes with delayed-cytoplasmic accumulation, which accumulate in the nucleus at early time points, and later in the cytoplasm (Figure 2). This result indicates transcript localization is fast and dynamic, proposing as a mechanism for tuning gene expression. Two previous studies reported a similar temporal fraction-dependent

regulation in plants, when the nuclear transcriptome was compared with the cellular fraction (total poly(A)+) in response to hypoxia conditions (Lee and Bailey-Serres, 2019; Reynoso et al., 2019). These studies identified nuclear-retained transcripts in plants under hypoxia associated with other stress functions. Also, they observed that after 1 hour of reaeration, *HSP70-4* increases its RNA levels in the poly(A)+ cellular fraction, and 1 hour after that the transcript was found in the polysome fraction (Lee and Bailey-Serres, 2019). The authors proposed this mechanism as a strategy for minimizing the energetic demands after conditions of limited reserves (Lee and Bailey-Serres, 2019). This kind of regulatory mechanism is conserved in rice, *Medicago*, and tomato (Reynoso et al., 2019), highlighting the plants' ability to change transcripts' availability in response to stimuli in a fast and dynamic manner.

Our study proposes a functional role for nucleocytoplasmic dynamics for fining tune gene expression in response to nitrate treatments. We show that five different localization patterns are observed in the nitrate response in a time course of 120 minutes (Figure 2, Supplemental Figure 6). Transcripts from these patterns were enriched in essential functions for the nitrate response (Figure 3). For example, in patterns with cytoplasmic and delayed-cytoplasmic accumulation, we found genes directly involved in nitrate-associated metabolism. This suggests that their accumulation in the cytoplasm is favored in order to rapidly express genes that play a key role to the stimulus. This kind of regulation has been previously described for mRNAs involved in the heat-shock response in *Saccharomyces cerevisiae*. In that case, a preferential binding of these transcripts to the export machinery favors their cytoplasmic delivery over that of transcripts with other cellular functions (Saavedra et al., 1996; Zander et al., 2016). The essential role for mRNA cytoplasmic accumulation in response to stress have also been described in plants under heat and cold (Yeap et al., 2019), and hypoxia (Lee and

Bailey-Serres, 2019) conditions. Nevertheless, we also identified enriched GO-terms associated with nitrogen processes (such as nucleotide biosynthesis and nitrate transporters) in nuclear-accumulated transcripts (Figure 3). Considering that nuclear-retained transcripts diminish their association to polysomes, and thus to the protein synthesis (Pastro et al., 2017; Benoit Bouvrette et al., 2018; Lee and Bailey-Serres, 2019; Reynoso et al., 2019), it is not clear why these transcripts are nuclear-retained. A possible explanation for this phenomenon is that those transcripts could increase their levels in the cytoplasm after the 120-minute period analyzed - such as occurred with the transcripts from the delayed-cytoplasmic accumulation pattern (Figure 2) - ; or the expression of these genes is non-essential in response to the stimulus – similar to that observed for general-function mRNAs in yeast in response to heat stress (Saavedra et al., 1996; Zander et al., 2016). Another hypothesis is that the accumulation of some transcripts in response to nitrate treatments is prompted for transcriptional activation of genomic neighborhood (Zhao et al., 2009; De and Babu, 2010). Some of these genes could not necessarily have direct functions in nutrition, so a post-transcriptional gene expression regulation should be required. In this way, possible functional roles for mRNA nucleocytoplasmic dynamics could be relevant for the control of gene expression in response to nitrate treatments.

Regulatory mechanisms associated with particular RNA features for nitrate-induced differential localization patterns

Possible mechanisms for the different localization patterns could be associated with variations in sequence features that are related to nuclear retention or nuclear-export control (Palazzo and Lee, 2018). We observed differences in splicing-junction density among DLTs and

established that nuclear-accumulated transcripts have higher splicing-junction density than transcripts that are not differentially localized, in contrast to the observed for those from the cytoplasmic accumulation pattern (Figure 4C). The contribution of splicing to mRNA localization is evident since the Transcription-EXport (TREX) complex is recruited by splicing proteins, and then it recruit export factors, directly connecting transcription with export (Yelina et al., 2010; Ehrnsberger and Grasser, 2019). Despite this mechanistic link between both processes, and in agreement with our results, - where many transcripts without introns showed cytoplasmic accumulation (Figure 4C)- intronless transcripts can still associate with export machinery and have faster delivery into the cytoplasm (Lei et al., 2011; Wang et al., 2018). Concomitantly, splicing is needed for multiple-exon transcripts export and this process preferentially enhances the expression of low-GC content mRNAs by promoting their association with nuclear export and translation machineries (Mordstein et al., 2020). In addition, nuclear accumulation for transcripts with a high density of splicing sites could increase the probability for intron retention and nuclear localization domains, and in this way, inhibit their cytoplasmic delivery (Lee et al., 2015; Monteuuis et al., 2019).

We also observed differences in length and GC content, which shows that the cytoplasmic accumulation and cytoplasmic reduction patterns differ the most from genes without differential localization (Figure 4A-B). Previous studies in flies, protists, and human cells have described that cytoplasmic-enriched RNAs are shorter than those accumulated in the nuclear or total fractions (Solnestam et al., 2012; Pastro et al., 2017; Benoit Bouvrette et al., 2018). Furthermore, low GC content has been correlated with cytoplasmic accumulation in *Trypanosoma* cells (Pastro et al., 2017). A possible mechanism relating cytoplasmic

accumulation and GC content could be associated with mRNA stability, especially if we consider that GC dinucleotides are substrates for decay (Takata et al., 2017).

Furthermore, sequence features are directly connected with the RNA-binding protein (RBP) specificity since particular nucleotide sequence motifs and secondary structures are determinants for protein-RNA recognition (Silverman et al., 2013; Gosai et al., 2015; Dedow and Bailey-Serres, 2019). The high diversity of these proteins allows them to regulate many cellular processes, having an essential role in nucleocytoplasmic distribution (Okamura et al., 2015; Wickramasinghe and Laskey, 2015; Chantarachot and Bailey-Serres, 2018; Yamada and Akimitsu, 2018). For instance, a positive correlation among nuclear accumulation, mRNA length, and specific motif-containing RBPs has been found in *Drosophila* and human cells (Benoit Bouvrette et al., 2018). Furthermore, mRNAs with cytoplasmic enrichment have lower free energy for the predicted secondary structure in carcinoma cells (Solnestam et al., 2012). According to our data, transcripts from the different localization patterns showed sequence differences (Figure 4, Supplemental Figure 8) that were associated with changes in RNA secondary structures. In fact, differences among DLTs in the predicted RNA folding energy were observed (Supplemental Figure 8G-I), suggesting these transcripts could bind with RBPs differentially in response to nitrate.

To respond to environmental and cellular stimulus faster, eukaryotic cells coordinate mRNA processes through RNA regulons (Keene, 2007; Culjkovic-Kraljacic and Borden, 2018). RBPs and regulatory RNA bind to sequence elements in RNAs that share biological functions to form RNA regulons (Keene, 2007; Hogan et al., 2008; Culjkovic-Kraljacic and Borden, 2018). Disrupted RBP activity alters mRNA splicing, stability, translation, export, and

localization (Keene, 2007; Culjkovic-Kraljacic and Borden, 2018). The role of RNA regulons in nucleocytoplasmic mRNA distribution has been described in the nuclear export of stress response transcripts in yeasts (Saavedra et al., 1996; Zander et al., 2016), and during proliferation (Chakraborty et al., 2008), differentiation (Mancini et al., 2010; Wang et al., 2013), and DNA repair (Wickramasinghe et al., 2013) in mammalian cells. Furthermore, a recent study in *Drosophila* cells showed that just a few RBPs have the highest impact in genome-wide nucleocytoplasmic mRNA distribution (Chen and Van Steensel, 2017). Plants have a higher diversity of RBP than other eukaryotic species, finding over 1800 of these proteins and suggesting a better ability to adapt stimuli responses (Marondedze et al., 2016; Köster et al., 2017; Chantarachot and Bailey-Serres, 2018). For example, the *Arabidopsis thaliana* genome encodes four orthologs for the human export protein RBP ALYREF (ALY1, ALY2, ALY3, and ALY4) (Pfaff et al., 2018). Nevertheless, these proteins seem to have specific functions since only ALY1 is associated with RNA-directed DNA-methylation transcripts in inflorescences (Choudury et al., 2019). Another specific role of RBPs has been described for the oil-palm EgRBP42 in the association to stress-response mRNAs in *Arabidopsis thaliana* (Yeap et al., 2019). In our data, 131 out of 426 genes with the annotated ‘mRNA binding protein’ molecular function were regulated in response to nitrate treatments, so specific RBPs could promote RNA regulon formation for controlling mRNA localization of functionally related transcripts during the nitrate response.

Differential localization of transcripts is associated with synthesis and decay changes in response to nitrate treatments

We measured changes in RNA polymerase II occupancy (as an estimation for synthesis) and decay rates in response to nitrate treatments with a focus on DLT localization patterns (Figure 5). The evidence support the role of RNA synthesis and degradation in modulating nuclear and cytoplasmic mRNA levels, considering the synthesis occurs in the nucleus and most of the degradation in the cytoplasm (Łabno et al., 2016). Our results show that RNPII occupancy changes are evident for genes that increase their levels after nitrate treatment, in accordance with previous research from our group (Alvarez et al., 2019). Interestingly, we also observed similar results for half-lives changes, which evidences a combined role for synthesis and decay in controlling mRNA steady-state levels.

Both DLT patterns with nuclear enrichment (delayed-cytoplasmic accumulation and nuclear accumulation patterns) showed significant increments in RNPII occupancy, which suggests that high synthesis rates may be responsible for nuclear accumulation (Figure 5A). We confirmed this hypothesis for *NIA1* with RNA smFISH experiments, which showed that most of the nuclear transcripts were located in the synthesis loci at 20 min of treatment (*NIA1* nuclear phase) (Figure 6B, Figure 6G). A previous research has previously proposed this hypothesis, when they observed higher transcript levels for nuclear-enriched RNA populations from *Arabidopsis* embryos (Palovaara and Weijers, 2019). Our results confirm this assumption and indicate that nuclear-accumulated transcripts are probably newly synthesized after the nitrate perception and do not reach the cytoplasm at the same rate as at which they are transcribed.

In addition, we observed a negative correlation for RNPII occupancy and half-life changes for genes that respond to nitrate, similar to results that have been reported for yeast, mouse, and fly cells under basal conditions (Miller et al., 2011; Tippmann et al., 2012; Chen and Van Steensel, 2017). We found a stronger negative correlation when only DLTs were considered (Figure 5C), which is comparable to the observed in yeasts for transcripts in response to osmotic stress (Miller et al., 2011). The increase of all RNA kinetic-rates is a strategy for controlling transient induction and diminishing transcriptional noise (Rabani et al., 2014). For instance, rapid turnover occurs co-translationally in plants during the response to excess-light stress for a faster tuning of the genetic response to the stimulus (Crisp et al., 2017). This evidence suggests that DLT-accumulated transcripts undergo a faster replacement, probably due to their specific role in the cellular response to nitrate.

Nuclear export as a possible mechanism for buffering cytoplasmic RNA levels during the nitrate response

mRNA nuclear-export is an essential mechanism for the control of gene expression, which distributes transcripts between the nucleus and cytoplasm (Bahar Halpern et al., 2015; Hansen et al., 2018). Export, synthesis and cytoplasmic decay rates are sufficient to predict nucleocytoplasmic mRNA levels in reported mathematical models (Bahar Halpern et al., 2015; Battich et al., 2015; Hansen et al., 2018), indicating that the contribution of other outputs for mRNA levels such as mRNA nuclear degradation (Das et al., 2003) and extracellular export (Thieme et al., 2015) is not considerable. In this study, we show that nucleocytoplasmic accumulation of transcripts is a dynamic process whereby hundreds of genes change their distribution between cellular compartments in response to nitrate treatments. Our results

indicate that the mRNA levels of a group of genes can go from nuclear enrichment to cytoplasmic in just a few minutes. A study for nucleocytoplasmic dynamics in *Drosophila* cells showed that genes involved in response to stress have a higher export rate than genes involved in constitutive functions (Chen and Van Steensel, 2017). Furthermore, mRNAs with stage-specific functions change between nuclear and cytoplasmic compartmentation during *Trypanosoma cruzi* development, regulating gene expression (Pastro et al., 2017). In *Arabidopsis thaliana*, the preferential cytoplasmic localization of transcripts followed by ribosome association occurs for specific genes involved in the hypoxia stress-response and is used as a mechanism to prioritize energetic demands (Lee and Bailey-Serres, 2019). The evidence presented in this study shows a similar regulation for a non-stress related nutritional response.

Intron retention is another mechanism to regulate gene expression via the modification of nuclear export, which provides the cells with the ability to respond to stress conditions earlier (Monteuuis et al., 2019). The intron retention is a systematic strategy in plants (Kim et al., 2007; McGuirre et al., 2008). mRNAs that accumulate in the nucleus in response to nitrate contained more splicing sites and longer sequences than those accumulated in the cytoplasm (Figure 4A and 4C). Intron retention occurs mainly in long transcripts because the excision of these mRNAs can be performed faster than their synthesis in response to cellular stimulus, a rationale that would not apply for short transcripts (Mauger et al., 2016; Chen and Van Steensel, 2017). Consequently, during the nitrate response, intron retention could signal mRNA nuclear retainment to store mRNAs that play a role later in the nutrient perception by the plant.

Furthermore, the identification of delayed-accumulated transcripts evidences the temporal decoupling of nuclear and cytoplasmic mRNA-level increment. This suggests that nuclear export is regulated in response to nitrate. While delayed-cytoplasmic accumulated transcripts did not show evident sequence differences from the nuclear accumulated pattern (transcripts mainly increase their levels in the nucleus during the whole study time-course) (Figure 4), they did show variations in synthesis and decay features (Figure 5). As we previously discussed, transcripts from the delayed-cytoplasmic accumulation pattern undergo the most significant changes for RNPII occupancy, which suggests that a strong synthesis triggers early nuclear-accumulation. A low export-rate would be required to maintain these high steady-state levels in the nucleus (if we do not consider possible contributions for extracellular export). In contrast, a high export-rate would be required to keep cytoplasmic levels high during later times when the synthesis rate decreases (assuming a low contribution of mRNA nuclear degradation). This hypothesis is supported by our data, which indicates that genes encoding for the export machinery are enriched in the cytoplasm in later times (Supplemental Figure 13), and by another nitrogen-responsive study that reported a similar time-dependent regulation for export machinery genes (Varala et al., 2018). In addition, in our experiments, delayed-cytoplasmic accumulated transcripts showed the highest destabilization among DLT patterns at 120 min (Figure 5B). Furthermore, decay profiles for *NIA1* and *VRN1* showed longer RNA half-lives during their nuclear phase (20 min of nitrate treatment) (Figure 6H-I, Supplemental Figure 12). These results suggest a connection between decay and export. A positive correlation between decay and export has been previously reported in flies (Chen and Van Steensel, 2017) and provides evidence on the importance of controlling the export-rate in order to maintain cytoplasmic mRNA levels in accordance to cell requirements.

In this context, we propose mRNA nuclear-export regulation as a mechanism for buffering the expression levels of important responsive genes for the nitrate response. The temporal retention of mRNAs in the nucleus has been defined as a strategy for controlling the expression of transcripts synthesized during bursts of transcription (Bahar Halpern et al., 2015; Tudek et al., 2019). According to the results shown in this work, the case of *NIA1* fits this hypothesis. *NIA1* is a gene that encodes for an enzyme for the first step of nitrate assimilation (Cheng et al., 1988; Santos-Filho et al., 2014), which strongly depends on transcriptional regulation (Zhao et al., 2018), and its decay is also finely controlled (Wu et al., 2020). A recent study showed that *NIA1* degradation generates many siRNAs, some of which regulate their own expression; this allows the plant to quickly adapt its metabolism in response to its nutritional state (Wu et al., 2020). This evidence highlights the importance of tuning some genes' expression (e.g., *NIA1*), especially when these are transcripts that need to be turned-over rapidly for an efficient cell-response.

We described the mRNA-nucleocytoplasmic dynamics in response to nitrate in *Arabidopsis* roots. The patterns observed for differentially localized transcripts could be explained by characteristic mRNA sequence features, synthesis or decay rates. Interestingly, transcripts with a delayed cytoplasmic accumulation showed the most substantial increments in RNPII occupancy and a reduction in RNA stability. We propose that nuclear export is a strategy for buffering RNA levels in the cytoplasm in order to tune the gene expression for transcripts that undergo a fast turn-over. Our research provides new insights into post-transcriptional regulation during the nitrate-genetic response, suggesting the role of mRNA nuclear-export in the regulation of gene expression under a non-stressful nutritional condition.

METHODS

Plant growth and nitrate treatment

Arabidopsis thaliana seedlings (Col-0 ecotype) were grown in hydroponic media for 15 days, using ammonium succinate as the only nitrogen source in the Phytatray™ system (Sigma, Cat.P1552). Treatments with KNO_3 (or KCl as control) to a final concentration of 5 mM were performed, according to Alvarez et al. (2014). Root tissue was collected at 0, 20, 60, and 120 min of treatment and immediately frozen in liquid nitrogen until processing.

RNA extraction from cellular fractions

Cell fractionation was achieved through differential centrifugation in a sucrose solution according to the protocol published by Xu & Copeland (2012): the pellets obtained correspond to the nuclear fraction, and the supernatants collected correspond to the cytoplasmic fraction. Unfractionated tissue was stored from ground roots for 'total' RNA extraction. RNA extraction, from all cellular fractions, was performed using an Acid Phenol-Chloroform protocol published by Darnell (2012). Finally, all extracted RNA samples were purified following the Clean-up for Liquid Samples protocol from PureLink® RNA Mini Kit (Ambion, Cat, 12183018A). Concentration, integrity, and purity parameters were evaluated for RNA extractions by capillary electrophoresis (Fragment Analyzer, STANDARD SENSITIVITY RNA ANALYSIS KIT DNF-471, Advanced Analytical Technologies) and spectrophotometry (Nanodrop2000, Thermo Scientific), procuring to have more than two micrograms of RNA, RNA Quality Number (RQN) higher than 6.0, and optimal absorbance ratios (A260/A280 and A260/A230) for each extraction

RT-qPCR measurements

cDNA was synthesized from nuclear and cytoplasmic RNA using Improm II RT (Promega, Cat. #A3800), and cDNA levels were measured by qPCR using the Brilliant III Ultra-Fast qPCR Kit (Agilent Technologies, Cat. #600880) and the StepOnePlus™ qPCR System (Agilent Technologies). Primers listed in Supplemental Table 3 were used for amplification. cDNA levels were calculated using the LinRegPCR software (Ramakers et al., 2003).

Nuclear transcript enrichment was evaluated by RT-qPCR detection of specific regions of unprocessed transcripts in genes with constitutive expression [*CLATHRIN COAT ASSEMBLY*, *RAN3*, and *EIF4G*]. Primers were designed for detecting intronic regions for unprocessed RNAs and between two exons (one at the end of an exon, and the other one at the beginning of the closest neighbor exon) for processed RNAs (Supplemental Table 3). The analysis was performed from cDNA synthesized from RNA extractions obtained for different cellular fractions using random primers (Promega, Cat. #C1181). Unprocessed RNA levels were normalized using the mean value of three processed mRNAs.

Differential RNA levels in the cellular fractions were confirmed, measuring *MPK9*, *SDR2*, *SUFE2*, *RCAR1*, *NRT2.2*, *BCA4*, *BZIP3*, *AT1G49230*, *NIA1* and *IDH1* (representative transcripts for DLT localization patterns). The mean RNA levels for *CLATHRIN COAT ASSEMBLY* and *RAN3* were used as a normalizer factor. For RNA decay evaluation by qPCR, *NIA1* and *VRN1* levels were measured from cordycepin-treated plants, using *YLS8* as a normalizer gene.

RNA sequencing from cellular fractions

cDNA libraries (from PolyA enriched RNA) were prepared by Macrogen service (South Korea), using TruSeq® Stranded mRNA LT Sample Preparation Kit (Illumina, Cat. RS-122-2101) from RNA of each cellular fraction (nuclear, cytoplasmic, and total), for control (KCl) and treated (KNO_3) conditions, and for the four time-points collected (0, 20, 60, and 120 minutes). Libraries were sequenced by Macrogen in Illumina Novaseq6000 platform with 100 bp pair-end reads.

RNA-seq data analysis

For most of the data analysis, R software packages (CRAN R Project) were used. The FastQC software (0.10.0 version, Babraham Bioinformatics) was used to check the reads' quality, and then the sequences were processed with Trimmomatic v0.36 (Bolger et al., 2014) for removing the low-quality reads. The sequences were mapped to the *Arabidopsis thaliana* genome (Araport11 annotation) using HISAT2 (Kim et al., 2015), and finally, Rsubread R Library (Liao et al., 2013) was used for counting the number of reads per gene. The number of Transcripts Per Million of reads (TPM) divided by the gene's length was calculated.

We used quantile normalization to identify differentially expressed genes in the cellular fractions (Smyth, 2005). This strategy was considered the best for reducing the bias generated by the different nature of the cellular fractions. Nuclear and Cytoplasmic TPMs/length were quantile normalized together (for comparisons between cellular fractions), and total TPMs/length was calculated separately. To identify genes that are differentially accumulated by the treatment and change during the time-course, a two-way ANOVA model was performed from the log2 (quantile normalized counts) of each cellular fraction, evaluating the effects of

treatment (KCl and KNO3), time (20, 60, 120 min) and their interaction through the model. In this way, transcripts that fit the model with a significant p-value for treatment (T) or its interaction with time (Treatment:Time) were considered as genes whose mRNA levels change within the cellular fraction in response to nitrate.

Given that nuclear and cytoplasmic fractions are not independent of each other, a ΔNC value (Normalized counts in nuclear fraction minus normalized counts in cytoplasmic fraction) was calculated in order to identify genes whose transcripts show different distributions between these cellular fractions. From these values, a similar analysis, as mentioned above, was performed. The transcripts whose ΔNC values fit the 2-way ANOVA model with a significant p-value for treatment or its interaction with time were considered as differentially localized transcripts (DLTs) in response to the nitrate treatments.

The different lists of regulated genes were compared using Sungear software (Poultney et al., 2007). Multiple Experiment Viewer (MeV) software (Saeed et al., 2003) was used to visualize and cluster the data. Gene groups were defined by hierarchical clustering from their Pearson correlation, using an average linkage method and defining a threshold distance of 0.5. Enrichment analysis of Gene Ontology (GO) and Kyoto Encyclopedia of Genes and Genomes (KEGG) terms was performed using the BioMaps software from VirtualPlant v1.3 (Katari et al., 2010), selecting terms with a p-value with FDR (False Discovery Rate) correction lower than 0.05. GO terms were summarized with REVIGO (http://revigo.irb.hr) set to obtain a medium-size list of terms according to Resnik similarity (Supek et al., 2011). The sequence features of these transcripts were analyzed, extracting the information from the Generic Feature Format (GFF) file of Araport11 annotation for each gene's most abundant isoform according to the

RNA-seq data. Prediction of mRNAs secondary structure was performed using the RNAfold function from ViennaRNA Package 2.0 (Lorenz et al., 2011).

RNA stability evaluation

In order to measure decay rates of DLTs during the nitrate response, *Arabidopsis thaliana* seedlings were treated with a transcription inhibitor after the treatment with the nutrient, and RNA decay rates and half-lives were calculated for each condition (KNO_3 and KCl). 15-day old *Arabidopsis thaliana* seedlings were treated as described above; after 20 or 120 min of nutrient treatment, the plants were transferred to a solution of Cordycepin 0.6 mM (Sigma Cat. #C3394) prepared in MS without nitrogen in a growth chamber with low agitation. Roots were collected at 0, 30, 60, and 120 min after the cordycepin treatment. RNA was extracted using TRIzol™ reagent (Invitrogen Cat. 15596) following the protocol described by Macrae (2007). RNA was used for cDNA synthesis and subsequent quantification by RNA-seq (for RNA from seedlings treated for 120 min with nitrate) or qPCR to evaluate stability at other treatment times.

For RNA-seq analysis, twenty-four different libraries were synthesized from RNA extracted from three independent experiments. cDNA libraries (from rRNA-depleted RNA) were prepared by Macrogen service (South Korea), using TruSeq® Stranded Total RNA Library Prep Plant (Illumina, Cat. 20020611) using RNA from nitrate or control conditions after the four time-points of cordycepin treatment. Libraries were sequenced by Macrogen in Illumina Novaseq6000 platform with 100 bp paired-end reads, requesting 40 million reads per sample. Raw data were analyzed as described above for RNA-seq from cellular fractions until obtaining TPM/length normalized counts. The Multiple Experiment Viewer (MeV) (Saeed et al., 2003)

software was used to visualize and cluster the data. Gene clusters were defined by hierarchical clustering from their Pearson squared correlation, using a complete linkage method, defining a threshold distance of 0.5.

Decay rates (k_{decay}) and then half-lives ($t_{1/2}$) were calculated by adjusting the measured RNA levels (C) as an exponential function of time (t). The mathematical adjustment for C(t) was developed assuming a constant decay rate, according to the function: $C(t) = e^{-kdecay * t}$ (Gutierrez et al., 2002; Narsai et al., 2007; Sorenson et al., 2018). 'RNA decay' R-package (Sorenson et al, 2018) was used for decay modeling for RNA-seq data. Models in which decay-rate changed or not between KNO_3 and KCl treatments were evaluated, and the model with the lowest Akaike Information Criterion (AIC) statistics was selected. Prism GraphPad 6 was used for qPCR data, assuming constant decay rates during the evaluation time for cordycepin treatment.

RNA polymerase II occupancy changes

Data from RNA Polymerase II Chromatin Immunoprecipitation sequencing (RNPII-ChIPseq) was analyzed (Alvarez et al., 2019). This data was obtained from *Arabidopsis thaliana* roots treated for 12 min with nitrate in the same conditions used to identify DLTs. Normalized sequence counts in regions between 500 bp upstream the TSS and 500 bp downstream the TTS were evaluated by differential accumulation with DESeq2 package (Love et al., 2014), calculating a fold change of RNPII occupancy between each gene's treated (KNO_3) and control condition (KCl).

RNA *in situ* detection

RNA single-molecule Fluorescence *in situ* Hybridization (RNA smFISH) was performed according to the protocol described in Duncan et al. (2017). Forty-eight probes were designed using the Stellaris Probe Designer software (version 2.0 from Biosearch Technologies) to recognize exonic regions for the *NIA1* transcript. Probes with Quasar670 fluorophore were synthesized by Stellaris. Probe sequences are listed in Supplemental Table 4.

Fifteen-day old *A. thaliana* seedlings were treated with nitrate (and KCl as control) for 20 and 120 min. Some of these plants were also treated with cordycepin 0.6 mM for 120 min after nutrient treatment for transcription site analysis. Roots were collected, fixed in 4% paraformaldehyde solution, and compressed on microscope slides to obtain cell monolayers. Fixed samples were hybridized with the probe set and then with DAPI 100 ng/mL. The visualization and imaging were performed with a Zeiss LSM800 inverted microscope, using an x63 oil-immersion objective and a cooled-electron multiplying-CCD (charge-coupled device) Andor iXon 897 camera. The following wavelengths were used for fluorescence detection: for Quasar670, an excitation line of 642nm with signal detection at 655–710 nm; for DAPI, an excitation line of 405 nm with signal detection at 420–480 nm. For all experiments, series of optical sections with z-steps of 0.2 µm were collected. Maximum projections and analysis of three-dimensional pictures were performed using Fiji. For image deconvolution and quantification, FISH-quant software was used (Mueller et al., 2013). Tutorial instructions for the batch analysis for "Mature mRNA quantification" and "Nascent mRNA quantification" were followed (Mueller et al., 2013).

Accession numbers

NIA1 (AT1G77760), *RAN3* (AT5G55190), *EIF4G* (AT3G60240), *CLATHRIN COAT ASSEMBLY PROTEIN* (AT4G24550), *MPK9* (AT3G18040), *SDR2* (AT3G51680), *SUFE2* (AT1G67810), *RCAR1* (AT1G01360), *NRT2.2* (AT1G08100), *BCA4* (AT1G70410), *BZIP3* (AT5G15830), *IDH1* (AT4G35260), *VRN1* (AT3G18990).

ACKNOWLEDGMENTS

We thank Luis Villarroel, Ph.D. (Pontificia Universidad Católica de Chile) for help with data normalization and statistics strategy. This work was supported by grants from the Fondo de Desarrollo de Áreas Prioritarias (FONDAP) Center for Genome Regulation (15090007), and the Agencia Nacional de Investigación y Desarrollo (ANID), through ANID–Millennium Science Initiative Program-Millennium Institute for Integrative Biology (iBio), FONDECYT 1180759 to R.A.G and Ph.D. scholarship (21161516) to A.F.

FIGURES

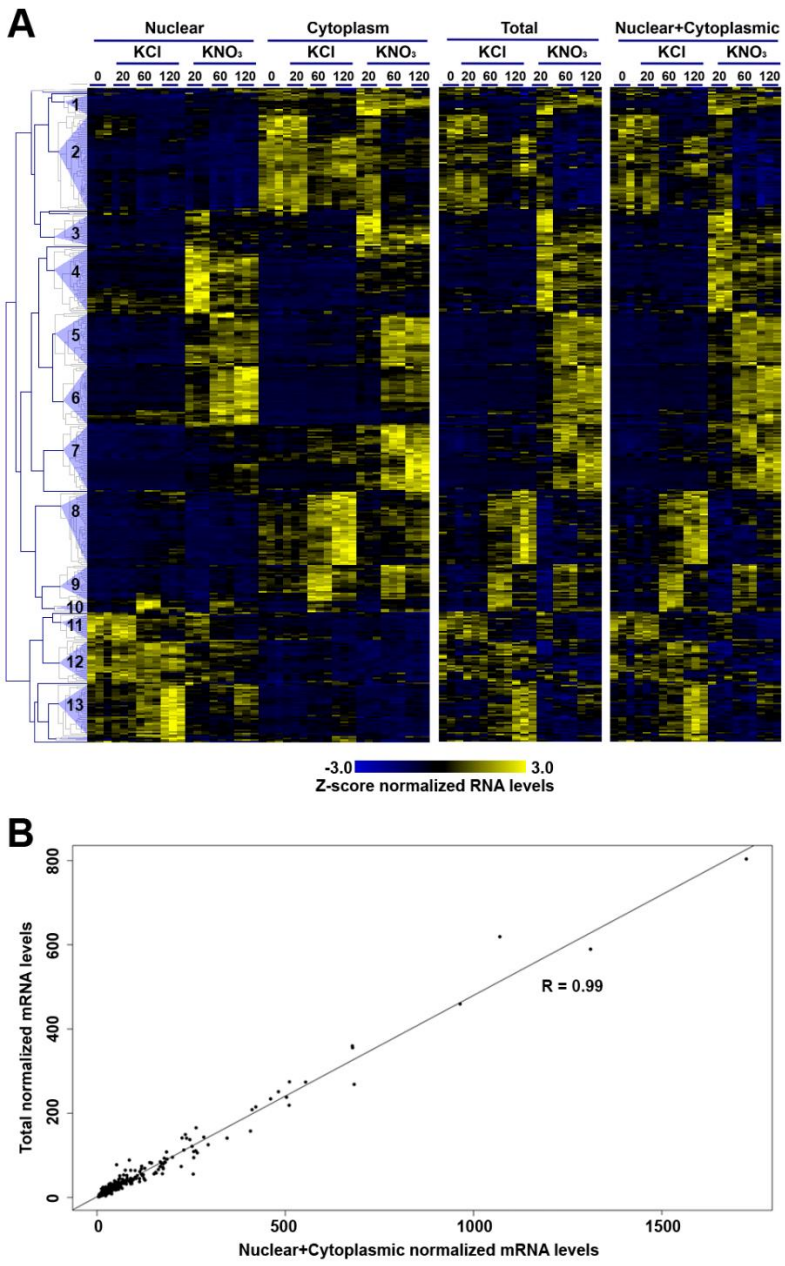

Figure 1. Differentially localized transcripts (DLTs) in response to nitrate treatments.

Heatmap with mRNA levels in cellular fractions for DLTs in response to nitrate treatments. Genes were hierarchically clustered using the correlation of mRNA levels in the nuclear and cytoplasmic fractions (panel I). mRNA levels in the total fraction are shown in panel II. We calculated Nuclear+Cytoplasmic mRNA levels, using data from each fraction, which are shown in panel III. Cluster numbers are indicated on the dendrogram to the left of the heatmap. Each column represents the mRNA levels for one replicate under each condition. **(B)** Scatter plot for comparing the mean mRNA levels of DLTs in the Total and Nuclear+Cytoplasmic data. The Pearson correlation (R) is indicated.

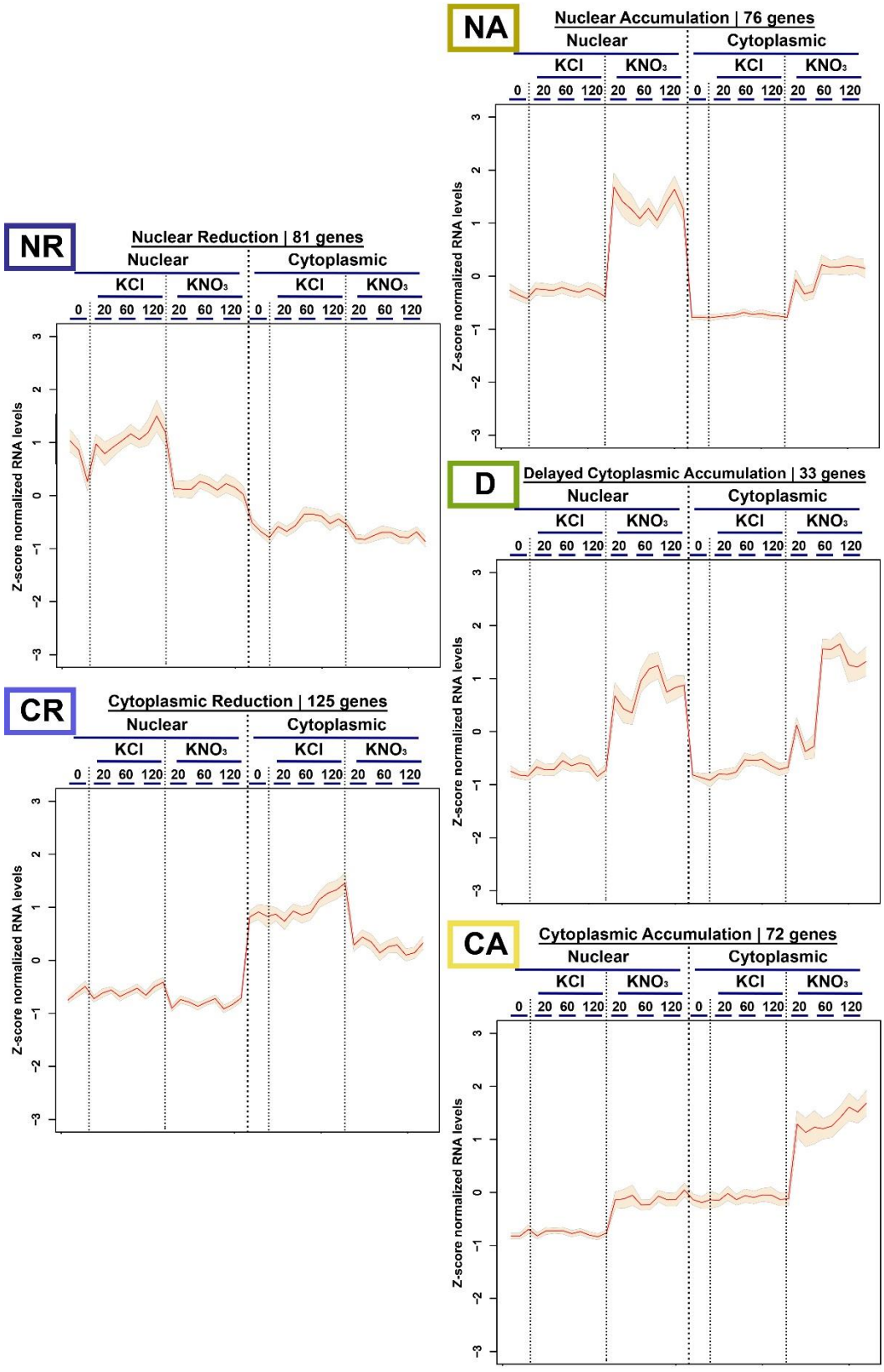
NA
Nuclear Accumulation | 76 genes
Nuclear
Cytoplasmic
KCl
KNO3
0 20 60 120 20 60 120 0 20 60 120 20 60 120
Z-score normalized RNA levels
NR
Nuclear Reduction | 81 genes
D
Delayed Cytoplasmic Accumulation | 33 genes
CR
Cytoplasmic Reduction | 125 genes
CA
Cytoplasmic Accumulation | 72 genes

Figure 2. DLT localization patterns in response to nitrate treatments.

Five different localization patterns (NR – Nuclear reduction, CR – Cytoplasmic reduction, NA – Nuclear accumulation, D – Delayed-cytoplasmic accumulation, and CA – Cytoplasmic accumulation) are identified. DLTs in response to nitrate treatments were separated by the cellular fraction where the main changes are observed (Nuclear or cytoplasmic), and if they show an accumulation or reduction of mRNA levels in the nitrate condition. Graphs show mean values of Z-scored normalized mRNA levels (orange line) and 95% confidence interval for mean values of each DLT for the three independent experiments (shadow).

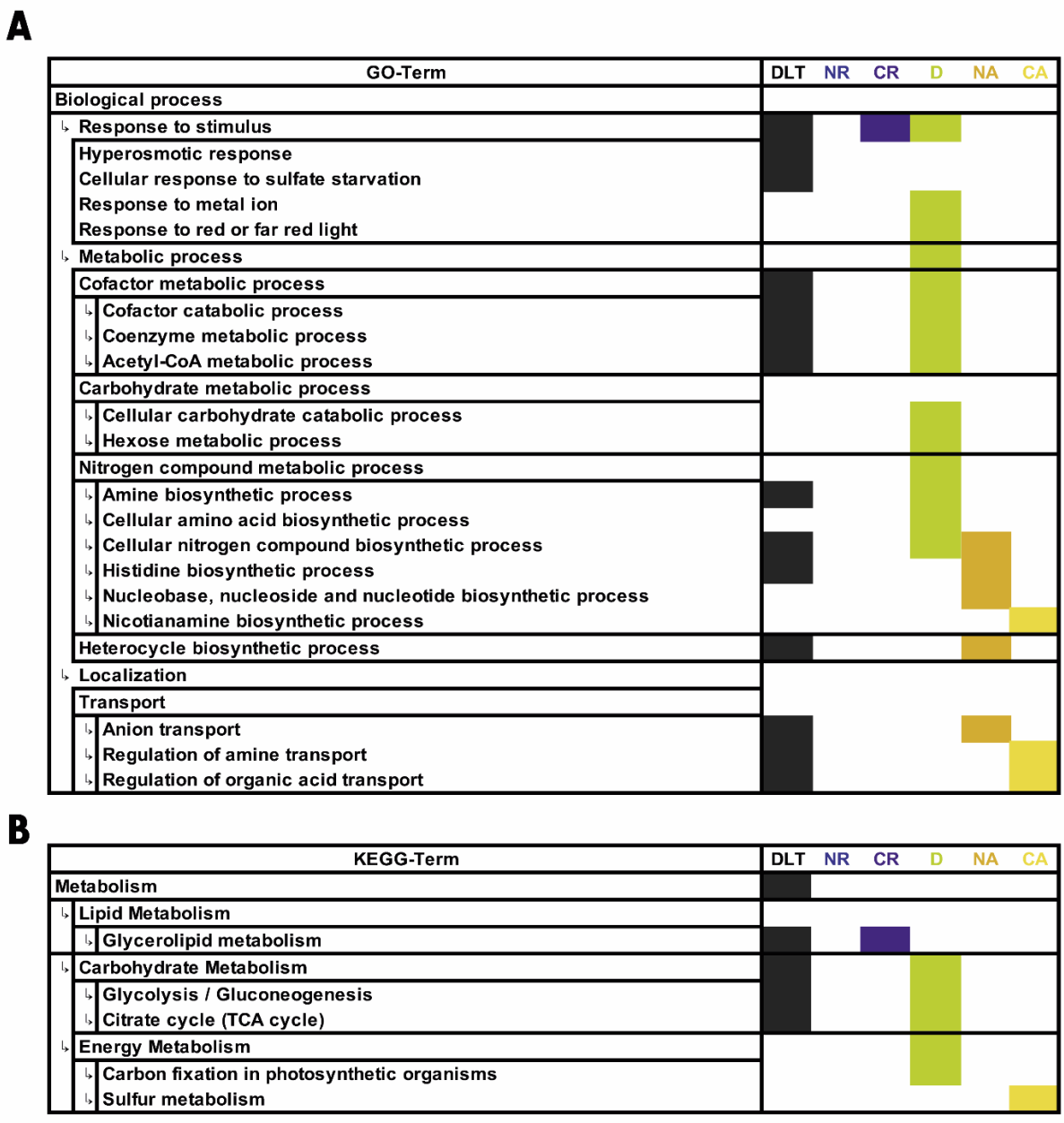

Figure 3. Over-represented terms in DLTs in response to nitrate treatments.

Summary of significant ($p<0.05$) over-representation of **(A)** GO, and **(B)** KEGG-Terms enriched in the lists of all DLTs, or the DLT localization patterns (NR – Nuclear reduction, CR – Cytoplasmic reduction, NA – Nuclear accumulation, D – Delayed-cytoplasmic accumulation, and CA – Cytoplasmic accumulation) according to VirtualPlant output (Katari et al., 2010). GO-terms were summarized by non-redundant 5 and 6 levels using REVIGO (Supek et al., 2011).

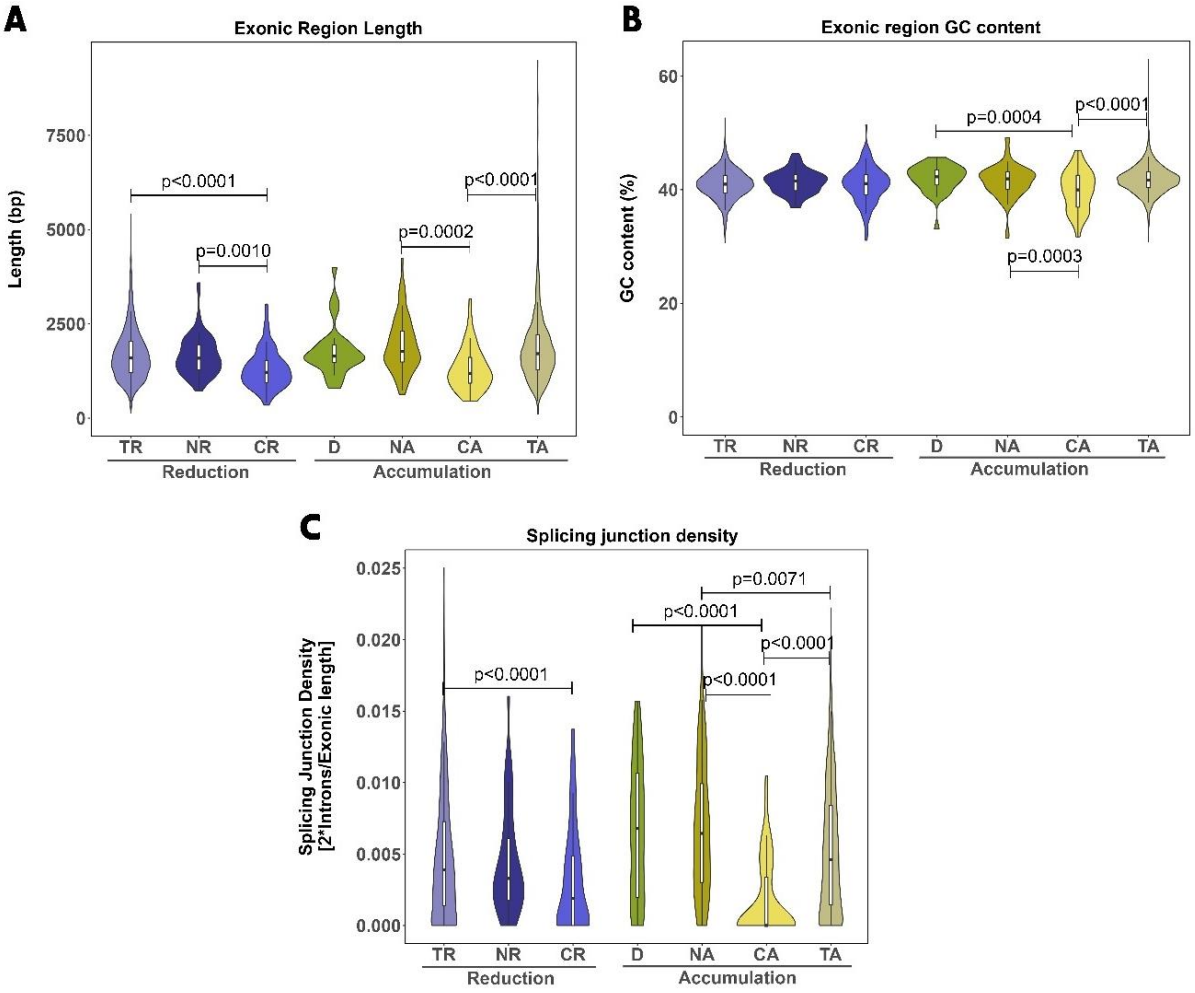

Figure 4. Differences in sequence-related features of DLTs in response to nitrate treatments.

Sequence features of the most abundant isoform for nitrate-regulated genes, according to Araport11 annotation. Violin plots show the distribution of **(A)** exonic region length, **(B)** exonic region GC content, and **(C)** splicing junction density for DLTs in each pattern (NR – Nuclear reduction, CR – Cytoplasmic reduction, NA – Nuclear accumulation, D – Delayed-cytoplasmic accumulation, and CA – Cytoplasmic accumulation). We also include nitrate-regulated genes in the total fraction that are not differentially localized as a control (TA – Total accumulated, or TR – Total reduced). Boxes inside show the interquartile range (IQR – 25-75%), the horizontal line indicates the median value. Whiskers show the ±1.58xIQR value. We compared the distributions using one-way ANOVA and Dunnett post-test. We include p-values and brackets to highlight relevant comparisons.

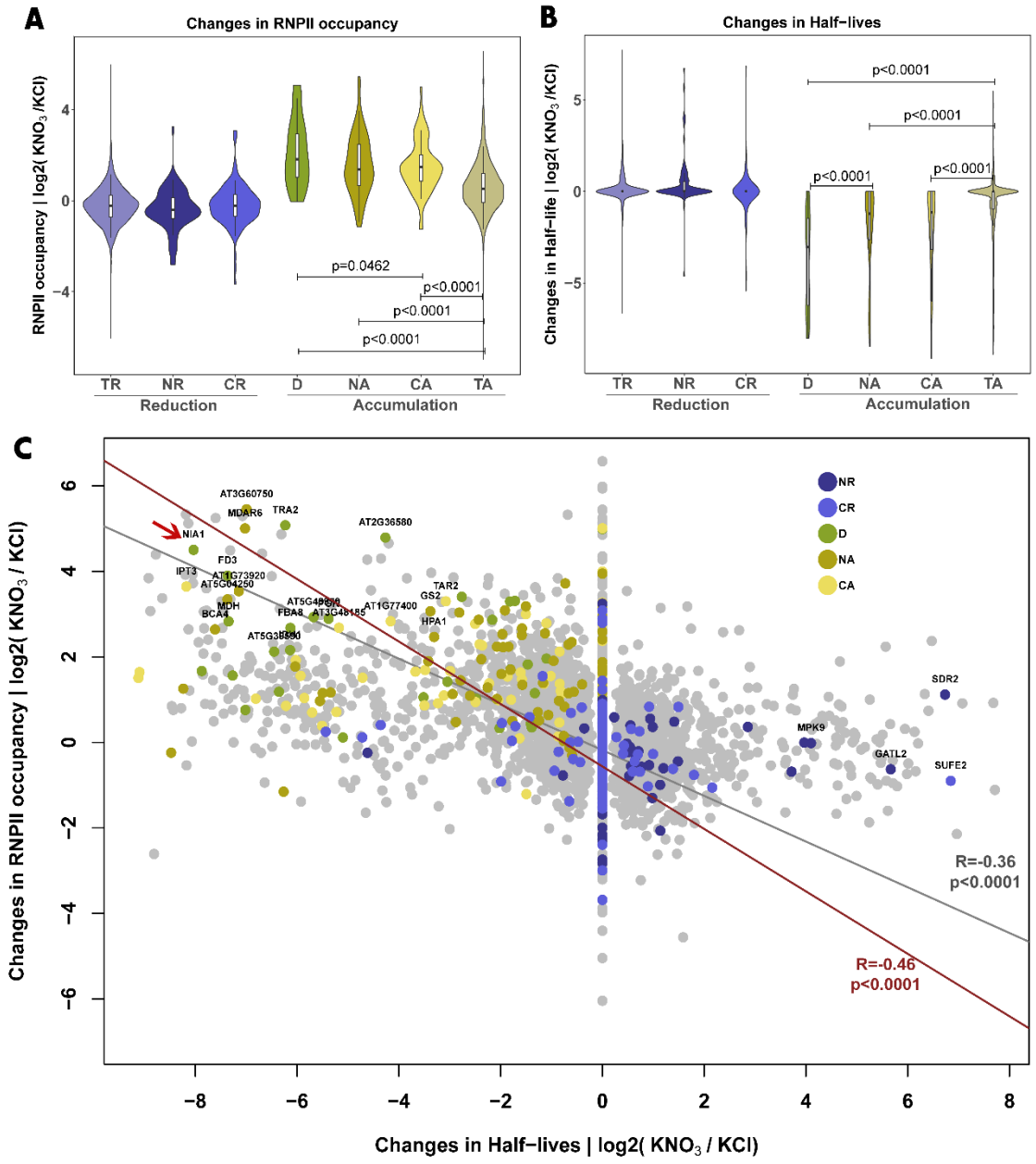
A
Changes in RNPII occupancy
RNPII occupancy | log2(KNO3 /KCl)
p=0.0462
p<0.0001
p<0.0001
p<0.0001
TR NR CR D NA CA TA
Reduction
Accumulation
B
Changes in Half−lives
Changes in Half−life | log2(KNO3 /KCl)
p<0.0001
p<0.0001
p<0.0001
p<0.0001
TR NR CR D NA CA TA
Reduction
Accumulation
C
Changes in RNPII occupancy | log2(KNO3 / KCl)
Changes in Half−lives | log2(KNO3 / KCl)
NR
CR
D
NA
CA
AT3G60750
MDAR6
TRA2
AT2G36580
NIA1
FD3
IPT3
AT1G73920
AT5G04250
TAR2
GS2
MDH
BCA4
FBA8
AT1G77400
HPA1
SDR2
MPK9
GATL2
SUFE2
R=-0.36
p<0.0001
R=-0.46
p<0.0001

Figure 5. Changes in RNA polymerase II (RNPII) occupancy and half-lies for DLTs in response to nitrate treatments.

(A) Changes in RNPII occupancy after 12 min and **(B)** Changes in half-lives after 120 min of nitrate treatment. Violin plots show the distribution for DLTs in each pattern (NR – Nuclear reduction, CR – Cytoplasmic reduction, NA – Nuclear accumulation, D – Delayed-cytoplasmic accumulation, and CA – Cytoplasmic accumulation). We also include nitrate-regulated genes in the total fraction that are not differentially localized as a control (TA – Total accumulated, or TR – Total reduced). Boxes inside show the interquartile range (IQR – 25-75%), indicating the median value as a horizontal line. Whiskers show the ±1.58xIQR value. We compared the distributions using one-way ANOVA and Dunnett post-test. We include p-values and brackets to highlight relevant comparisons. **(C)** Scatter plot showing the relationship between changes in RNPII occupancy and half-lives for all genes that respond to nitrate in any cellular fraction. Linear regression and Pearson correlation coefficient are indicated for all data (gray) and DLTs only (red). The red arrow shows *NITRATE REDUCTASE 1* (*NIA1*) as the DLT with the greatest changes in RNPII occupancy as well as half-life values.

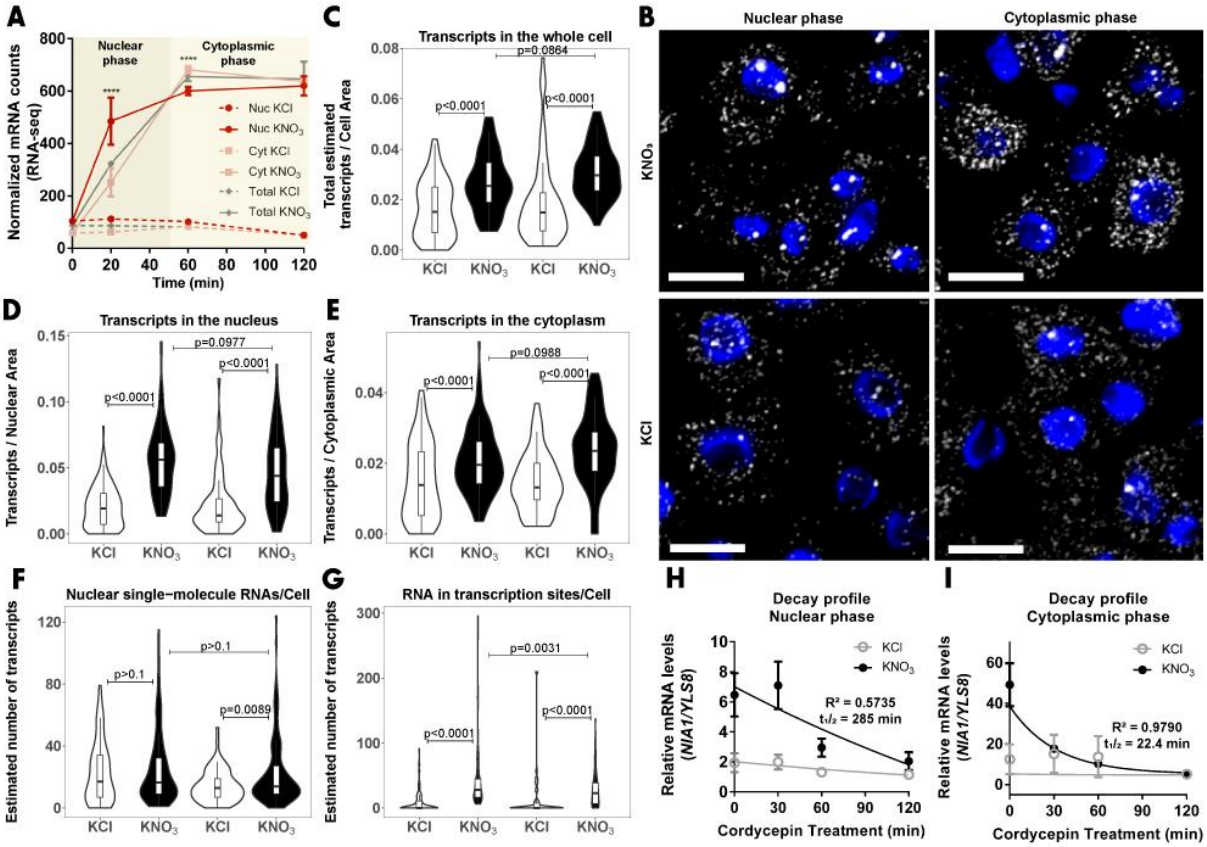
A
Normalized mRNA counts (RNA-seq)
Nuclear phase
Cytoplasmic phase
Nuc KCl
Nuc KNO3
Cyt KCl
Cyt KNO3
Total KCl
Total KNO3
Time (min)
B
Nuclear phase
Cytoplasmic phase
KNO3
KCl
C
Transcripts in the whole cell
Total estimated transcripts / Cell Area
p<0.0001
p=0.0864
p<0.0001
D
Transcripts in the nucleus
Transcripts / Nuclear Area
p<0.0001
p=0.0977
p<0.0001
E
Transcripts in the cytoplasm
Transcripts / Cytoplasmic Area
p<0.0001
p=0.0988
p<0.0001
F
Nuclear single−molecule RNAs/Cell
Estimated number of transcripts
p>0.1
p>0.1
p=0.0089
G
RNA in transcription sites/Cell
Estimated number of transcripts
p<0.0001
p=0.0031
p<0.0001
H
Decay profile
Nuclear phase
Relative mRNA levels (NIA1/YLS8)
KCl
KNO3
R² = 0.5735
t1/2 = 285 min
Cordycepin Treatment (min)
I
Decay profile
Cytoplasmic phase
Relative mRNA levels (NIA1/YLS8)
KCl
KNO3
R² = 0.9790
t1/2 = 22.4 min
Cordycepin Treatment (min)

Figure 6. RNA single-molecule FISH detection and decay profiles for *NIA1* transcript in nuclear and cytoplasmic accumulation phases

(A) mRNA levels in cellular fractions measured by RNA-seq. (****) indicates statistical differences between nuclear and cytoplasmic fractions.

(B) Representative microscopy images *NIA1 in situ* detection in *Arabidopsis* root cells by RNA single-molecule FISH (smFISH). White color corresponds to signal detected for *NIA1* specific fluorescent probes. Blue color corresponds to the DAPI stain. Scale bar = 10 µm.

(C-G) Quantification of the RNA smFISH. Violin plots show the distribution for transcript quantification in the nitrate (KNO_3, black) or control (KCl, white) conditions at 20 or 120 min after the treatment. Boxes inside show the interquartile range (IQR – 25-75%), indicating the median value as a horizontal line. Whiskers show the ±1.58xIQR value. **(C)** Estimated number of transcripts per cell area in whole cells (nucleus+cytoplasm). **(D)** Number of transcripts per nuclear area. The number of transcripts from single-molecule signals and the estimated number of transcripts in transcription sites is included. **(E)** Number of transcripts from single-molecule signals in the cytoplasmic area. **(F)** Number of active transcription sites per cell. **(G)** Estimated number of transcripts in each active transcription site

(H-I) Comparison of half-life values ($t_{1/2}$) between *NIA1* nuclear and cytoplasmic phases. RNA levels were determined by RT-qPCR. Half-lives and coefficients of determination for regression models are indicated in each graph.

SUPPLEMENTAL FIGURES

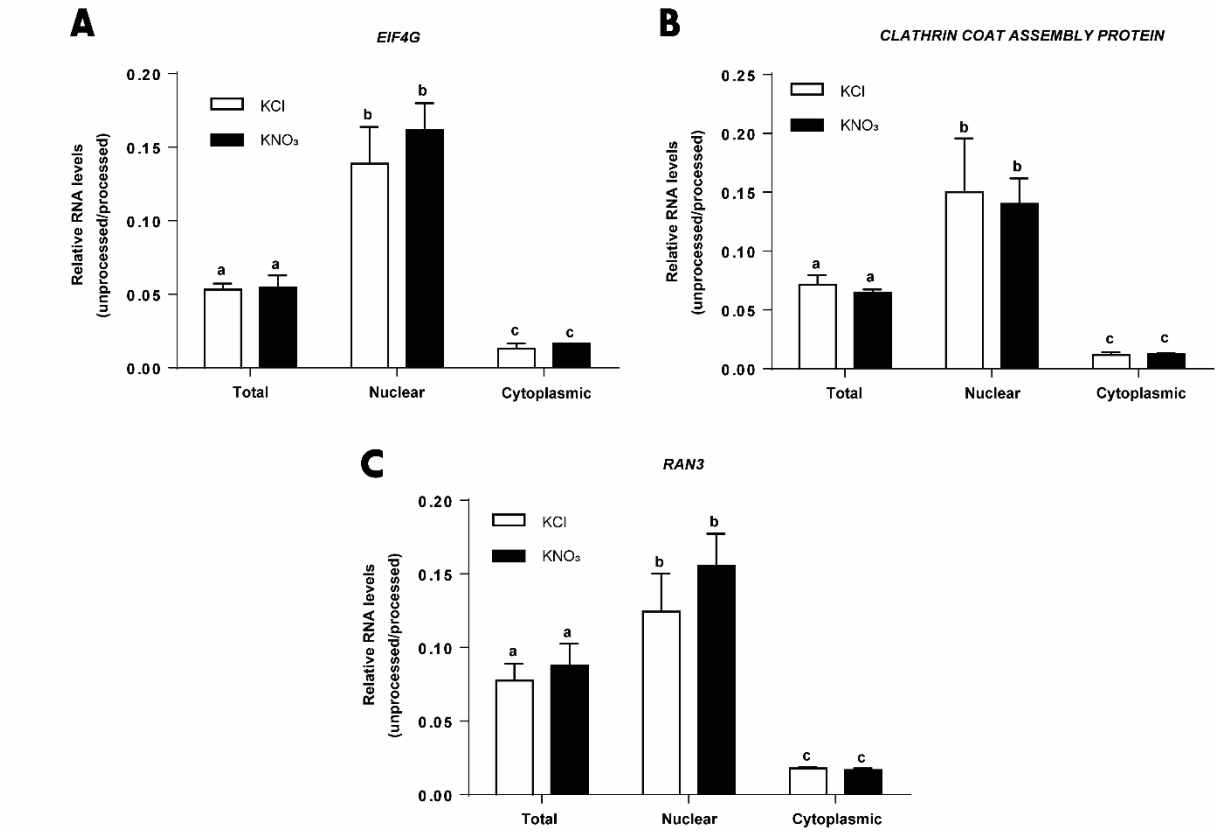

Supplemental Figure 1. Unprocessed transcripts are enriched in nuclear fractions and reduced in cytoplasmic fractions.

RNA detection by RT-qPCR for unprocessed transcripts in the different cellular fractions (Total, nuclear, and cytoplasmic) obtained from root tissue from nitrate- or control-treated seedlings for 60 min (KNO_3 or KCl, respectively). Three different constitutive-expressed transcripts were detected: **(A)** *EIF4G*, **(B)** *CLATRHIN COAT ASSEMBLY PROTEIN*, and **(C)** *RAN3*. RNA values were normalized with mean processed RNA levels. Detection was performed using primers flanking (processed RNA) or inside (unprocessed RNA) intronic regions for each gene. Bars represent the mean ± standard error of 3 independent experiments. Statistical analysis was performed using ANOVA/Tukey's HSD test. Different letters above bars denote statistically significant differences (ANOVA/Tukey's HSD test, $p<0.05$).

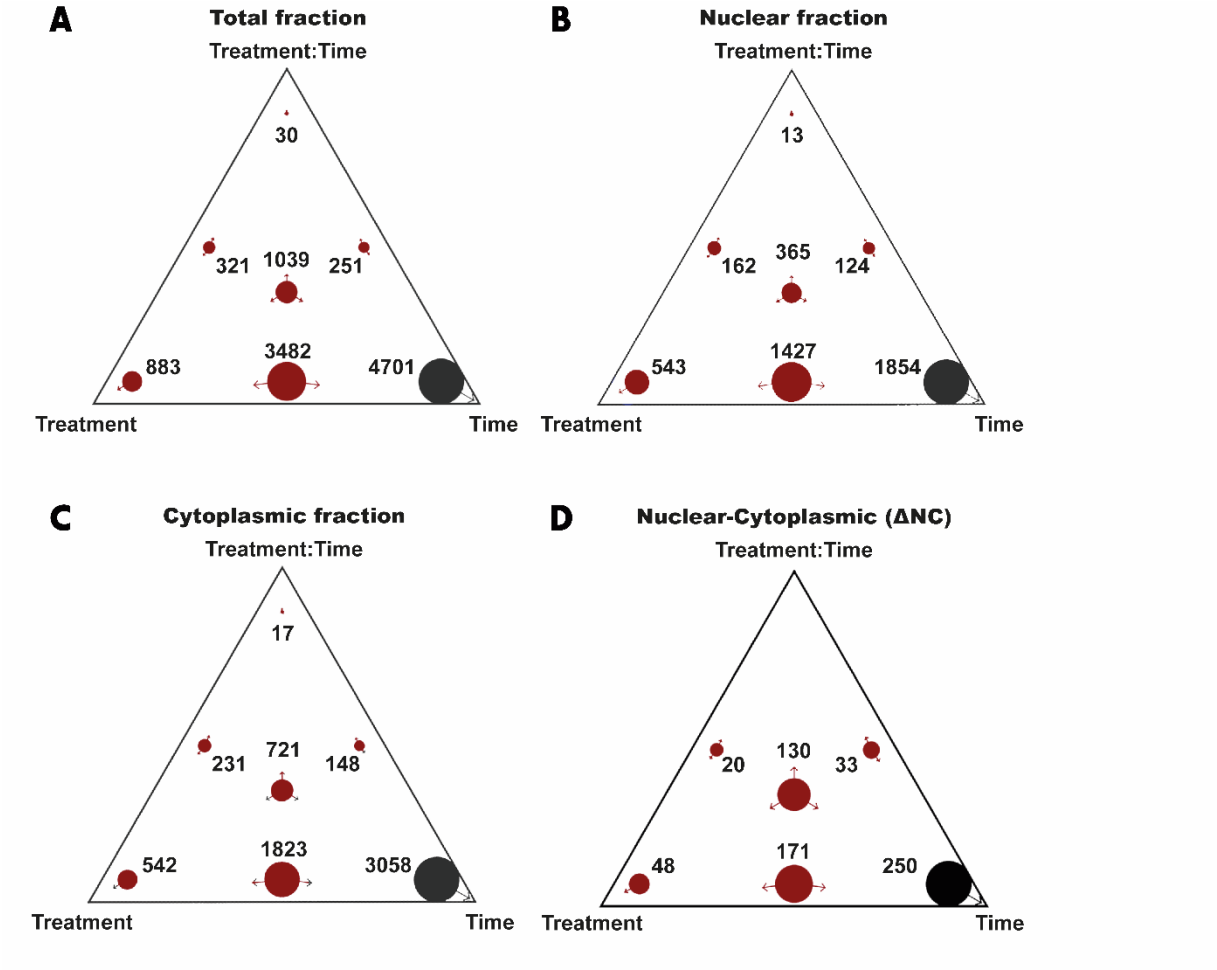

Supplemental Figure 2. Number of differentially expressed genes in cellular fractions

The list of genes with significant factors obtained by two-way ANOVA analysis of RNAseq data is represented using the Sungear tool (Poultney et al., 2007). The triangle shows the factors at the vertices (Treatment, time, and the interaction between both (Treatment:Time). The circles inside the triangle represent the genes controlled by the different factors, as indicated by the arrows around the circles. The size of each circle is proportional to the number of genes associated with that circle. The number of genes in the circle is shown next to the corresponding circle. **(A)** Total fraction, **(B)** Nuclear fraction, **(C)** Cytoplasmic fraction, and **(D)** Nuclear-Cytoplasmic subtraction. Differentially expressed genes in response to nitrate treatments are colored in red.

A

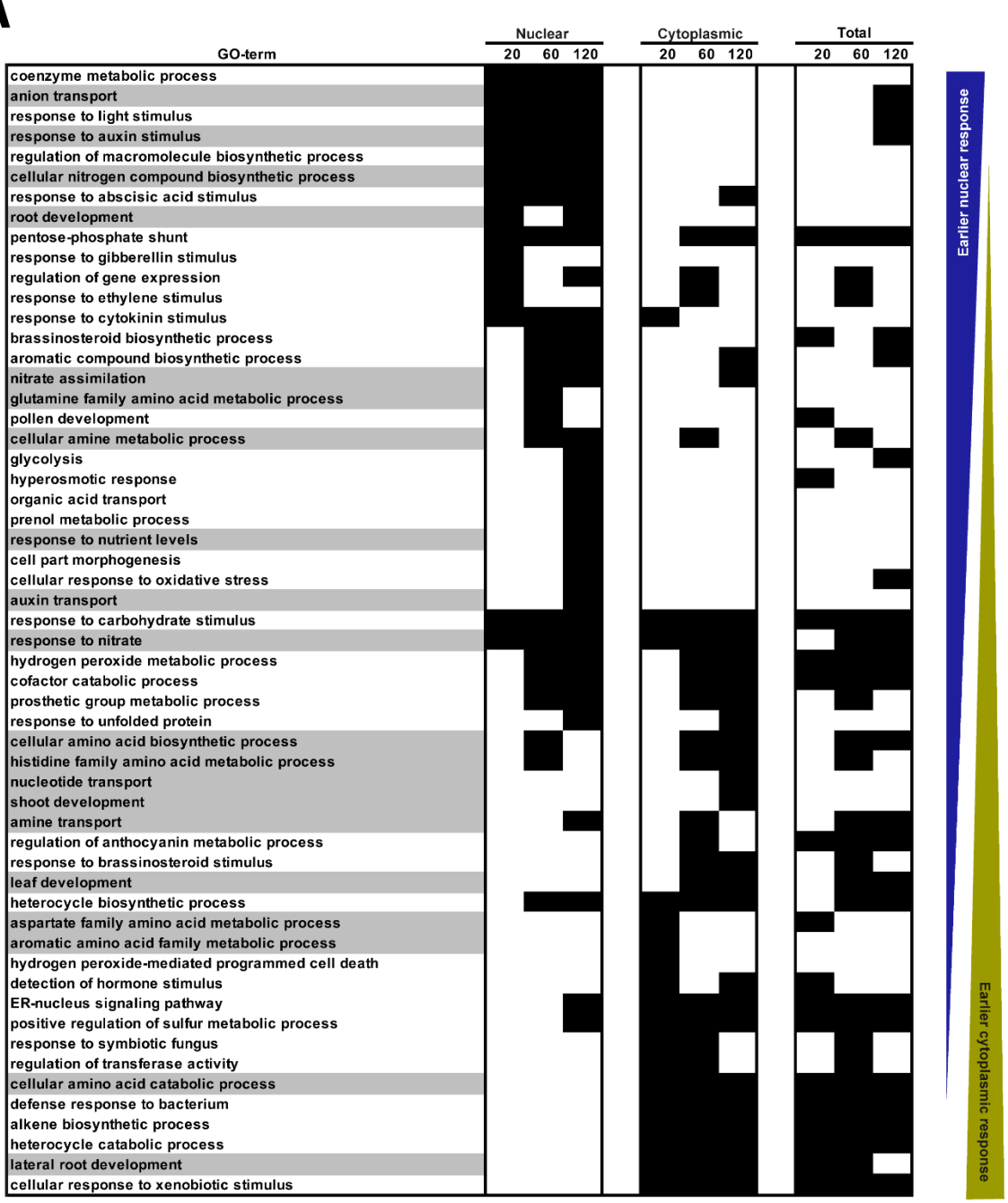
GO-term
Nuclear
Cytoplasmic
Total
20 60 120
20 60 120
20 60 120
coenzyme metabolic process
anion transport
response to light stimulus
response to auxin stimulus
regulation of macromolecule biosynthetic process
cellular nitrogen compound biosynthetic process
response to abscisic acid stimulus
root development
pentose-phosphate shunt
response to gibberellin stimulus
regulation of gene expression
response to ethylene stimulus
response to cytokinin stimulus
brassinosteroid biosynthetic process
aromatic compound biosynthetic process
nitrate assimilation
glutamine family amino acid metabolic process
pollen development
cellular amine metabolic process
glycolysis
hyperosmotic response
organic acid transport
prenol metabolic process
response to nutrient levels
cell part morphogenesis
cellular response to oxidative stress
auxin transport
response to carbohydrate stimulus
response to nitrate
hydrogen peroxide metabolic process
cofactor catabolic process
prosthetic group metabolic process
response to unfolded protein
cellular amino acid biosynthetic process
histidine family amino acid metabolic process
nucleotide transport
shoot development
amine transport
regulation of anthocyanin metabolic process
response to brassinosteroid stimulus
leaf development
heterocycle biosynthetic process
aspartate family amino acid metabolic process
aromatic amino acid family metabolic process
hydrogen peroxide-mediated programmed cell death
detection of hormone stimulus
ER-nucleus signaling pathway
positive regulation of sulfur metabolic process
response to symbiotic fungus
regulation of transferase activity
cellular amino acid catabolic process
defense response to bacterium
alkene biosynthetic process
heterocycle catabolic process
lateral root development
cellular response to xenobiotic stimulus
Earlier nuclear response
Earlier cytoplasmic response

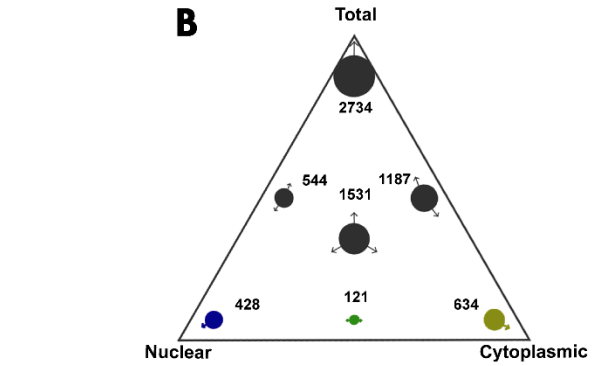
B
Total
2734
544
1187
1531
121
428
634
Nuclear
Cytoplasmic

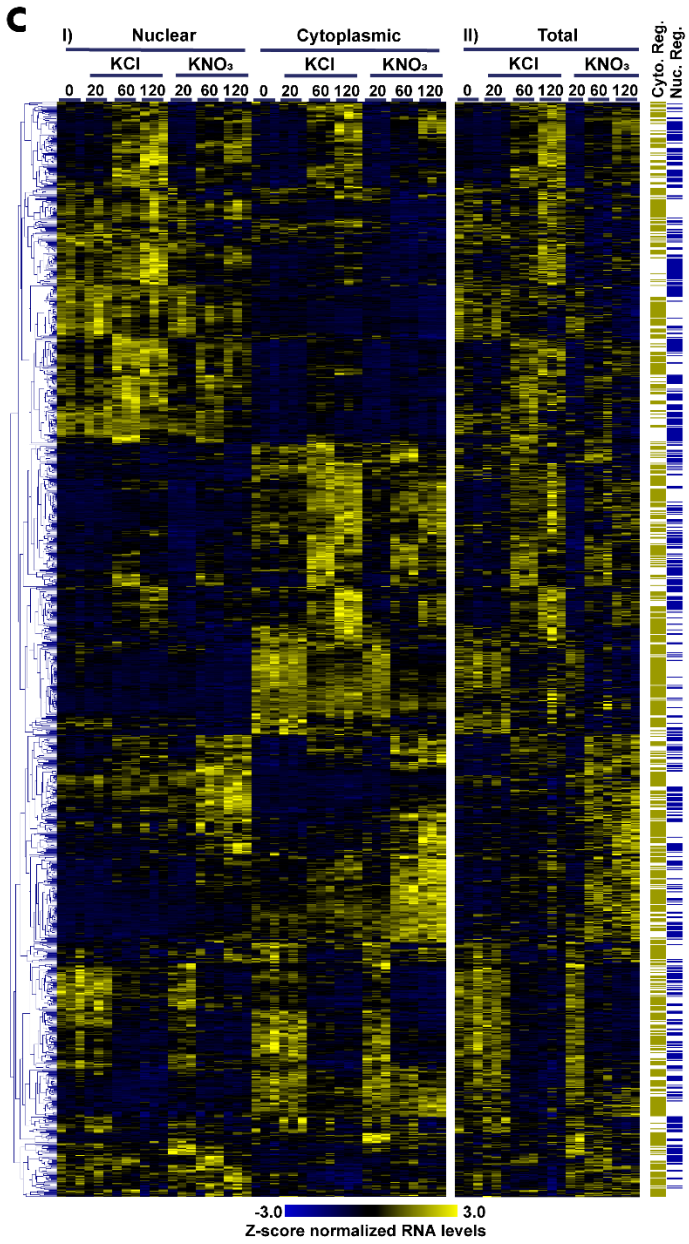
C
I)
Nuclear
Cytoplasmic
II)
Total
KCl
KNO3
0 20 60 120 20 60 120 0 20 60 120 20 60 120 0 20 60 120 20 60 120
Cyto. Reg.
Nuc. Reg.
-3.0
3.0
Z-score normalized RNA levels

Supplemental Figure 3. Differentially expressed genes in response to nitrate treatment in cellular fractions.

(A) Over-represented biological functions (level 5 GO-Terms) from differentially expressed genes in cellular fractions after 20, 60, and 120 min of nitrate treatment. Biological functions associated with nutrition, development, and nitrogen-containing metabolites are highlighted (shadow).

(B) Sungear representation for comparing the lists of differentially expressed genes in Total, nuclear, and cytoplasmic fractions (vertexes) in response to nitrate (KNO_3) compared with control (KCl) treatments. Circles indicate the number of genes shared among each list.

(C) Heatmap with mRNA levels in cellular fractions for differentially expressed genes in cellular fractions that are not identified in the total fraction. Genes were hierarchically clustered using the correlation of mRNA levels in the nuclear and cytoplasmic fractions (panel I). mRNA levels in the total fraction are shown in the panel II. Each column represents the mRNA levels for one replicate under each condition. Nuclear (Nuc) or Cytoplasmic (Cyt) regulation is indicated at the figure's right side. Three replicates from independent experiments are shown as separated columns for each condition.

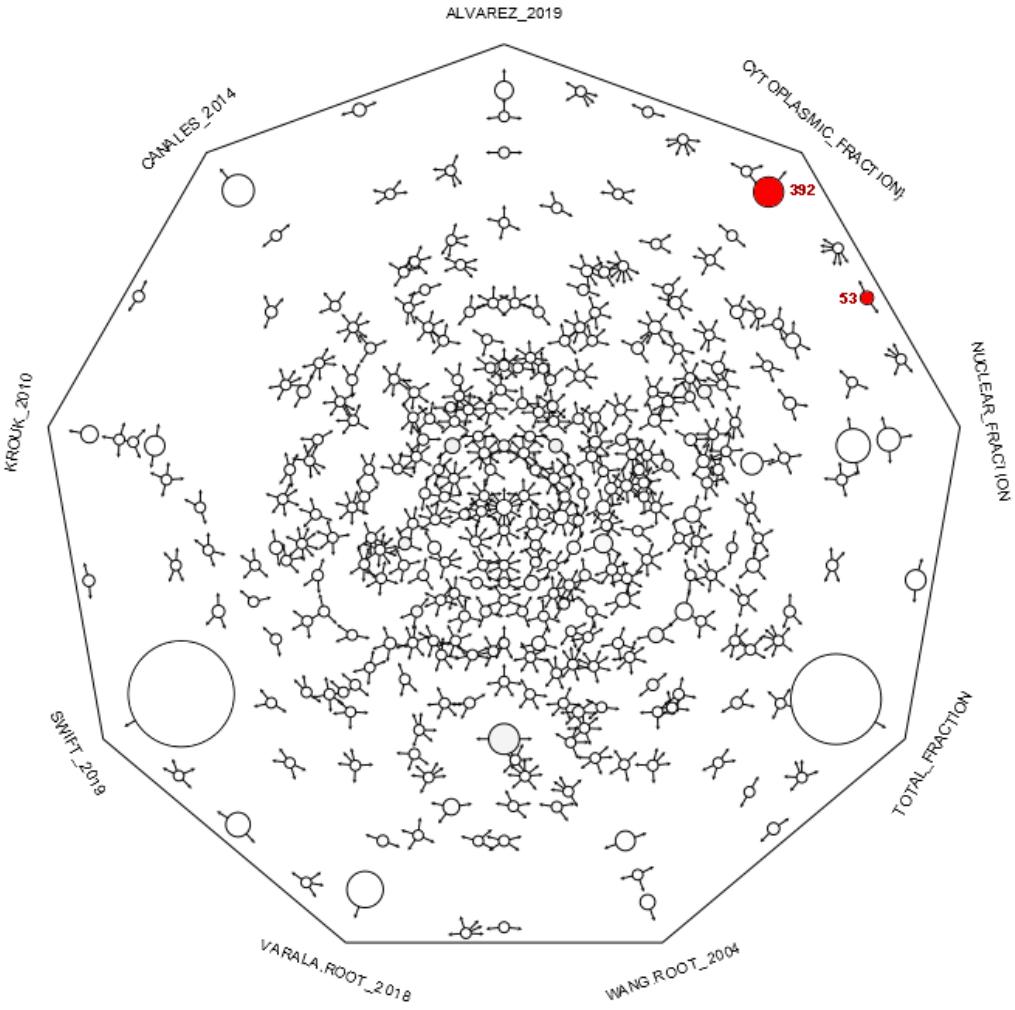

Supplemental Figure 4. Comparison of regulated genes in response to nitrate treatments from different transcriptomic studies

The lists of differentially expressed genes in response to nitrate in different transcriptomic studies are represented using the Sungear tool (Poultney et al., 2007). Vertexes of the polygon show different lists for ALVAREZ_2019 (Alvarez et al., 2019), CANALES_2014 (Canales et al., 2014), KROUK_2010 (Krouk et al., 2010), Swift_2019 (Swift et al., 2020), VARALA.ROOT_2018 (Results for root tissue in Varala et al., 2018), WANG.ROOT_2004 (Results for root tissue in Wang et a., 2004), TOTAL_FRACTION, NUCLEAR_FRACTION, and CYTOPLASMIC_FRACTION (results from this work). The circles inside the polygon represent the identified genes from each work, as indicated by the arrows around the circles. The size of each circle is proportional to the number of genes associated with that circle. Genes only identified in cellular fractions are colored in red, and the number of these genes in each list is indicated as text.

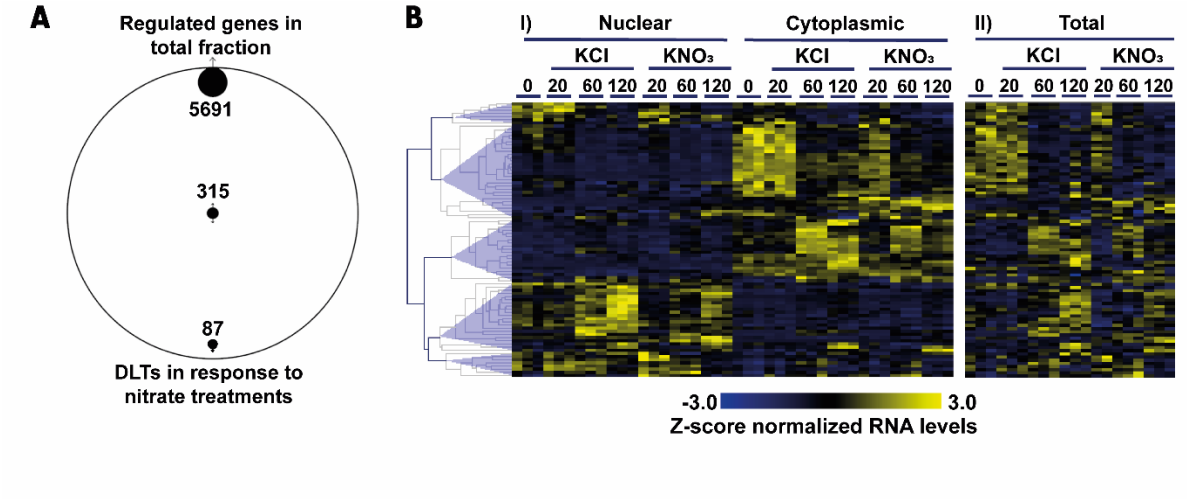

Supplemental Figure 5. DLTs in response to nitrate treatments that are not regulated in the total fraction.

(A) Sungear representation for comparing lists of total differentially regulated genes and DLTs in response to nitrate treatment.

(B) Heatmap with mRNA levels in cellular fractions for DLTs that are not identified in the total fraction. Genes were hierarchically clustered using the correlation of mRNA levels in the nuclear and cytoplasmic fractions (panel I). mRNA levels in the total fraction are shown in the panel II. Each column represents the mRNA levels for one replicate under each condition.

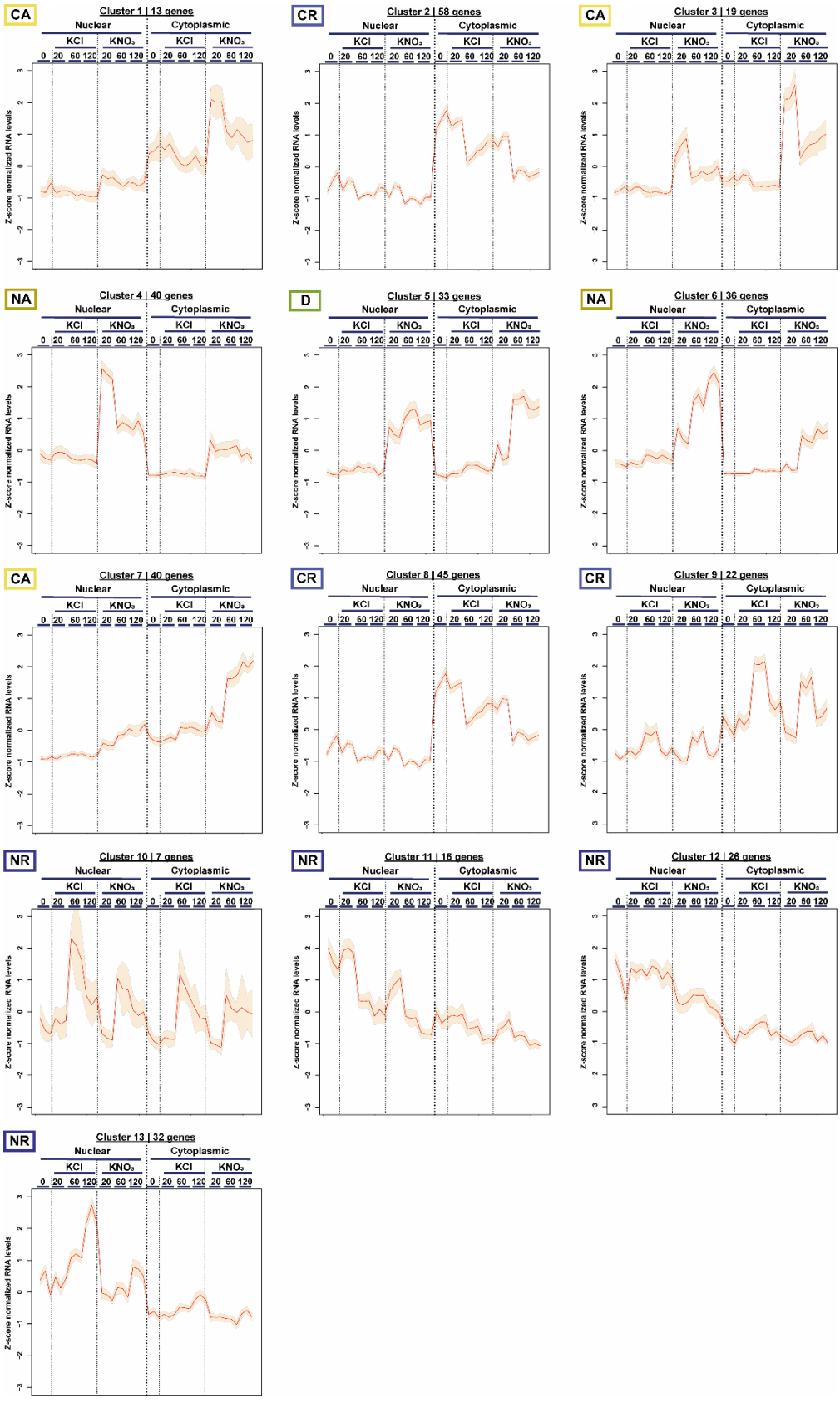
CA
Cluster 1 | 13 genes
CR
Cluster 2 | 58 genes
CA
Cluster 3 | 19 genes
NA
Cluster 4 | 40 genes
D
Cluster 5 | 33 genes
NA
Cluster 6 | 36 genes
CA
Cluster 7 | 40 genes
CR
Cluster 8 | 45 genes
CR
Cluster 9 | 22 genes
NR
Cluster 10 | 7 genes
NR
Cluster 11 | 16 genes
NR
Cluster 12 | 26 genes
NR
Cluster 13 | 32 genes
Nuclear
Cytoplasmic
KCl
KNO3
0 20 60 120 20 60 120 0 20 60 120 20 60 120
Z-score normalized RNA levels

Supplemental Figure 6. DLT expression clusters for the different localization patterns in response to nitrate treatments.

Thirteen expression clusters (from Figure 1) for DLTs in response to nitrate treatments are identified. The localization pattern (NR – Nuclear reduction, CR – Cytoplasmic reduction, NA – Nuclear accumulation, D – Delayed-cytoplasmic accumulation, and CA – Cytoplasmic accumulation) each cluster represent is indicated in the colored box. DLTs in response to nitrate treatments were separated by the cellular fraction where the main changes are observed (Nuclear or cytoplasmic), and if they show an accumulation or reduction of in the nitrate condition. Graphs show mean values of Z-scored normalized RNA levels (orange line) and 95% confidence interval for mean values for three biological replicates (shadow).

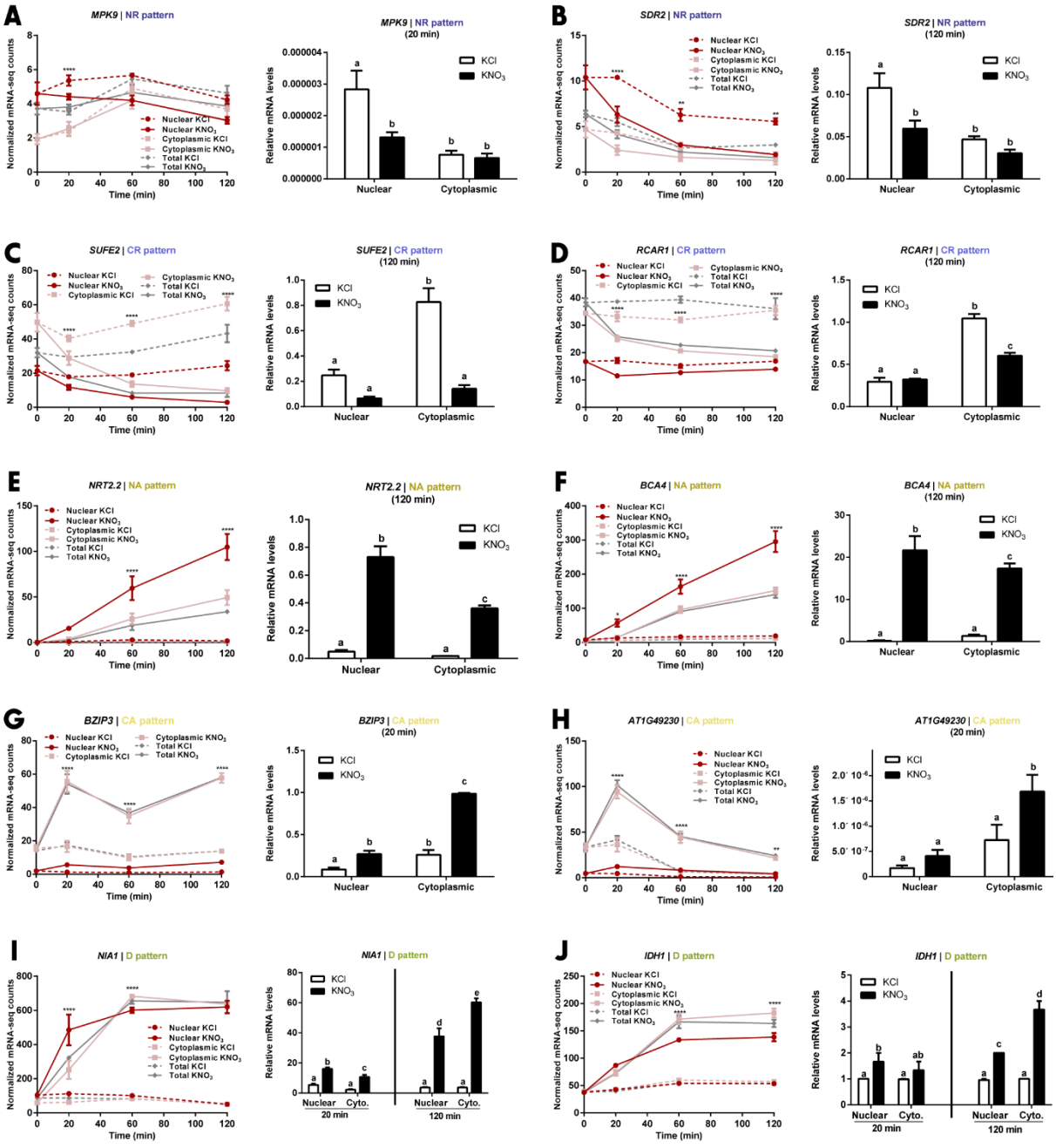
A
MPK9 | NR pattern
Normalized mRNA-seq counts
Time (min)
Nuclear KCl
Nuclear KNO3
Cytoplasmic KCl
Cytoplasmic KNO3
Total KCl
Total KNO3
MPK9 | NR pattern
(20 min)
Relative mRNA levels
KCl
KNO3
Nuclear
Cytoplasmic
B
SDR2 | NR pattern
SDR2 | NR pattern
(120 min)
C
SUFE2 | CR pattern
SUFE2 | CR pattern
(120 min)
D
RCAR1 | CR pattern
RCAR1 | CR pattern
(120 min)
E
NRT2.2 | NA pattern
NRT2.2 | NA pattern
(120 min)
F
BCA4 | NA pattern
BCA4 | NA pattern
(120 min)
G
BZIP3 | CA pattern
BZIP3 | CA pattern
(20 min)
H
AT1G49230 | CA pattern
AT1G49230 | CA pattern
(20 min)
I
NIA1 | D pattern
NIA1 | D pattern
Nuclear Cyto.
20 min
120 min
J
IDH1 | D pattern
IDH1 | D pattern

Supplemental Figure 7. qPCR validation for differential accumulation of representative DLTs.

mRNA levels for representative genes from DLT localization patterns in response to nitrate. The mRNA levels were analyzed in the time-point where the biggest differences between nuclear and cytoplasmic levels are observed in RNAseq data.The **left panels** show the mRNA levels in all time-course measured by RNA-seq. The asterisks indicate statistical differences between nuclear and cytoplasmic levels in a specific time-point (Two-way ANOVA, Tukey post-test. *; $p<0.05$; **: $p<0.01$, ***: $p<0.001$, ****: $p<0.0001$). The **right panels** show the mRNA levels measured by RT-qPCR. The different letters denote statistically significant differences (Two-way ANOVA, Tukey post-test, $p<0.05$).

(A) RNA levels for *MPK9* (nuclear reduction – NR - pattern). qPCR measurements were performed at 20 min of treatment.

(B) RNA levels for *SDR2* (nuclear reduction – NR - pattern). qPCR measurements were performed at 120 min of treatment.

(C) RNA levels for *SUFE2* (cytoplasmic reduction – CR - pattern). qPCR measurements were performed at 120 min of treatment.

(D) RNA levels for *RCAR1* (cytoplasmic reduction – CR - pattern). qPCR measurements were performed at 120 min of treatment.

(E) RNA levels for *NRT2.2* (nuclear accumulation – NA - pattern). qPCR measurements were performed at 120 min of treatment.

(F) RNA levels for *RCA4* (nuclear accumulation – NA - pattern). qPCR measurements were performed at 120 min of treatment.

(G) RNA levels for *BZIP3* (cytoplasmic accumulation – CA - pattern). qPCR measurements were performed at 20 min of treatment.

(H) RNA levels for *AT1G49230* (cytoplasmic accumulation – CA - pattern). qPCR measurements were performed at 20 min of treatment.

(I) RNA levels for *NIA1* (delayed cytoplasmic accumulation – D - pattern). qPCR measurements were performed at 20 and 120 min of treatment.

(J) RNA levels for *IDH1* (delayed cytoplasmic accumulation – D - pattern). qPCR measurements were performed at 20 and 120 min of treatment.

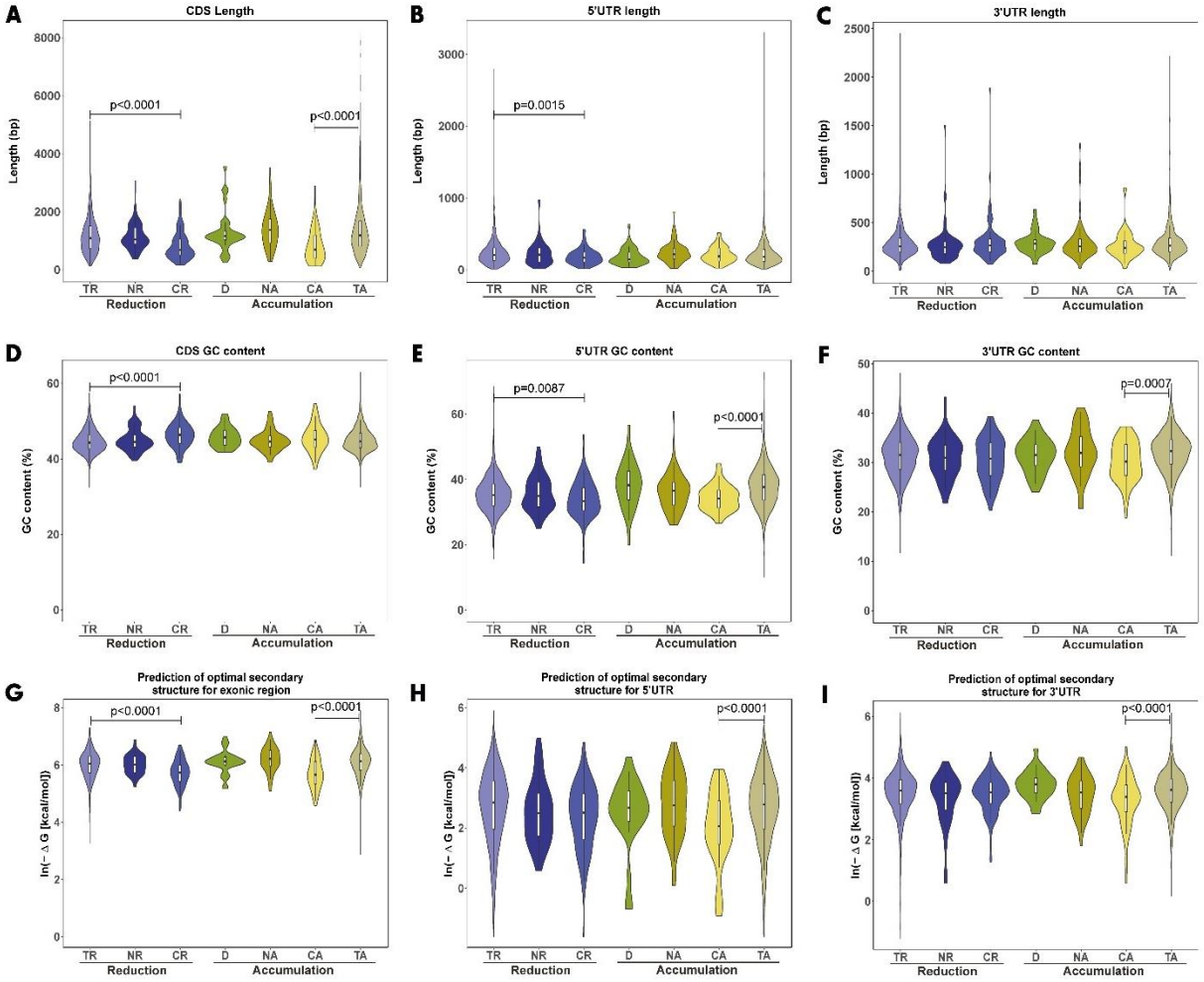

Supplemental Figure 8. Detailed sequence-related features for DLTs in response to nitrate treatments.

Sequence features of the most abundant isoform for nitrate-regulated genes, according to Araport11 annotation. Violin plots show the distribution of **(A-C)** length features, **(D-E)** GC content, and **(G-H)** free energy for optimal secondary structure prediction (RNAfold software) for DLTs localization patterns (NR – Nuclear reduction, CR – Cytoplasmic reduction, NA – Nuclear accumulation, D – Delayed-cytoplasmic accumulation, and CA – Cytoplasmic accumulation). We also include nitrate-regulated genes in the total fraction that are not differentially localized as a control (TA – Total accumulated, or TR – Total reduced). Boxes inside show the interquartile range (IQR – 25-75%), indicating the median value as a horizontal line. Whiskers show the ±1.58xIQR value. We compared the distributions using one-way ANOVA and Dunnett post-test. We include p-values and brackets to highlight relevant comparisons.

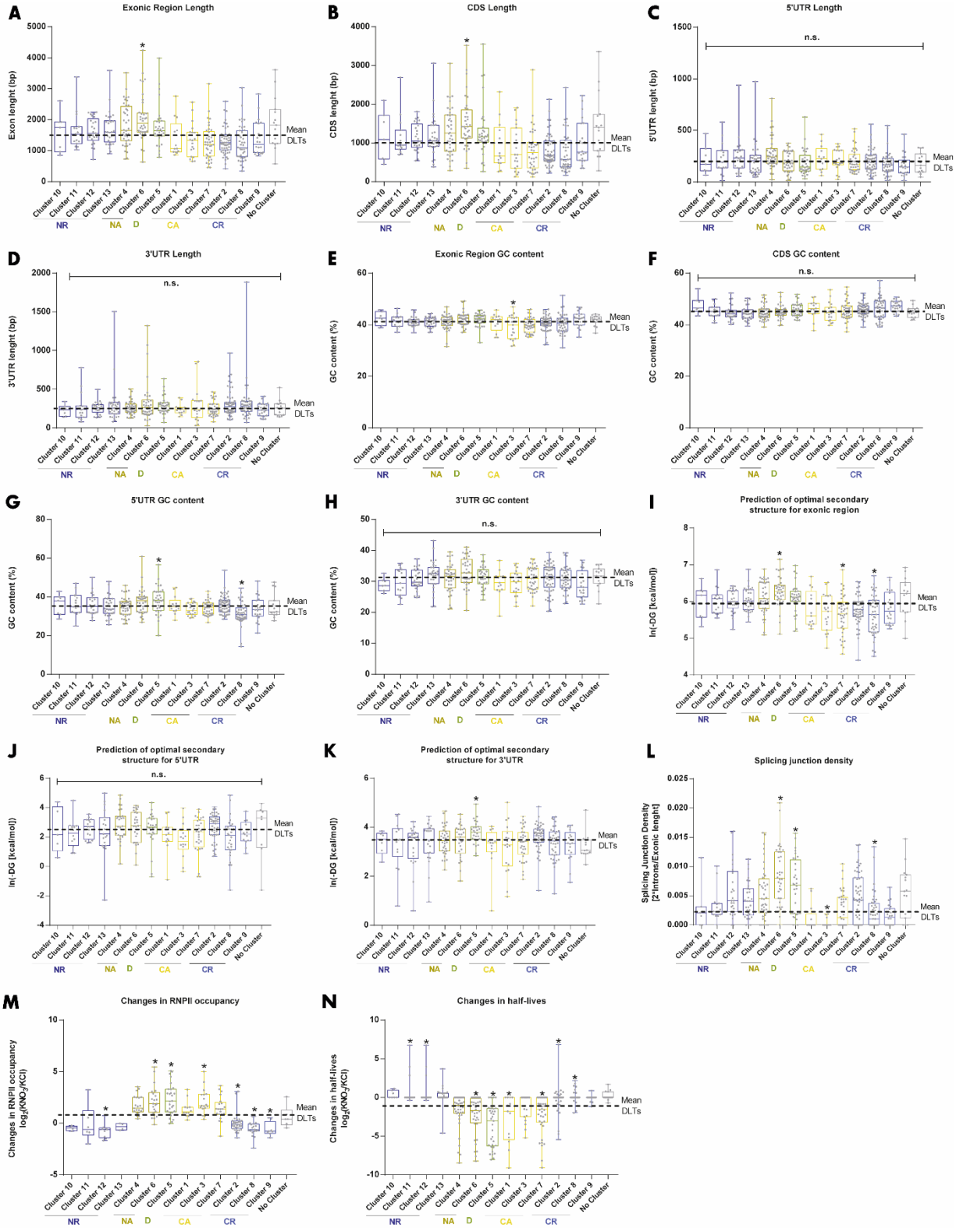
A
Exonic Region Length
Exon lenght (bp)
B
CDS Length
CDS lenght (bp)
C
5'UTR Length
5'UTR lenght (bp)
n.s.
D
3'UTR Length
3'UTR lenght (bp)
n.s.
E
Exonic Region GC content
GC content (%)
F
CDS GC content
GC content (%)
n.s.
G
5'UTR GC content
GC content (%)
H
3'UTR GC content
GC content (%)
n.s.
I
Prediction of optimal secondary structure for exonic region
ln(-DG [kcal/mol])
J
Prediction of optimal secondary structure for 5'UTR
ln(-DG [kcal/mol])
n.s.
K
Prediction of optimal secondary structure for 3'UTR
ln(-DG [kcal/mol])
L
Splicing junction density
Splicing Junction Density [2*Introns/Exonic lenght]
M
Changes in RNPII occupancy
Changes in RNPII occupancy log2(KNO3/KCl)
N
Changes in half-lives
Changes in half-lives log2(KNO3/KCl)
Mean DLTs
Cluster 10
Cluster 11
Cluster 12
Cluster 13
Cluster 4
Cluster 6
Cluster 5
Cluster 1
Cluster 3
Cluster 7
Cluster 2
Cluster 8
Cluster 9
No Cluster
NR
NA
D
CA
CR

Supplemental Figure 9. Sequence features for DLTs in response to nitrate treatments separated by expression cluster.

Sequence features of the most abundant isoform for DLTs, according to Araport11 annotation. Box plots show min to max (bars) and 5-95 percentile (boxes) distributions. Clusters were grouped based on their localization pattern patterns (NR – Nuclear reduction, CR – Cytoplasmic reduction, NA – Nuclear accumulation, D – Delayed-cytoplasmic accumulation, and CA – Cytoplasmic accumulation). The mean value from all DLTs is indicated in the dashed line. (*) show statistical differences ($p<0.05$) among clusters and DLTs distribution from One-way ANOVA, Tukey post-test analysis. **(A-D)** Length features **(E-H)** GC content features **(I-K)** Free energy for optimal secondary structure prediction (RNA fold software) **(L)** Splicing junction density (Calculated as two times the number of introns divided by exonic region length. **(M)** Changes in RNPII occupancy after 12 min. Values are graphed as the fold change (FC) of the KNO_3/KCl ratio in a logarithmic scale (log2). **(N)** Changes in half-life after 120 min of nitrate treatment. Values are graphed as the fold change (FC) of the KNO_3/KCl ratio in a logarithmic scale (log2).

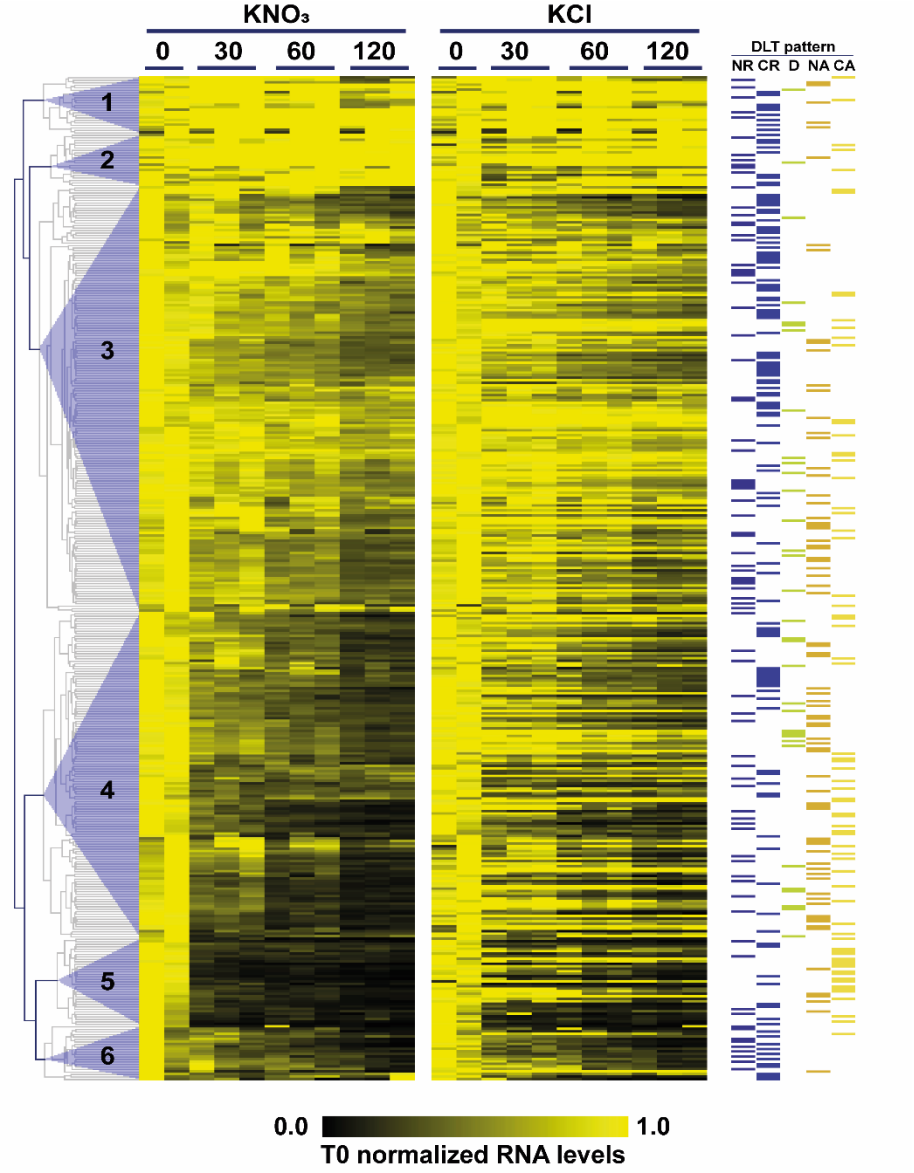

Supplemental Figure 10. Decay profiles and half-lives for DLTs in response to nitrate treatments.

Decay profiles for the 402 DLTs in response to nitrate treatments. RNA levels were measured by RNAseq from KNO_3 (Left panel), or KCl (Right panel) treated roots for 120 min and then treated with cordycepin for 0, 30, 60, or 120 min. The RNA levels were normalized using the mean value at 0 min (T0) of cordycepin treatment. Genes were hierarchically clustered in six groups according to their decay profiles in the KNO_3 condition (indicated in the left part of the figure). The localization patterns whose each DLT belongs is indicated in the right part of the figure. Replicates from independent experiments are shown as separate columns for each condition.

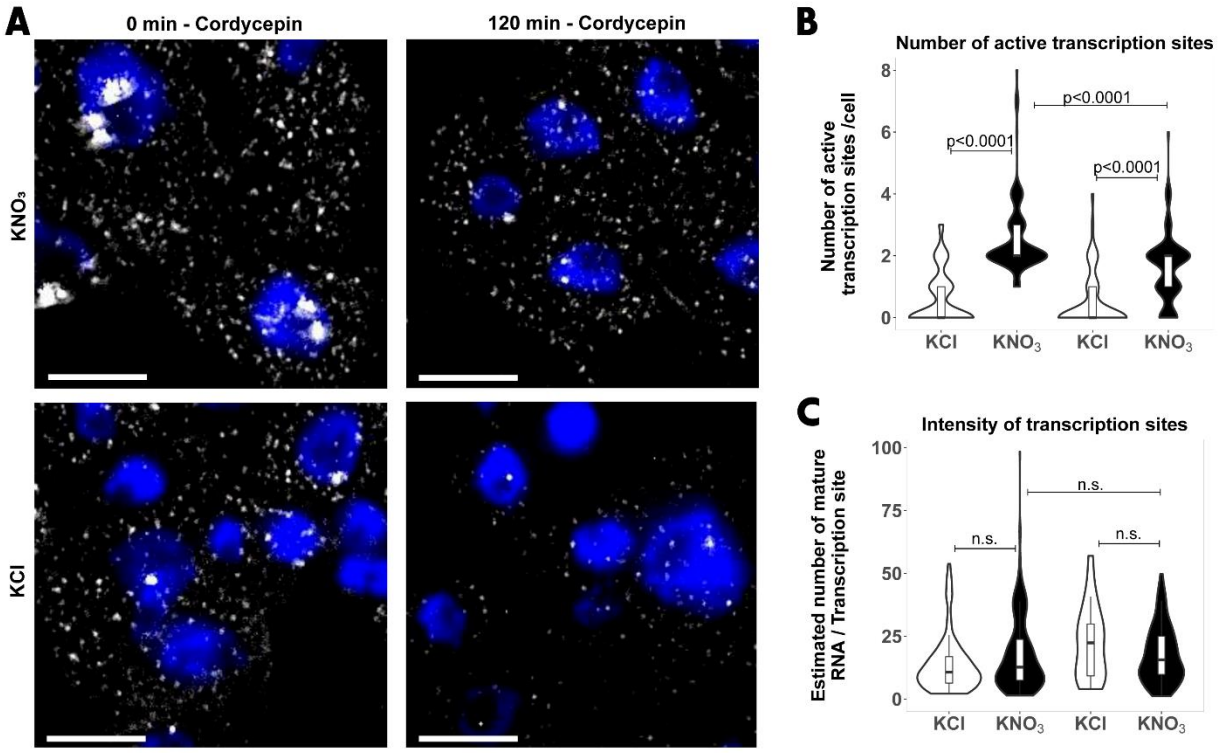

Supplemental Figure 11. Transcription sites analysis by RNA single-molecule FISH during nitrate treatment.

(A) Representative microscopy images from two independent experiments for *NIA1* detection in *Arabidopsis* root cells from nitrate (KNO_3, top) or control (KCl, bottom) for 20 min, and then treated with cordycepin 0.6 mM for 0 (left) or 120 (right) min. The white signal corresponds to specific probes for *NIA1* associated with Quasar670 fluorophore. The Blue signal corresponds to the DAPI stain. Scale bar = 10 µm.

(B-C) ranscription site analysis. Violin plots show the distribution for transcript quantification in the nitrate (KNO_3, black) or control (KCl, white) condition after 20 or 120 min of treatment (Figure 6E). Boxes inside show the interquartile range (IQR – 25-75%), indicating the median value as a horizontal line. Whiskers show the ±1.58xIQR value. One-way ANOVA Tukey post-test p-values for significant differences are indicated (n.s: non-significant, p-value>0.1). Four images from different roots from two independent experiments were quantified for each time/condition. **(B)** Number of identifiable active transcription sites per cell. **(C)** Estimated number of transcripts by each active transcription site.

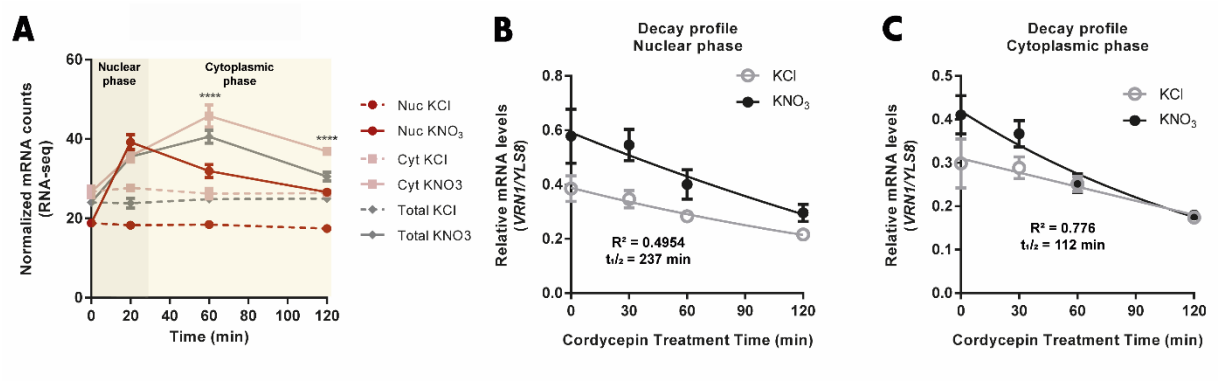

Supplemental Figure 12. Decay profiles for *VRN1* transcript in response to nitrate treatments

(A) mRNA levels in cellular fractions measured by RNA-seq for *VRN1*. Asterisks (****) indicate statistical differences between nuclear and cytoplasmic fractions, according to two-way ANOVA, Tukey post-test,. SEM from three independent experiments is shown as error bars.

(B-C) Comparison of half-lives ($t_{1/2}$) for *VRN1* between nuclear **(B)** and cytoplasmic **(C)** phases. RNA levels were determined by RT-qPCR. Measured half-lives and the determination coefficient for linear regression are indicated for each graph. SEM from three independent experiments is shown as error bars.

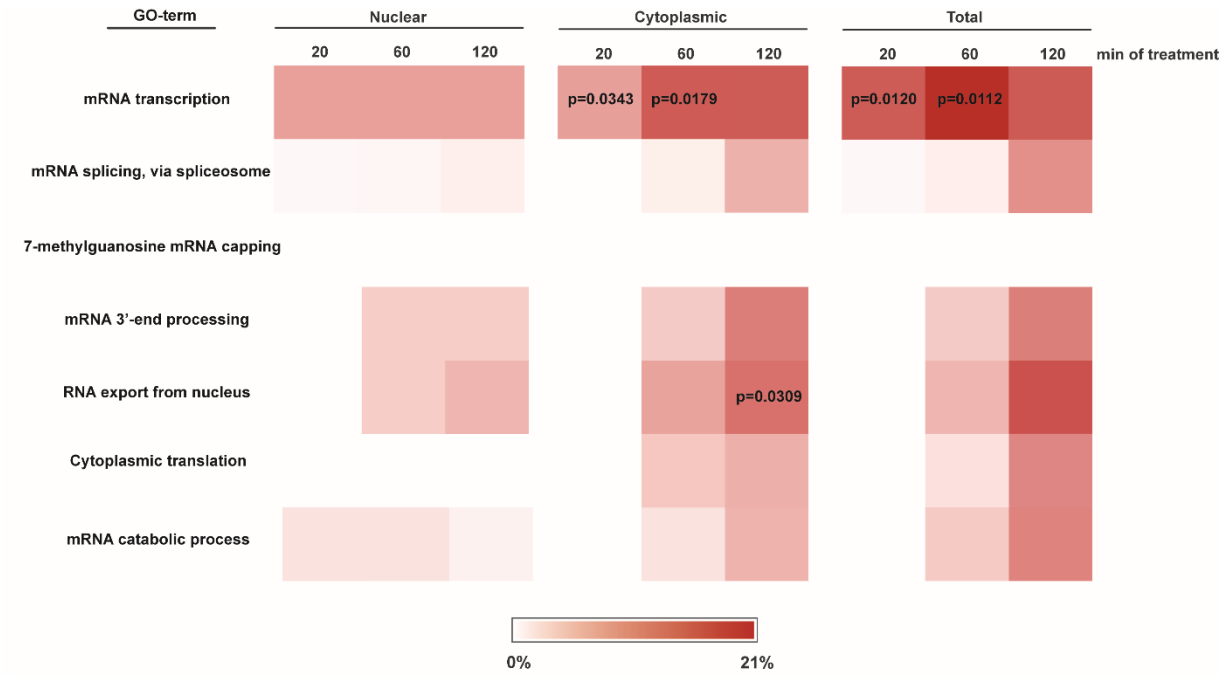

Supplemental Figure 13. Percentage of annotated genes regulated by nitrate for different mRNA processes in cellular fractions.

Heatmap showing the percentage of annotated genes in GO-terms associated with RNA processes. The percentage is based on the number of genes with differential expression between KNO_3 and KCl condition during the treatment in nuclear, cytoplasmic, and total fractions from RNA-seq data. The p-values for hypergeometric tests are indicated when $p<0.05$, considering the total number of genes regulated in each point.

SUPPLEMENTAL TABLES

Supplemental Table 1. RNA-seq libraries parameters from total and cellular fractions.

Parameter	Total	Nuclear	Cytoplasmic
Library concentration range (nM)	22.49 - 356.94	72.53 - 136.50	50.03 - 119.51
Library size range (bp)	316 - 353	274 - 300	270 - 292
Number of reads (in millions) [Mean ± SD]	68.92 ± 9.26	70.57 ± 7.33	70.75 ± 5.37
Q_{30} (%) [Mean ± SD]	94.72 ± 0.31	93.98 ± 0.19	93.69 ± 0.32
Reads after quality filters (%) [Mean ± SD]	93.31 ± 0.54	89.56 ± 0.44	88.92 ± 0.60
Mapped reads to genome (%) [Mean ± SD]	92.01% ± 1.44%	86.05% ± 3.80%	84.12% ± 6.91%
Correlation between replicates [Mean ± SD]	0.988 ± 0.002	0.984 ± 0.003	0.984 ± 0.003

Supplemental Table 2. 5% Top ranking for RNA polymerase II occupancy and half-life changes for DLTs

AGI	log2(Fold change for RNPII occupancy)	log2(Fold change for Half-life)	Pattern	Rank RNPII	Rank HL	Mean rank*
AT1G77760	4.501620483	-8.03387428	D	7	6	6.5
AT3G63110	3.642572016	-8.17646288	CA	12	5	8.5
AT3G60750	5.449888133	-6.99098716	NA	1	16	8.5
AT1G63940	5.003402905	-7.02239935	NA	4	14	9
AT2G27510	3.898664347	-7.36525023	D	10	10	10
AT5G13420	5.077476651	-6.2313914	D	2	21	11.5
AT5G04250	3.342976238	-7.36993171	NA	15	9	12
AT1G73920	3.535756169	-7.14477493	NA	13	13	13
AT3G47520	2.83039771	-7.34495462	D	38	11	24.5
AT2G36580	4.788445348	-4.26437858	D	6	44	25
AT1G70410	2.641988051	-7.61204945	NA	46	8	27
AT5G48970	2.930203694	-5.67513393	D	32	30	31
AT3G52930	2.676877939	-6.13066842	D	44	24	34
AT1G79550	2.889127666	-5.38119271	D	34	35	34.5
AT4G24670	3.298600937	-3.07721565	CA	17	55	36
AT5G15070	3.404484005	-2.76387192	D	14	62	38
AT5G35630	3.065846801	-3.37910574	NA	28	51	39.5
AT5G39590	2.122968421	-6.44981091	D	63	18	40.5
AT3G48185	2.678889525	-5.17642543	CA	43	38	40.5

(*) Mean rank: mean value between Rank RNPII (RNA polymerase II occupancy) and Rank HL (Half-life change)

Supplemental Table 3. List of primers

Primer sequence (5'->3')	Gene	Sense	Use	Experiment
CAACACGCTTCCTTGCCTAGAG	*MPK9*	Forward	qPCR	DLT confirmation (NR pattern)
GGGTCGTGACTAAAGACGCTATGG	*MPK9*	Reverse	qPCR	DLT confirmation (NR pattern)
TGGAATGGGACCACACGCTTAC	*SDR2*	Forward	qPCR	DLT confirmation (NR pattern)
TAGCTCACACGCTGCGTTCTTG	*SDR2*	Reverse	qPCR	DLT confirmation (NR pattern)
CGTGGCACAACGTGTTGATGAG	*SUFE2*	Forward	qPCR	DLT confirmation (CR pattern)
TTTGATGCGCCACGTCAGTAGC	*SUFE2*	Reverse	qPCR	DLT confirmation (CR pattern)
ACCAGTGTACCTCTGCTCTTGTC	*RCAR1*	Forward	qPCR	DLT confirmation (CR pattern)
TCATGGGAATCTTGGTGCTCACG	*NRT2.2*	Forward	qPCR	DLT confirmation (CR pattern)
ACGGCGTACCATAGAATCTTTCCG	*NRT2.2*	Reverse	qPCR	DLT confirmation (NA pattern)
GCATCAGCGAGGAACAAGATCAAG	*BCA4*	Forward	qPCR	DLT confirmation (NA pattern)
AGCGATACGTTCACAGCTTCCTTC	*BCA4*	Reverse	qPCR	DLT confirmation (NA pattern)
TCTCCGTACAAGTGACCAAACGAG	*RCAR1*	Reverse	qPCR	DLT confirmation (NA pattern)
TCTCACAGGTTGCTTGGCT	*BZIP3*	Forward	qPCR	DLT confirmation (CA pattern)
GATGTGATAACCTGACGAAGCTCC	*BZIP3*	Reverse	qPCR	DLT confirmation (CA pattern)
ATGCGAGAAGATTGCCGACTGC	*AT1G49230*	Forward	qPCR	DLT confirmation (CA pattern)
TGATGCTGTCTTGTGGTGGTTGAG	*AT1G49230*	Reverse	qPCR	DLT confirmation (CA pattern)
AAGGCAAAGGCAACTTCCTGGT	*NIA1*	Forward	qPCR	DLT confirmation (D pattern) | Decay
TCATCCTCGGTTCTGTTTGCGT	*NIA1*	Reverse	qPCR	DLT confirmation (D pattern) | Decay
GTCATGCCTGGAGGAAATGTTGGG	*IDH1*	Forward	qPCR	DLT confirmation (D pattern)
TGCTGATGCACCTTGCTCGAATAC	*IDH1*	Reverse	qPCR	DLT confirmation (D pattern)
TTACTGTTTCGGTTGTTCTCCATTT	*YLS8*	Forward	qPCR	Normalizer
CACTGAATCATGTTCGAAGCAAGT	*YLS8*	Reverse	qPCR	Normalizer
AGGCACATCAGTATCAACTGGGG	*CLATHRIN COAT ASSEMBLY PROTEIN*	Forward	qPCR	Normalizer | Processed RNA (fraction control)
ACCCCTGAACCTGAAGAACTCCT	*CLATHRIN COAT ASSEMBLY PROTEIN*	Reverse	qPCR	Normalizer | Processed RNA (fraction control)
AATACGCGCTGAGTTCCCTT	*CLATHRIN COAT ASSEMBLY PROTEIN*	Forward	qPCR	Unprocessed RNA (fraction control)
AGCACCGGGTTCTAACTC	*CLATHRIN COAT ASSEMBLY PROTEIN*	Reverse	qPCR	Unprocessed RNA (fraction control)
ATCTGCGTCATTCCTAAGCTCAC	*RAN3*	Forward	qPCR	Normalizer | Processed RNA (fraction control)
GTTTGCTGGTTAGGTAGAGCCATC	*RAN3*	Reverse	qPCR	Normalizer || Processed RNA (fraction control)
TGCTGCTTTGACTTAGTTTGTCTG	*RAN3*	Forward	qPCR	Unprocessed RNA (fraction control)
GCCAAATGCATCCAACTACTGA	*RAN3*	Reverse	qPCR	Unprocessed RNA (fraction control)
ATGCTCACTCTCGCTCTCAAGGAG	*EIF4G*	Forward	qPCR	Processed RNA (fraction control)
AGGTCCGGTGTTTCTGTTGAACG	*EIF4G*	Reverse	qPCR	Processed RNA (fraction control)

TGTGTCTCGAACTTTGCTTCTG	*EIF4G*	Forward	qPCR	Unprocessed RNA (fraction control)
CAGGCCAGCAAATCGCAATA	*EIF4G*	Reverse	qPCR	Unprocessed RNA (fraction control)
GTACCAGCCAACAAAGGGTATGC	*VRN1*	Forward	qPCR	Decay
GGCGTTGGCTCTTCAGCTTTAAC	*VRN1*	Reverse	qPCR	Decay

Supplemental Table 4. List of probes for *NIA1* smFISH

Target	Probe name	Sequence (5'->3')	Probe position	GC Percentage
NIA1	NIA1_1	tggttttggtttggtttgtg	52	40.00%
NIA1	NIA1_2	ataatggcggttatcgacgg	128	50.00%
NIA1	NIA1_3	ggtcgaatgagcgaggagaa	195	55.00%
NIA1	NIA1_4	atgacgtcgagagtttggtt	229	45.00%
NIA1	NIA1_5	gtgatgacttcggtttcttt	271	40.00%
NIA1	NIA1_6	gagtcgtcgtaactgtctac	298	50.00%
NIA1	NIA1_7	cagctctttgtagtaaggga	356	45.00%
NIA1	NIA1_8	gacggttctaaatcgctgtt	388	45.00%
NIA1	NIA1_9	ttgaatccaactatcagccg	434	45.00%
NIA1	NIA1_10	cggcgttgaatggatgtttt	483	45.00%
NIA1	NIA1_11	ggagtgatgaatccatggtg	526	50.00%
NIA1	NIA1_12	attgaccagtctgaccaatt	592	40.00%
NIA1	NIA1_13	ctggggaactcggagattag	661	55.00%
NIA1	NIA1_14	agagaagtagatactccggc	772	50.00%
NIA1	NIA1_15	ctccttcgaagcaaacgttt	861	45.00%
NIA1	NIA1_16	ccttcttaatacttgttccg	915	40.00%
NIA1	NIA1_17	catgatccggcgttaaaagc	990	50.00%
NIA1	NIA1_18	acaatgacccgaaccggaaa	1012	50.00%
NIA1	NIA1_19	ttgaggcgtgacgatgattc	1073	50.00%
NIA1	NIA1_20	aaaatctctgcgtgaccagg	1234	50.00%
NIA1	NIA1_21	acggcttctgagtagtgaat	1266	45.00%
NIA1	NIA1_22	cagaaacaccagcaccagaa	1417	50.00%
NIA1	NIA1_23	tctttagcactgagcagatc	1459	45.00%
NIA1	NIA1_24	ggttccagatgagtttatca	1521	40.00%
NIA1	NIA1_25	ggtcgggtgttcgaaaacta	1616	50.00%
NIA1	NIA1_26	ggaaatctcaagctgacgct	1673	50.00%
NIA1	NIA1_27	ttcgaggcagtgttcatgaa	1735	45.00%
NIA1	NIA1_28	caatctgtacctgcgtttat	1882	40.00%
NIA1	NIA1_29	ccaaaagcttcttggctttg	1932	45.00%
NIA1	NIA1_30	gtgatgagttcaccgatacg	1960	50.00%
NIA1	NIA1_31	cgttaggggaagagtcgtag	1986	55.00%
NIA1	NIA1_32	tttgaggcaccatgaactga	2008	45.00%
NIA1	NIA1_33	ggagttagctctttgattgg	2047	45.00%
NIA1	NIA1_34	gggttgaccaaagcaatgtt	2074	45.00%
NIA1	NIA1_35	ttacgaacgtcgtgcgagat	2134	50.00%
NIA1	NIA1_36	acgggtaaaccaagctgttg	2182	50.00%
NIA1	NIA1_37	tctgagacagagtttgtcgt	2234	45.00%
NIA1	NIA1_38	ccttggatgaacgtctttga	2318	45.00%
NIA1	NIA1_39	tcattgacccgattggtaac	2376	45.00%
NIA1	NIA1_40	cattgctagtttcttggcaa	2471	40.00%
NIA1	NIA1_41	aagaatgtcatcctcggttc	2591	45.00%

NIA1	NIA1_42	aaatctttagcctctcctta	2646	35.00%
NIA1	NIA1_43	ttcctttgcgatttcaacga	2672	40.00%
NIA1	NIA1_44	cagcttcagttataaacccg	2709	45.00%
NIA1	NIA1_45	tagatttggctgcaacgcaa	2807	45.00%
NIA1	NIA1_46	ttaagagatcctccttcacg	2844	45.00%
NIA1	NIA1_47	gtgcccaaataaccatgtat	2937	40.00%
NIA1	NIA1_48	catgagtcctgacatgcaat	3112	45.00%

CHAPTER 2: Functional characterization of transcription factors with a differential mRNA localization in response to nitrate treatments.

Functional characterization of transcription factors with a differential mRNA localization in response to nitrate treatments.

Alejandro Fonseca and Rodrigo A. Gutiérrez

Affiliations

ANID–Millennium Science Initiative Program-Millennium Institute for Integrative Biology (iBio), Santiago, Chile

Departamento de Genética Molecular y Microbiología, Facultad de Ciencias Biológicas, Pontificia Universidad Católica de Chile, Santiago, Chile

FONDAP Center for Genome Regulation, Santiago, Chile

*Corresponding author: Email: rgutierrez@bio.puc.cl, Rodrigo A. Gutiérrez

ABSTRACT

Plant development is strongly regulated by nutrient availability. Nitrate is a potent controller of gene expression to modulate the root system architecture (RSA). Different strategies have allowed identifying many transcription factors (TFs) that orchestrate plants' genetic response to nitrate. Previous results (Chapter 1) described a group of differentially localized transcripts (DLTs) in response to nitrate treatments in *Arabidopsis thaliana* roots. In this chapter, we analyzed the influence of transcription factors with differential changes in their cytoplasmic mRNA levels in response to nitrate treatments using gene network and reverse genetics strategies. We identified BZIP3, VRN1, WRKY24, ERF105, VIP1, and COG1 as the main hubs among TFs with DLTs for the regulation of nitrate-responsive genes. BZIP3 and VRN1 stood out for being TFs with mRNA cytoplasmic accumulation in response to nitrate. They regulate gene-targets involved in nitrate transport, nitrate assimilation, and developmental processes. Preliminary analyses for nitrate RSA elicited changes in insertional mutants of *BZIP3* and *VRN1* genes showed differences in the primary root length and lateral root emergence. Besides, we observed slight differences in the induction of mRNA levels for genes that encode nitrate reductases and transporters. These results describe uncharacterized regulators of the nitrate response and give insights into how cytoplasmic mRNAs levels control critical elements for plant nutritional adaptation.

INTRODUCTION

Plant development and growth depend on the nutritional state, where nitrogen is considered an indispensable element (Andrews et al., 2013; Gutiérrez, 2013; Fredes et al., 2019; Vidal et al., 2020). Most plants uptake the inorganic nitrogen as nitrate (NO_3^-) or ammonium (NH_4^+) (Masclaux-Daubresse et al., 2010; Andrews et al., 2013). Nevertheless, the low concentration of nitrogen sources in soil and the environmental issues associated with fertilizer use generate increasing interest in improving nitrogen use efficiency in commercial crops (Hirel et al., 2011). Understanding the molecular mechanisms related to plants' nitrogen processes is necessary to achieve this goal (Gutiérrez, 2013; O'Brien et al., 2016; Vidal et al., 2020).

Among the nitrogen sources, nitrate stands out as the most abundant in agricultural soils (Owen and Jones, 2001) and can activate a signaling cascade inside the cell (Scheible et al., 1997). NPF6.3/NRT1.1 acts as a dual-affinity transceptor (Ho et al., 2009) whose affinity changes by post-translational modifications. For instance, under low nitrate conditions, the CBL-INTERACTING PROTEIN KINASE 23 (CIPK23) phosphorylates the transporter, increasing its affinity (Liu and Tsay, 2003). The increase of cellular nitrate levels activates calcium influx through phospholipase C (PLC) activity (Riveras et al., 2015), which acts as a second messenger triggering the activation of transcription factors, such as NIN-LIKE PROTEIN 7 (NLP7), regulating the gene expression for plant physiological adaptation to the nutritional condition (Marchive et al., 2013; Undurraga et al., 2017; Vidal et al., 2020). The modulation of different regulators at the local and systemic level orchestrate downstream responses affecting nutrient metabolism and a series of developmental processes associated with

growth, root development, leaf development, seed dormancy, and flowering time (Fredes et al., 2019; Vidal et al., 2020).

In addition to NLP7, more than forty TFs regulate plant physiology, growth, and development in response to nitrate (Vidal et al., 2020). Gene regulatory networks (GNR) have worked as an efficient systems-biology strategy for understanding temporal and dynamic layers of transcriptional regulation (Gaudinier et al., 2018; Varala et al., 2018; Brooks et al., 2019), and also have allowed integrating transcriptomic data for the understanding of regulatory mechanisms for root and shoot architecture system modifications (Canales et al., 2014; Vidal et al., 2015).

As we described in the previous chapter, different regulated genes were identified when nuclear and cytoplasmic transcriptomes are analyzed separately (Chapter 1). Accordingly, 402 transcripts were described as differentially localized in the nucleus or cytoplasm in response to nitrate treatments, where we identified mRNAs that codify for many regulatory proteins. The changes in the subcellular distribution of mRNAs that codify for transcription factors could alter the plant's physiological response (Lee and Bailey-Serres, 2019). For instance, some TFs with cytoplasmic mRNA accumulation are the BASIC LEUCINE-ZIPPER 3 (BZIP3) and REDUCED VERNALIZATION RESPONSE 1 (VRN1) proteins. BZIP3 is a basic leucine zipper domain-containing transcription factor responsible for the leaf development control in response to sugars (Matiolli et al., 2011; Sanagi et al., 2018). VRN1 (also called REPRODUCTIVE MERISTEM 39, REM39) is an AP2/B3-like transcriptional factor family protein, mainly described in the developmental control of reproductive tissue (Chandlrer et al., 1996; Levy et al., 2002; Zhou et al., 2019). High throughput experiments have shown that BZIP3

and VRN1 significantly impact the roots' nitrogen-regulated gene expression (Brooks et al., 2019). Nevertheless, no direct effects on root phenotype in response to nitrate have been reported.

We performed a gene network coupled with reverse genetic analyses to elucidate physiological effects that could generate the differential localization of transcripts in response to nitrate treatments. BZIP3 and VRN1 (two transcription factors with cytoplasmic accumulation) were identified as central regulators of nitrate-responsive targets. Preliminary experiments with mutant plants for *BZIP3* and *VRN1* genes showed differences in the nitrate-elicited changes for root architecture system and gene expression. Further characterization of these transcription factors could give new insights into the sophisticated nitrate gene regulation and stand out the role of differential mRNA localization in response to nitrate treatments.

RESULTS

Identification of transcription factors with a differential mRNA localization in response to nitrate treatments

We performed a gene network analysis to identify important regulatory elements with differentially localized mRNAs in response to nitrate treatments. We analyzed RNA-seq data obtained from cytoplasmic and total fractions in KNO_3 and KCl treatments (Chapter 1). We calculated the correlations for predicted TF-target interactions among TFs with differentially localized transcripts (DLTs, Chapter 1) and targets that respond to the treatment. Five thousand nine hundred forty-nine significant correlations ($p \leq 0.01$) were found for 3,899 targets. These correlations involve 14 TFs with differential mRNA localization. Interestingly 1,142 TF-target interactions (19.2%) showed a significant correlation only in the cytoplasmic data (and not in the total). This result indicates the difference between cytoplasmic and total mRNA levels allow identifying new gene connections.

For network visualization, we filtered by TF-target interactions with experimental evidence (DAP-seq data) (O'Malley et al., 2016). One thousand three hundred ninety-nine significant correlations were kept after applying this filter, involving 1,279 genes. Community clustering (GLay) allowed identifying 6 TF hubs, all of them with greater mRNA levels in the cytoplasm than in the nucleus. BZIP3, a TF whose transcript accumulate in the cytoplasm, was the main hub with 465 connections. VRN1, a TF with delayed-cytoplasmic mRNA accumulation, showed interactions with 263 targets. We identified four other hubs: *WRKY24* (AT5G41570), *ERF105* (AT5G51190), *VIP1* (AT1G43700), and *COG1* (AT1G29160) with

324, 147, 113, and 87 connections, respectively. All these four TFs reduce their mRNA levels in response to nitrate treatments.

Enriched gene ontology (GO) term analysis from these clusters showed that BZIP3 target genes are associated with response to stimulus and nitrate transport (*NRT2.1*, *NRT2.2,* and *CLCA*). We also observed essential genes in the nitrate assimilation (e.g., *NITRATE REDUCTASE 1*, *NIA1*). When VRN1 targets were analyzed, we identified genes that encode for the nitrate transceptor NRT1.1 and the NITRATE REDUCTASE 2 (NIA2), as well as genes with functions of development and nitrogen metabolism. For the other identified hubs, we observed genes associated with cell growth, amino acid metabolism, response to stimulus, and signaling (Table 1). This network analysis suggests that the cytoplasmic mRNA levels of some regulatory elements during the nitrate response are related to important genes' expression for the nutritional response.

Root system architecture analysis for *BZIP3* and *VRN1* mutant plants

For functional analysis we worked with insertional mutant plants in the genes that encode BZIP3 and VRN1 (*bzip3-1* and *vrn1-6*, respectively). We selected homozygous lines by PCR genotyping (Supplemental Figure 1). RSA was analyzed in 15-day-old seedlings grown in hydroponic media (T0) and after three days of 5 mM KNO_3 treatment (or 5mM KCl as control). We measured the primary root length (Figure 2A) and lateral root density for two independent experiments (Figure 2B). The number of initiating, emerging, and emerged lateral roots were quantified (Supplemental Figure 2). We observed a primary root inhibition elongation in response to nitrate for all genotypes. Nevertheless, this effect seems to be less for the *bzip3-1* line, having longer roots than WT plants in the nitrate condition (Figure 2A). Furthermore,

mutant plants showed differences for lateral root density, observing an increase between nitrate and control conditions for both mutant genotypes (Figure 2B). This difference is due to the increase in emerging root density (Supplemental Figure 2). We observed basal differences for the *vrn1-6* line, having a lower lateral root density before the treatments (T0) (Figure 2B). These plants showed a higher initiating root density and a lower density for emerged lateral roots before the treatments, suggesting their lateral root formation is delayed (Supplemental Figure 1). These results propose a role BZIP3 and VRN1 transcription factors in mediating RSA changes in response to nitrate treatments.

Nitrate genetic response analysis for *BZIP3* and *VRN1* mutant plants

To analyze the genetic response of *bzip3-1* and *vrn1-6* plants to nitrate treatments, we performed RT-qPCR measurements for genes codifying for nitrate reductases (*NIA1* and *NIA2*) and nitrate transporters (*NRT1.1, NRT2.1, NRT2.2, NRT3.1*). Preliminary results for this experiment are reported since only two measurements from different experiments have been completed (Figure 3). We identified slight differences for *NIA2* and *NRT1.1* mRNA levels. The *bzip3-1* plants showed a lower mean mRNA level for these genes, contrary to the observed for *vrn1-6,* where higher mean values were observed. These results suggest that BZIP3 and VRN1 transcription factors have a role in the induction of important nitrate responsive genes.

DISCUSSION

This chapter described a preliminary characterization of the nitrate response for mutant plants in genes that codify for transcription factors with differential mRNA localization. We identified *BZIP3* and *VRN1* as main hubs for nitrate-regulated genes, having both cytoplasmic mRNA accumulation in response to nitrate treatments. We observed slight differences in nitrate-induced changes for RSA and gene expression in mutant plants, suggesting these TFs could be important regulators of the nitrate response. We are performing additional biological replicates to complement these results.

The TF-target network described here (Figure 1) allowed the identification of six transcription factors (BZIP3, VRN1, WRKY24, VIP1, COG1, and ERF105) whose transcripts were differentially accumulated in the cytoplasm (according to the analysis showed in Chapter 1) and they had a high target-connectivity with nitrate-regulated genes. Most of these TFs had not been previously characterized in the nitrate response. For instance, mutant plants for the *VIP1* gene showed differences in primary root length under high nitrate concentrations (Gaudinier et al., 2018). Nevertheless, no similar analyses have been reported for the other five TFs, although BZIP3 and VRN1 showed to be nitrogen-response regulators in a recent system biology analysis (Brooks et al., 2019).

BZIP3 is a transcription factor whose expression is reduced in high sugar concentrations through transcriptional and decay control (Matiolli et al., 2011). The molecular role of this TF is not fully understood. Nevertheless, the involvement of BZIP3 in abscisic acid mediated-sugar signaling and leaf development suggests it as an integrator of nutritional signals for plant growth (Matiolli et al., 2011; Sanagi et al., 2018). Furthermore, BZIP3 has been identified in

transcriptomic analysis as a nitrate-responsive gene (Canales et al., 2014) and recently as a high-influencing regulator of genes that change their RNA levels in shoot and root tissue after treatments with ammonium nitrate, identifying many target-genes involved in nitrate use, such as *NIA1*, *NIA2*, *NRT1.2*, and *BT2* (Brooks et al., 2019). The evidence shown in this work, based on correlation and interaction evidence (Grant et al., 2011; O'Malley et al., 2016), also suggests a role of BZIP3 in the regulation of nitrate transport and nitrate assimilation genes (Figure 1, Table 1), proposing its function as an integrator not only for carbon nutritional state but also nitrogen signals. Carbon and nitrogen metabolisms have a close interplay to control plants' growth and development (Gutiérrez et al., 2007; Santos-Filho et al., 2014; Bloom, 2015), so the role of BZIP3 could be related to this interaction.

Similarly, VRN1 is also involved in developmental processes, mainly having a role in reproductive tissue by repressing the flowering repressor FLC expression during vernalization (Chandlrer et al., 1996; Levy et al., 2002). *VRN1*-overexpressor plants showed shoot developmental defects, but no molecular mechanisms have been described (Mylne et al., 2006; King et al., 2013). Likewise to the observed for BZIP3, VRN1 was identified as a transcription factor with a strong influence on the RNA levels of nitrogen-responsive genes, exclusively in the roots (Brooks et al., 2019). However, any direct evidence for VRN1 control of root development has been reported. In this context, according to our results, VRN1 showed to be a potential controller of many target-genes involved in developmental processes and nitrogen metabolism in roots (Table 1), even observing a phenotype in the emergence of roots under basal conditions in mutant seedlings (Figure 2).

Nitrate has an essential role in root system architecture, observing that high nitrate concentrations inhibit primary root growth, increases root hair density, and regulates root meristem cell dynamics (Fredes and Moreno 2020). The phenotypic analysis of RSA in expression-altered mutant or transgenic plants have been extensively used for characterizing regulators of the nitrate response (Zhang and Forde, 1998; Vidal et al., 2010; Alvarez et al., 2014; Ma et al., 2014; Walker et al., 2017; Gaudinier et al., 2018). Nevertheless, in this work, more replicates are needed to clearly observe reported phenotypes under similar experimental conditions (Vidal et al., 2010; Alvarez et al., 2014).

In this work, new nitrate-responsive genes were identified following the cell fractionation/RNA-seq strategy explained above, finding many regulatory proteins that have not been previously characterized (Chapter 1). Furthermore, when the correlation was analyzed using only the cytoplasmic data, we identified gene connections not detected in the data from the total fraction (Figure 1). For instance, *VRN1* significant correlations with *NRT2.1* and *NIA2* were only identified in cytoplasmic data, an interaction that had not been reported in previous works (Brooks et al., 2019). These new connections can be identified due to the differences among nuclear, cytoplasmic, and cellular transcriptomes, which is a reported feature in many eukaryotic species (Barthelson et al., 2007; Djebali et al., 2012; Solnestam et al., 2012; Bahar Halpern et al., 2015; Battich et al., 2015; Chen and Van Steensel, 2017; Pastro et al., 2017; Benoit Bouvrette et al., 2018; Reynoso et al., 2018; Lee and Bailey-Serres, 2019; Palovaara and Weijers, 2019).

Considering that transcripts for *VRN1* and *BZIP3* are both mainly accumulated in the cytoplasm, we propose the hypothesis that these regulators are preferentially exported to

increase their expression, and in this way, efficiently control other genes involved in the nitrate response. This hypothesis is more robust for BZIP3, whose transcript levels are not induced in the nucleus, but they reach high cytoplasmic levels at the earliest time of treatment (Supplemental Figure 7G, Chapter 1). Similar mechanisms to the observed for HSP genes in yeast in response to heat could be acting in *Arabidopsis* during the nitrate response, where HSP transcripts bind to export machinery over other transcripts, being preferentially exported into the cytoplasm during stress (Saavedra et al., 1996; Zander et al., 2016). Likewise, this kind of mechanism is also suggested for plants, for example, in the nuclear-retention and subsequent polysome-association of the *HSP70-4* transcript during hypoxia-reaeration stages (Lee and Bailey-Serres, 2019).

In conclusion, we identified transcription factors with cytoplasmic mRNA level changes as important regulators of nitrate-responsive genes. Through a cell-fractionation/RNA-seq strategy coupled with gene network analysis, BZIP3 and VRN1 were recognized as uncharacterized potential regulators of the nitrate response by controlling the expression of genes involved in nitrate use and root architecture system modulation. Further experimental evidence is required for elucidating the role of these TFs in the nitrate response. Nevertheless, this preliminary evidence proposes them as possible export-regulated transcripts to modulate the genetic response of *Arabidopsis thaliana* roots to nitrate treatments.

METHODS

Plant material

Insertional mutants for *BZIP3* and *VRN1* were ordered according to available stocks in the Arabidopsis Biological Research Center (ABRC). Mutant lines for *bzip3-1* (SAIL_261_F01) and *vrn1-6* (SALK_061401) plants were selected in BASTA and Kanamicin, respectively, and then genotyped by PCR (Primers are listed in Table 2). Homozygous lines were propagated for the reported experiments.

Plant growth and nitrate treatment

Arabidopsis thaliana seedlings (from wild type or mutant genotypes) were grown in hydroponic media for 15 days, using ammonium succinate as the only source of nitrogen in the Phytatray^{TM} system (Sigma, Cat.P1552). Treatments with KNO_3 (or KCl as control) to a final concentration of 5 mM were performed, according to the described by Alvarez et al. (2014). Root tissue was collected after 120 min of treatment and immediately frozen in liquid nitrogen until processing for RNA extraction. The root phenotype was analyzed after three days of the treatment.

Root architecture system analysis

Roots of nitrate-treated and control plants were analyzed three days after the treatment to characterize their primary and lateral roots. For this, formaldehyde-fixed roots, collected after the treatment, were scanned, and primary root length was measured with the ImageJ software. Furthermore, roots were observed in an optical microscope (Nikon Eclipse 80i) for determining lateral root density, as described by Vidal et al. (2010).

RT-qPCR measurements

RT-qPCR evaluated the RNA levels of key elements in the nitrate response. RNA was extracted from nitrate-treated and control roots. cDNA was synthesized using Improm II RT (Promega, Cat. #A3800) and then measured by qPCR using the Brilliant III Ultra-Fast qPCR Kit (Agilent Technologies, Cat. #600880) and the StepOnePlus^{TM} qPCR System (Agilent Technologies). *YLS8* was used as a reference gene. Primers listed in Table 1 were used for amplification. cDNA levels were calculated using LinRegPCR software (Ramakers et al., 2003).

Gene network analysis

A correlation-based Transcription Factor (TF) – Target network was built based on the RNAseq counts obtained for 42 sequenced libraries for Cytoplasmic and Total fractions in KNO_3 and KCl treatments (Chapter 1). TF-Target information was obtained from experimental evidence of DAP-seq experiments (O'Malley et al., 2016) and motif-based sequence analysis with FIMO (Grant et al., 2011), using the CIS-BP (Weirauch et al., 2014), PlantTFDB (Jin et al., 2017), and Plant Cistrome (O'Malley et al., 2016) databases. To visualize the network, Cytoscape software (Shannon et al., 2003) was used. In this network, genes were considered as nodes and TF-target interactions as edges. Only significant correlated interactions (p-value ≤ 0.01) for TFs with a differentially localized transcript (identified in Chapter 1) were maintained. The community clustering (GLay) tool (Su et al., 2010) was used for the visual separation of clusters according to their topology. Gene ontology (GO) enrichment analysis was performed using the BinGO tool (Maere et al., 2005), selecting terms with a p-value lower than 0.05. GO-terms were summarized with REVIGO software (http://revigo.irb.hr), setting to obtain a tiny-size list of terms according to Resnik similarity (Supek et al., 2011)

Accession numbers

BZIP3 (AT5G15830), *VRN1* (AT3G18990), *NIA1* (AT1G77760), *NIA2* (AT1G37130), *NRT1.1* (AT1G12110), *NRT2.1* (AT1G08090), *NRT2.2* (AT1G08100), *NRT3.1* (AT5G50200), *YLS8* (AT5G08290).

ACKNOWLEDGMENTS

We thank Tomás Moyano, Ph.D., for the help with network analysis. This work was supported by grants from the Fondo de Desarrollo de Areas Prioritarias (FONDAP) Center for Genome Regulation (15090007), ANID–Millennium Science Initiative Program-Millennium Institute for Integrative Biology (iBio), and Fondo Nacional de Desarrollo Científico y Tecnológico (FONDECYT) 1180759 to R.A.G. A.F. was supported by ANID Ph.D. scholarship (21161516).

TABLES

Table 1. Enriched GO-Terms for clusters in network analysis

GO-ID	Description	Corrected p-value	Genes in the set
		BZIP3 cluster	
GO:0009719	response to endogenous stimulus	2.60E-02	AT1G09540| AT5G49720| AT5G64750| AT5G65430| AT2G37630| AT3G57040| AT3G02850| AT5G63160| AT4G24670| AT5G53160| AT3G63010| AT4G37790| AT3G61890| AT3G12560| AT1G20440| AT2G46680| AT4G37610| AT1G76180| AT3G48360| AT5G59220| AT3G11410| AT4G16780
GO:0009725	response to hormone stimulus	2.60E-02	AT1G09540| AT5G49720| AT5G64750| AT5G65430| AT2G37630| AT3G57040| AT3G02850| AT5G63160| AT4G24670| AT5G53160| AT3G63010| AT4G37790| AT3G61890| AT3G12560| AT1G20440| AT2G46680| AT4G37610| AT1G76180| AT3G48360| AT5G59220| AT3G11410| AT4G16780
GO:0015706	**nitrate transport**	2.60E-02	AT5G40890| AT1G08100| AT1G08090
		VRN1 cluster	
GO:0006812	cation transport	2.44E-02	AT5G03570| AT3G24450| AT4G30110| AT2G26650| AT3G06370| AT2G18960| AT3G42050| AT1G05300| AT2G19110
GO:0009719	response to endogenous stimulus	3.75E-03	AT1G58250 |AT4G25420 |AT2G14920| AT5G20990| AT3G55610| AT3G50660| AT1G56010| AT5G25220| AT1G56650| AT1G29395| AT1G59940| AT2G18960| AT5G66350| AT4G37580| AT1G73730| AT2G26980| AT1G08920| AT4G34750| AT2G46990| AT3G12830 |AT4G34000
GO:0032501	multicellular organismal process	4.74E-03	AT4G25420| AT1G56010| AT5G42970| AT3G54990| AT4G02380| AT3G03900| AT1G66470| AT1G13245| AT2G39200| AT3G14370| AT1G73680| AT1G69780| AT3G44540| AT4G37580| AT3G05090| AT2G46990| AT1G43710| AT4G36870| AT4G24660| AT1G79280| AT3G55610| AT3G50660| AT4G30960| AT5G21140| AT2G17820| AT1G14720| AT5G03150| AT4G36380| AT2G26650| AT2G28890| AT4G33650| AT5G53290| AT2G28550
GO:0032502	**developmental process**	4.78E-03	AT4G25420| AT1G56010| AT5G42970| AT3G54990| AT4G02380| AT1G66470| AT1G13245| AT2G39200| AT3G14370| AT1G73680| AT1G69780| AT3G44540| AT4G37580| AT3G05090| AT2G46990| AT1G43710| AT4G36870| AT4G24660| AT1G79280| AT3G55610| AT3G50660| AT4G30960| AT5G21140| AT2G17820| AT4G05320| AT1G14720| AT1G17060| AT5G03150| AT4G36380| AT2G26650| AT2G28890| AT4G33650| AT5G53290| AT2G28550
GO:0042558	pteridine and derivative metabolic process	1.58E-02	AT5G20990| AT2G43820| AT3G07270
GO:0048856	anatomical structure development	5.49E-03	AT4G25420| AT1G56010 |AT1G66470| AT1G13245| AT2G39200| AT3G14370| AT1G73680| AT1G69780| AT4G37580| AT3G05090| AT2G46990| AT1G43710| AT4G36870| AT4G24660| AT1G79280| AT3G55610| AT3G50660| AT5G21140| AT2G17820| AT1G14720| AT1G17060| AT5G03150| AT4G36380| AT2G26650| AT2G28890| AT4G33650| AT5G53290| AT2G28550
GO:0050896	response to stimulus	2.09E-04	AT1G67900| AT1G12110| AT4G25420| AT1G37130| AT1G56010| AT5G42970| AT1G61560| AT1G56650| AT1G29395| AT4G02380| AT5G43060| AT2G39200| AT1G72890| AT3G18990| AT1G08920| AT5G43350| AT3G50660| AT5G50200| AT5G25220| AT4G05320| AT4G09000| AT5G35620| AT1G17060| AT4G36040| AT1G69850| AT1G47128| AT1G58250| AT2G14920| AT3G13405| AT1G59740| AT5G26660| AT1G59940| AT2G18960| AT4G36010| AT1G73680| AT1G69780| AT4G37580| AT2G44490| AT5G03780| AT2G26980| AT4G34750| AT2G46990| AT3G12830| AT3G53990| AT5G20990| AT3G55610| AT5G51830| AT4G30960| AT1G66760| AT2G17820| AT1G16420| AT5G66350| AT1G73730| AT3G47520| AT2G26650| AT3G06370| AT2G22010| AT3G30775| AT4G34000
GO:0065007	biological regulation	4.82E-02	AT1G58250| AT4G25420| AT2G14920| AT3G13405| AT1G13460| AT2G29060| AT3G30260| AT1G63100| AT3G54990| AT1G56650| AT5G50210| AT1G59940| AT2G34150| AT2G18960| AT1G12630| AT5G57660| AT3G14370| AT1G72890| AT1G69780| AT4G37580| AT3G46640| AT1G76350| AT1G79280| AT1G67810| AT1G10120| AT3G50660| AT4G30960| AT4G24620| AT1G62262| AT5G54840| AT3G01330| AT4G04770| AT2G18160| AT1G17060| |AT5G03150| AT4G36380| AT5G62430| AT1G51140| AT1G05805| AT5G03570| AT2G26650| AT2G22010| AT5G53290| AT2G28550| AT4G34000

GO:0065008	regulation of biological quality	4.82E-02	AT1G58250| AT4G25420| AT2G14920| AT3G50660| AT4G30960| AT1G62262| AT4G04770| AT3G14370| AT1G17060| AT4G37580| AT4G36380| AT5G03570| AT2G26650
GO:0046483	heterocycle metabolic process	2.95E-02	AT5G20990| AT3G55610| AT1G68710| AT2G44490| AT1G56430| AT2G43820| AT4G30110| AT3G07270| AT3G42050| AT3G30775
GO:0008202	steroid metabolic process	4.32E-02	AT2G14920| AT1G17060| AT3G50660| AT4G36380
GO:0010817	regulation of hormone levels	2.44E-02	AT2G14920| AT3G14370| AT1G17060| AT3G50660| AT4G30960| AT4G36380
GO:0009414	response to water deprivation	4.60E-03	AT1G12110| AT4G30960| AT2G17820| AT1G29395| AT4G02380| AT1G47128| AT2G18960| AT1G08920| AT4G34000
GO:0015833	peptide transport	1.32E-02	AT1G65730| AT1G59740| AT5G62680| AT3G54140| AT2G02040
GO:0009165	nucleotide biosynthetic process	4.32E-02	AT1G32380| AT1G68710| AT5G50210| AT4G30110| AT3G42050
GO:0044271	**cellular nitrogen compound biosynthetic process**	9.57E-03	AT3G44720| AT1G32380| AT5G20990| AT3G55610| AT1G68710| AT1G37130| AT1G56430| AT5G50210| AT4G30110| AT3G07270| AT3G42050| AT3G30775
GO:0071495	cellular response to endogenous stimulus	5.89E-03	AT4G25420| AT5G20990| AT3G50660| AT4G37580| AT1G73730| AT1G56010| AT1G59940| AT2G26980| AT5G66350| AT4G34000
GO:0009628	response to abiotic stimulus	8.46E-04	AT1G67900| AT1G12110| AT4G25420| AT1G37130| AT5G42970| AT1G56650| AT5G26660| AT1G29395| AT1G59940| AT4G02380| AT2G18960| AT5G43060| AT4G37580| AT3G18990| AT2G26980| AT1G08920| AT2G46990| AT3G53990| AT3G55610| AT4G30960| AT5G25220| AT2G17820| AT1G16420| AT1G17060| AT3G47520| AT1G47128| AT2G26650| AT3G06370| AT4G34000
			WRKY24 cluster
GO:0009653	**anatomical structure morphogenesis**	2.62E-02	AT5G23530| AT3G01470| AT5G25890| AT5G64340| AT2G41370| AT5G56320| AT2G46225| AT5G02260| AT2G20750| AT4G22910| AT2G26420| AT5G46700| AT5G41315| AT1G74380
GO:0009664	**plant-type cell wall organization**	2.81E-02	AT5G56320| AT5G41040| AT5G02260| AT2G20750| AT5G33290
GO:0040007	**growth**	4.08E-02	AT5G23530| AT5G56320| AT5G02260| AT2G20750| AT4G22910| AT5G64340| AT2G26420| AT3G21510| AT1G74380
GO:0045488	pectin metabolic process	1.97E-02	AT4G01750| AT5G41040| AT5G33290
GO:0065007	biological regulation	1.79E-02	AT5G23530| AT3G55980| AT4G22910| AT2G30710| AT4G26080| AT1G52280| AT2G46370| AT1G80840| AT5G58670| AT5G40910| AT5G41570 |AT3G05690| AT3G20550| AT2G30880| AT1G73670| AT2G23320| AT1G16490| AT1G28340| AT4G30980| AT3G56800| AT4G18430| AT2G25180| AT5G44530| AT5G25890| AT5G64340| AT3G16280| AT5G66320| AT3G21510| AT1G22770| AT3G47610| AT1G17590| AT2G20400| AT1G78010| AT2G26420| AT4G17695| AT2G28160| AT5G43890| AT3G01470| AT3G04420| AT5G21482| AT1G04610| AT1G49560| AT5G56320| AT5G02260| AT2G20750| AT3G62420| AT4G26070| AT1G79430| AT5G10280| AT2G44940| AT3G04070| AT4G14690| AT1G74380
GO:0090066	regulation of anatomical structure size	2.81E-02	AT5G23530| AT5G56320| AT5G02260| AT2G20750| AT4G22910| AT5G64340| AT2G26420| AT3G21510| AT1G74380
GO:0016049	**cell growth**	2.60E-02	AT5G23530| AT5G56320| AT5G02260| AT2G20750| AT4G22910| AT5G64340| AT2G26420| AT3G21510| AT1G74380
GO:0042180	cellular ketone metabolic process	8.57E-03	AT3G03780 |AT5G41040| AT5G45340| AT5G16240| AT1G67730| AT1G80340| AT3G28910| AT5G17920| AT5G64050| AT2G36880| AT5G58860| AT2G45300| AT1G01120| AT5G65800| AT1G09620| AT2G46370| AT2G43750| AT1G77590
GO:0044255	cellular lipid metabolic process	2.62E-02	AT5G58860| AT2G37940| AT1G01120| AT5G41040| AT5G45340| AT5G16240| AT1G67730| AT1G80340| AT3G28910| AT2G46370| AT2G18640| AT1G77590
GO:0019438	aromatic compound	4.08E-02	AT5G58860| AT4G23690| AT2G45300| AT5G41040| AT1G16490| AT3G21230| AT4G34135

	biosynthetic process		
GO:0042398	**cellular amino acid derivative biosynthetic process**	8.57E-03	AT5G58860| AT4G23690| AT5G41040| AT5G65800| AT5G53120| AT1G16490| AT3G21230| AT4G34135| AT2G36880
GO:0044281	small molecule metabolic process	8.57E-03	AT3G03780| AT5G40390| AT5G41040| AT5G45340| AT5G16240| AT1G80340| AT3G21230| AT3G25610| AT2G36310| AT2G45300| AT5G53120| AT4G34135| AT2G46370| AT4G23690| AT1G67730| AT3G28910| AT1G31220| AT2G31390| AT5G17920| AT5G64050| AT2G36880| AT5G58860| AT1G01120| AT5G65800| AT1G16490| AT1G09620| AT2G43750| AT1G77590
GO:0009415	response to water	2.62E-02	AT5G40390| AT5G37500| AT5G45340| AT5G52310| AT4G26070| AT5G58670| AT5G59220| AT4G38410
GO:0050794	regulation of cellular process	3.81E-02	AT2G25180 |AT3G55980 |AT5G25890| AT3G16280| AT5G66320| AT1G22770| AT3G47610| AT1G17590| AT4G22910| AT2G30710| AT4G26080| AT2G20400 |AT1G78010| AT1G52280| AT2G46370| AT1G80840| AT5G58670| AT4G17695| AT5G40910| AT2G28160| AT3G01470| AT3G04420| AT5G41570| AT3G05690| AT2G30880| AT1G73670| AT1G49560| AT2G23320| AT1G16490| AT3G62420| AT1G28340| AT4G26070| AT1G79430| AT5G10280| AT4G30980| AT2G44940| AT3G04070| AT3G56800| AT4G14690| AT4G18430
GO:0032787	monocarboxylic acid metabolic process	2.60E-02	AT5G58860| AT1G01120| AT5G41040| AT5G45340| AT5G16240| AT1G67730| AT1G80340| AT3G28910| AT2G46370| AT1G77590
		ERF105 cluster	
GO:0002682	regulation of immune system process	4.49E-02	AT3G15210 |AT3G18690| AT3G11820
GO:0006575	**cellular amino acid derivative metabolic process**	4.49E-02	AT4G25640| AT4G08920| AT2G47460| AT4G11280| AT1G20510| AT3G59050
GO:0006950	response to stress	4.49E-02	AT3G05210| AT4G08920| AT2G16500| AT5G63790| AT2G17870| AT1G64280| AT1G48000| AT1G72450| AT1G52200| AT3G15210| AT3G14110| AT2G40970| AT2G32920| AT5G41750| AT1G50170| AT4G11280| AT3G11820| AT3G16720| AT1G20510
GO:0031408	oxylipin biosynthetic process	4.00E-02	AT3G14110| AT1G20510| AT5G63380
		VIP1 cluster	
GO:0042221	response to chemical stimulus	4.53E-02	AT3G50060| AT5G44790| AT1G30270| AT3G57530| AT1G32450| AT1G70410| AT1G19840| AT4G21670| AT4G14640| AT2G44350| AT4G17500| AT5G53460| AT4G37260| AT4G31550| AT4G33630| AT4G11290| AT4G30270| AT3G15500
		COG1 cluster	
GO:0023034	intracellular signaling pathway	3.49E-02	AT3G28650| AT5G03520| AT2G02680| AT1G61840
GO:0042592	homeostatic process	4.01E-02	AT5G58530| AT5G61440| AT4G08930| AT2G26710

Table 2. List of primers

Primer sequence (5'->3')	Gene	Sense	Use
GCAGATTTACACAGCAACGTGT	*BZIP3*	Forward	Genotyping
ACTTTGGTACGTAGTTAAACGGT	*BZIP3*	Reverse	Genotyping
GCTTCCTATTATATCTTCCCAAATTACCAATACA	*T-DNA (SALK)*	Reverse	Genotyping
TGTGCAGAGGGTCCCAGATA	*VRN1*	Forward	Genotyping
GCAGCTCAAACACACAGACG	*VRN1*	Reverse	Genotyping
ATTTTGCCGATTTCGGAAC	*T-DNA (SAIL)*	Reverse	Genotyping
TTACTGTTTCGGTTGTTCTCCATTT	*YLS8*	Forward	qPCR
CACTGAATCATGTTCGAAGCAAGT	*YLS8*	Reverse	qPCR
AAGGCAAAGGCAACTTCCTGGT	*NIA1*	Forward	qPCR
TCATCCTCGGTTCTGTTTGCGT	*NIA1*	Reverse	qPCR
AACTCGCCGACGAAGAAGGTTG	*NIA2*	Forward	qPCR
CTCGTGACATGGCGTCGTAATC	*NIA2*	Reverse	qPCR
AATCCAAGCCACGGGTGTTT	*NRT1.1*	Forward	qPCR
CACTTGCTTGTTCGCAGTGA	*NRT1.1*	Reverse	qPCR
CCACAGATCCAGTGAAAGGTACAG	*NRT2.1*	Forward	qPCR
CACCCTCTGACTTGGCGTTCT	*NRT2.1*	Reverse	qPCR
TCATGGGAATCTTGGTGCTCACG	*NRT2.2*	Forward	qPCR
ACGGCGTACCATAGAATCTTTCCG	*NRT2.2*	Reverse	qPCR
GTTGATGCCATTGGCCATGAAG	*NRT3.1*	Forward	qPCR
GACACTGAAACAGATGGAGGCAA	*NRT3.1*	Reverse	qPCR

FIGURES

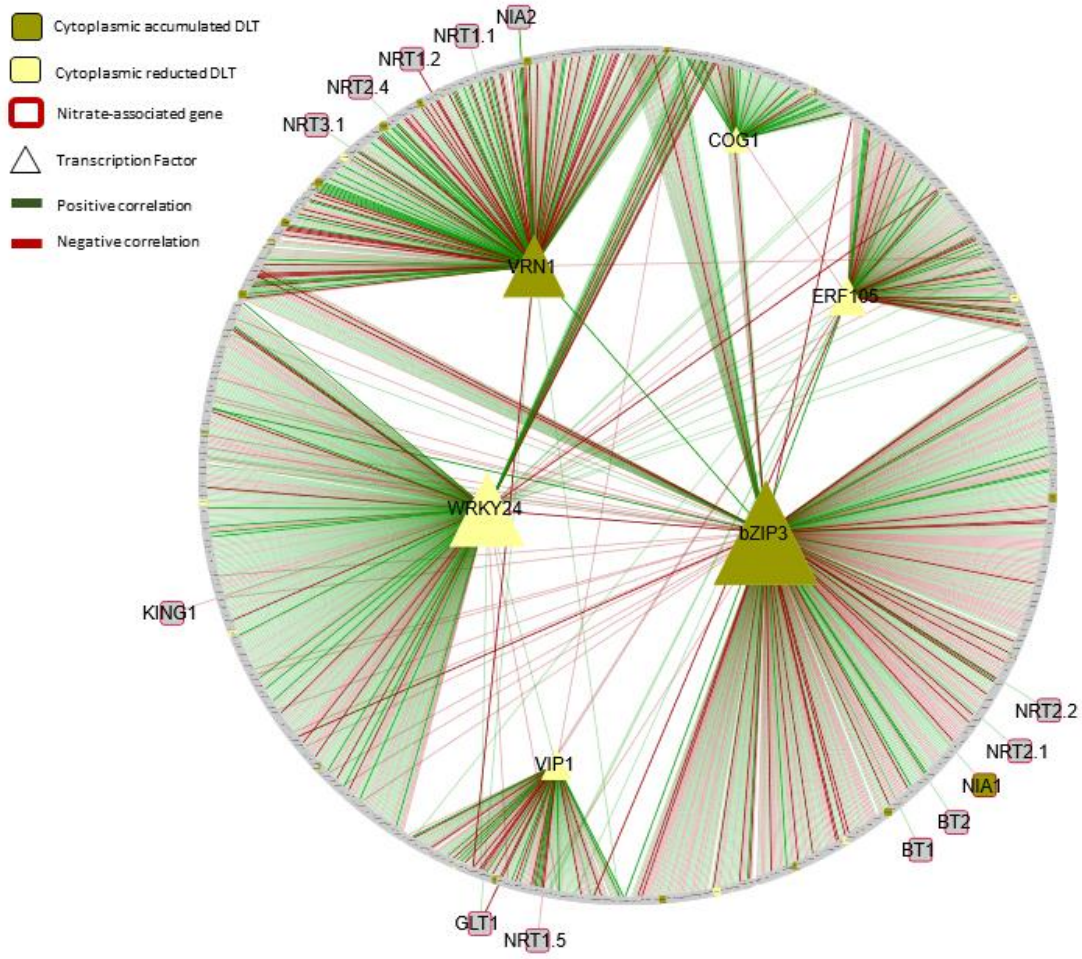

Figure 1. TF-target correlation network identifies main hubs with differential cytoplasmic mRNA accumulation during the nitrate response.

A correlation TF-target network was built as described in the Methods section. Clustering analysis identified six main hubs, which represent transcription factors with differential localization in response to nitrate treatments (DLTs, chapter 1). Triangles represent transcription factors. Edges show TF-target interaction showing positive (green) or negative (red) correlation. Darker edges are indicated when the correlation is not significant in total data. Differentially localized transcripts are highlighted in yellow tones differentiating genes with increasing (mustard) from decreasing (light yellow) RNA levels. Genes directly associated with nitrate functions are indicated with a red border.

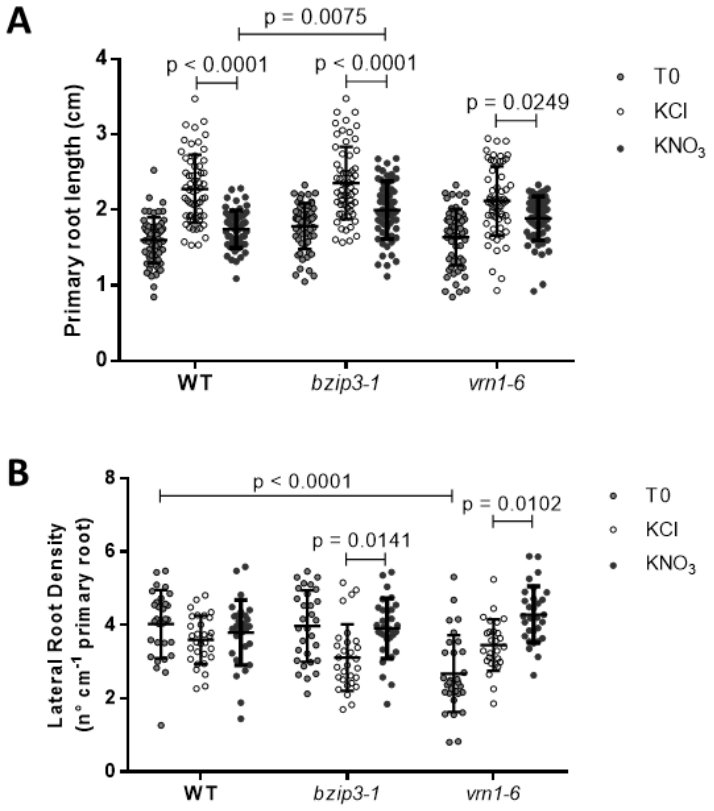

Figure 2. Root system architecture phenotype for *bzip3-1* and *vrn1-6* mutants in response to nitrate treatments.

Primary root length **(A)** and lateral root density **(B)** were calculated for 15 day-old seedling before (T0) and after three days of nitrate (KNO_3) or control (KCl) treatments. Wild type (WT), *bzip3-1*, and *vrn1-6* genotypes were evaluated. Lateral root density was calculated as the number of emerging or totally emerged lateral roots divided by primary root length (in centimeters). Each point represents the measurement for one plant from two independent experiments. Two-way ANOVA Tukey post-test p values for significative differences are indicated (p value<0.05) for WT-mutant comparison in the same condition and for KNO_3-KCl comparison within each genotype. Error bars show standard deviation.

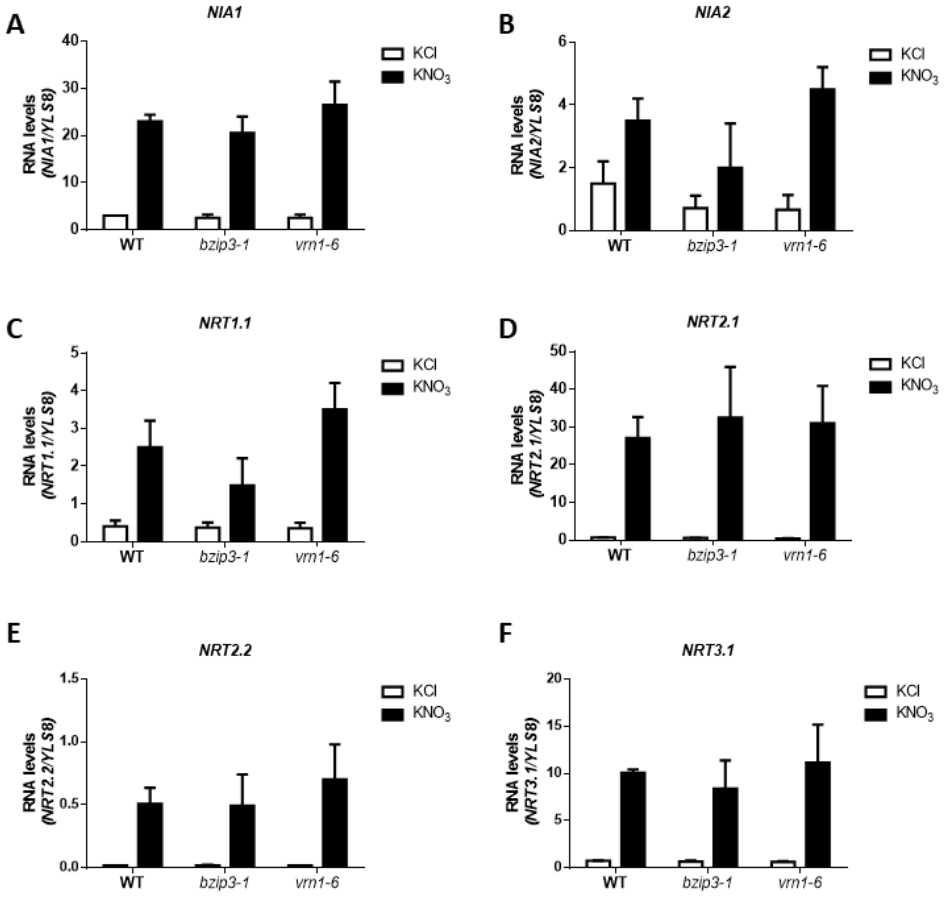

Figure 3. Nitrate responsive gene mRNA levels for *bzip3-1* and *vrn1-6* in response to nitrate treatments.

mRNA levels measurements by RT-qPCR for nitrate-responsive genes in roots of 15-day old seedling after two hours of nitrate (KNO_3) or control (KCl) treatments. Values were normalized by *YLS8* levels. *NIA1* (A), *NIA2* (B), *NRT1.1* (C), *NRT2.1* (D), *NRT2.2* (E), and *NRT3.1* (F) genes were analyzed. Bars show mean + SEM for measurements from two independent experiments.

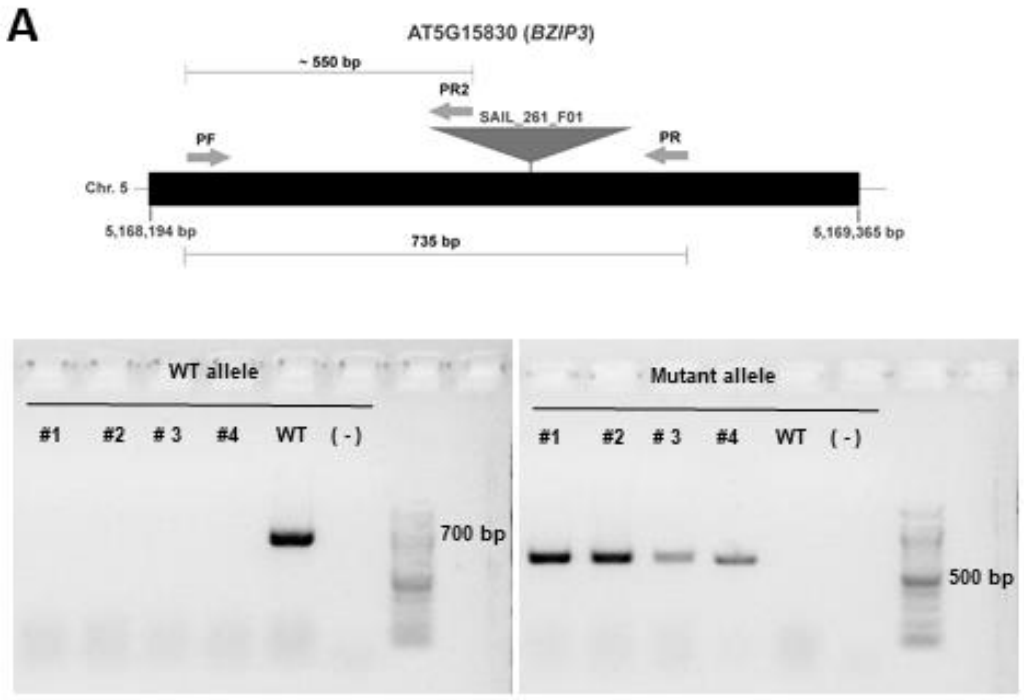
A
AT5G15830 (BZIP3)
~ 550 bp
PR2
SAIL_261_F01
PF
PR
Chr. 5
5,168,194 bp
5,169,365 bp
735 bp
WT allele
#1 #2 # 3 #4 WT (-)
700 bp
Mutant allele
#1 #2 # 3 #4 WT (-)
500 bp

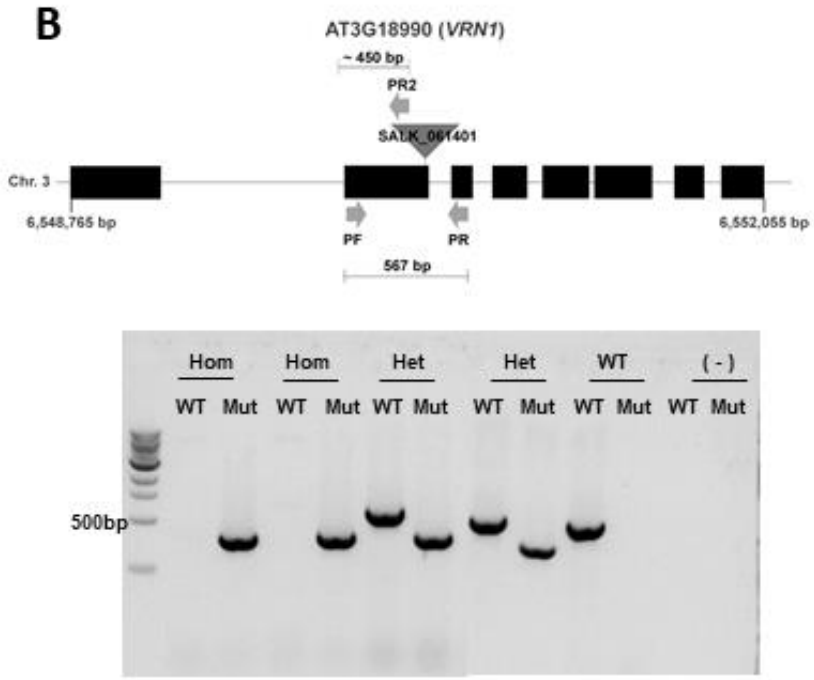
B
AT3G18990 (VRN1)
~ 450 bp
PR2
SALK_061401
Chr. 3
6,548,765 bp
6,552,055 bp
PF
PR
567 bp
Hom Hom Het Het WT (-)
WT Mut WT Mut WT Mut WT Mut WT Mut WT Mut
500bp

Supplemental Figure 1. Mutant lines genotyping

Antibiotic-resistant seedlings for SAIL_261_F01 (*bzip3-1*) (**A)** and SALK_061401 (*vrn1-6*) **(B)** lines were genotyped by PCR using the strategies shown at the top of the figure. The WT allele (WT) was amplified using PF and PR primers that hybridize the gene sequence, and the mutant allele (Mut) was amplified using PR2 (which recognizes T-DNA left border) instead. For *bzip3-1* mutants, only homozygous plants were obtained (identified as #1, #2, #3, and #4), contrary to *vrn1-6* mutants were homozygous (Hom) and heterozygous (Het) plants were identified. Genomic DNA from Col-0 wild type (WT) plants was used as control. Negative control for PCR reaction (-) was also included for both reactions.

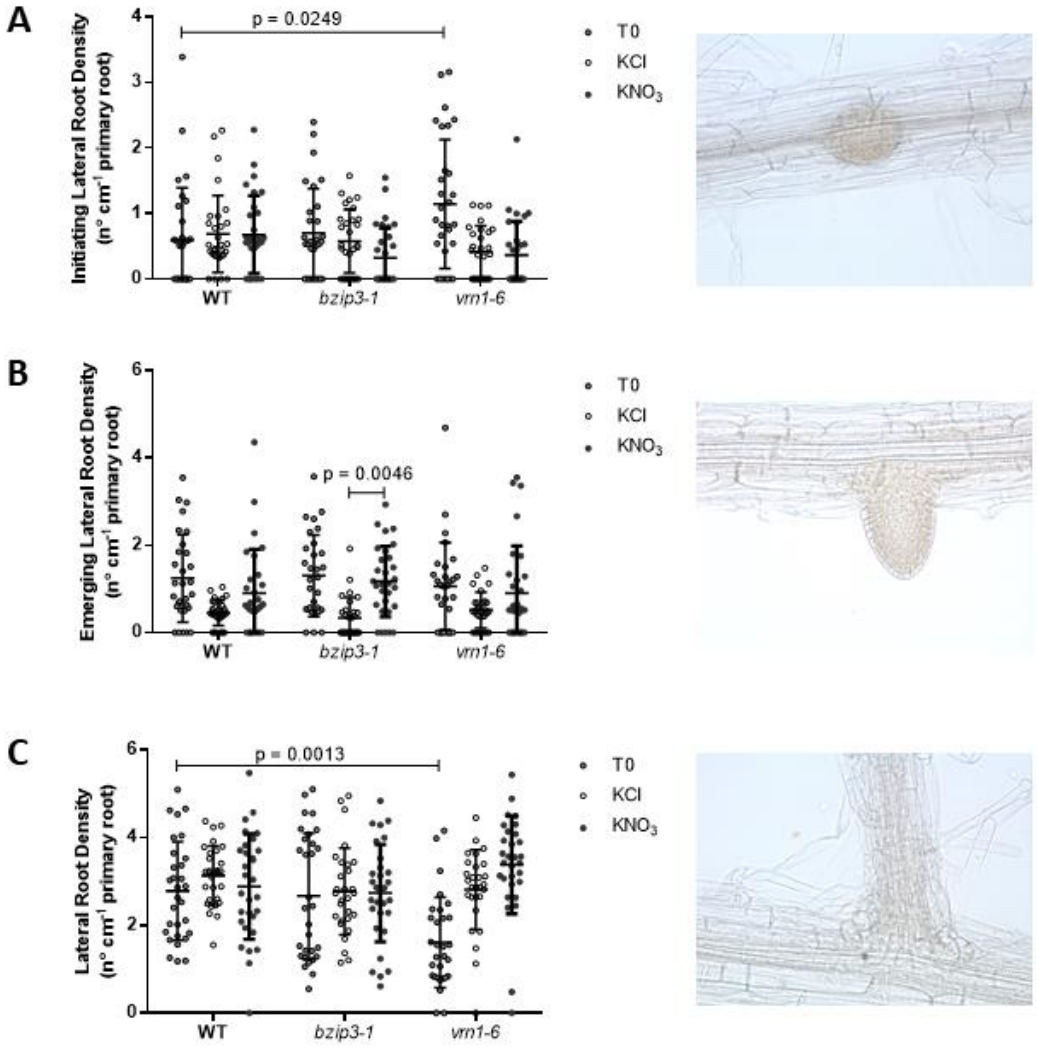

Supplemental Figure 2. Detailed lateral root phenotype for *bzip3-1* and *vrn1-6* mutants in response to nitrate treatments.

Lateral root density was calculated for 15-day old seedling before (T0) and after three days of nitrate (KNO_3) or control (KCl) treatment. Wild type (WT), *bzip3-1*, and *vrn1-6* genotypes were evaluated. Lateral roots were quantified separately for initiating (A), emerging (B), and emerged (C) roots. Examples for each type of lateral root state are shown in (D). Each point represents the measurement for one plant from two independent experiments. Two-way ANOVA Tukey post-test p values for significative differences are indicated (p value<0.05) for WT-mutant comparison in the same condition and for KNO_3-KCl comparison within each genotype. Error bars show standard deviation.

CONCLUSIONS

This work described the dynamics for nucleocytoplasmic distribution in *Arabidopsis thaliana* root cells in response to nitrate treatments. Transcripts with changes in their mRNA distribution during the treatments showed five different localization patterns. The differences in RNA sequence, processing site density, synthesis, and decay rates suggest the participation of many cellular processes affecting nuclear and cytoplasmic steady-state levels. Remarkably, these results suggest a role for mRNA nuclear export in controlling the nucleocytoplasmic distribution of transcripts in response to nitrate, taking into consideration: 1) Genes with differential mRNA accumulation in the nucleus or the cytoplasm had important function for the nutritional response, indicating a nuclear-retention or a successful delivery into the cytoplasm in order to modulate gene expression in response to the treatment. 2) Transcripts from the delayed-cytoplasmic accumulation pattern had the most significant nitrate-elicited increments in their RNA polymerase II occupancy and turnover rates, indicating these mRNAs are rapidly replaced. The control of mRNA nucleocytoplasmic dynamics could extend the time that these transcripts are expressed. 3) The mRNAs for essential regulatory elements of the nitrate response, such as VRN1 and BZIP3 transcription factors, were identified as transcripts preferentially accumulated in the cytoplasm, potentially affecting physiological regulation processes in the roots. Altogether, during the nitrate response, the regulation of the nucleocytoplasmic dynamic of transcripts could allow fine-tuning gene expression to keep mRNA levels according to the nutritional condition, suggesting a relevant role for mRNA nuclear export in the plant's adaptive response to nitrogen nutrient signals.

REFERENCES

Alboresi A, Gestin C, Leydecker M, Bedu M, Meyer C, Truong H (2005) Nitrate, a signal relieving seed dormancy in Arabidopsis. Plant Cell Environ **28**: 500–512

Alvarez JM, Riveras E, Vidal EA, Gras DE, Contreras-López O, Tamayo KP, Aceituno F, Gómez I, Ruffel S, Lejay L, et al (2014) Systems approach identifies TGA1 and TGA4 transcription factors as important regulatory components of the nitrate response of Arabidopsis thaliana roots. Plant J **80**: 1–13

Alvarez M, Moyano C, Zhang T, Gras DE, Herrera FJ, Brien AO, Carrillo L, Araus V, Jiang J, Gutie RA (2019) Local Changes in Chromatin Accessibility and Transcriptional Networks Underlying the Nitrate Response in Arabidopsis Roots. Mol Plant **12**: 1545–1560

Andrews M, Raven JA, Lea PJ (2013) Do plants need nitrate? the mechanisms by which nitrogen form affects plants. Ann Appl Biol **163**: 174–199

Bahar Halpern K, Caspi I, Lemze D, Levy M, Landen S, Elinav E, Ulitsky I, Itzkovitz S (2015) Nuclear Retention of mRNA in Mammalian Tissues. Cell Rep **13**: 2653–2662

Barthelson RA, Lambert GM, Vanier C, Lynch RM, Galbraith DW (2007) Comparison of the contributions of the nuclear and cytoplasmic compartments to global gene expression in human cells. BMC Genomics **8**: 1–15

Battich N, Stoeger T, Pelkmans L (2015) Control of Transcript Variability in Single Mammalian Cells. Cell **163**: 1596–1610

Benoit Bouvrette LP, Cody NAL, Bergalet J, Lefebvre FA, Diot C, Wang X, Blanchette M, Lécuyer E (2018) CeFra-seq reveals broad asymmetric mRNA and noncoding RNA distribution profiles in Drosophila and human cells. RNA **24**: 98–113

Bloom AJ (2015) Photorespiration and nitrate assimilation: A major intersection between plant carbon and nitrogen. Photosynth Res **123**: 117–128

Bolger AM, Lohse M, Usadel B (2014) Trimmomatic: A flexible trimmer for Illumina sequence data. Bioinformatics **30**: 2114–2120

Bouguyon E, Perrine-walker F, Pervent M, Rochette J, Cuesta C, Benkova E, Martinière A, Bach L, Krouk G, Gojon A, et al (2016) Nitrate Controls Root Development through Posttranscriptional Regulation of the NRT1.1/NPF6.3 Transporter/Sensor. Plant Physiol **172**: 1237–1248

Brooks MD, Cirrone J, Pasquino A V, Alvarez JM, Swift J, Mittal S, Juang C, Varala K, Gutiérrez RA, Krouk G, et al (2019) Network Walking charts transcriptional dynamics

of nitrogen signaling by integrating validated and predicted genome-wide interactions. Nat Commun **10**: 1–13

Canales J, Contreras-López O, Álvarez JM, Guti RA (2017) Nitrate induction of root hair density is mediated by TGA1 / TGA4 and CPC transcription factors in Arabidopsis thaliana. Plant J **92**: 305–316

Canales J, Moyano TC, Villarroel E, Gutiérrez RA (2014) Systems analysis of transcriptome data provides new hypotheses about Arabidopsis root response to nitrate treatments. Front Plant Sci **5**: 1–14

Castro Marín I, Loef I, Bartetzko L, Searle I, Coupland G, Stitt M, Osuna D (2011) Nitrate regulates floral induction in Arabidopsis , acting independently of light , gibberellin and autonomous pathways. Planta **233**: 539–552

Chakraborty P, Wang Y, Wei J, Deursen J Van, Yu H, Malureanu L, Dasso M, Forbes DJ, Levy DE, Seemann J, et al (2008) Nucleoporin Levels Regulate Cell Cycle Progression and Phase-Specific Gene Expression. Dev Cell **15**: 657–667

Chandlrer J, Wilson A, Dean C (1996) Arabidopsis mutants showing an altered response to vernalization. Plant Jour **10**: 637–644

Chantarachot T, Bailey-Serres J (2018) Polysomes, Stress Granules, and Processing Bodies: A Dynamic Triumvirate Controlling Cytoplasmic mRNA Fate and Function. Plant Physiol **176**: 254–269

Chen J, Yu Y, Sui X, Qiao L, Dong, C-H (2019) Arabidopsis CPR5 regulates ethylene signaling via interacting with ETR1 N-terminus and controlling mRNAs nucleocytoplasmic transport. J Integr Plant Biol **November**: 810–824

Chen T, Van Steensel B (2017) Comprehensive analysis of nucleocytoplasmic dynamics of mRNA in Drosophila cells. PLoS Genet **13**: 1–25

Cheng C, Dewdney J, Nam H, Boer BGW Den, Goodman HM (1988) A new locus (NIA1) in Arabidopsis thaliana encoding nitrate reductase. EMBO J **7**: 3309–3314

Choudury SG, Shahid S, Cuerda-gil D, Panda K, Cullen A, Ashraf Q, Sigman M, McCue A, Slotkin RK (2019) The RNA Export Factor ALY1 Enables Genome-Wide RNA-Directed DNA Methylation. Plant Cell **31**: 759–774

Crisp PA, Ganguy DR, Smith AB, Murray KD, Estavillo GM, Searle I, Ford E, Bogdanovic O, Lister R, Borevitz JO, et al (2017) Rapid Recovery Gene Downregulation during Excess-Light Stress and Recovery in Arabidopsis. Plant Cell **29**: 1836–1863

Culjkovic-Kraljacic B, Borden KLB (2018) The Impact of Post-transcriptional Control: Better Living Through RNA Regulons. Front Genet **9**: 1–11

Darnell R (2012) Identification of RNAs Bound by a Specific Protein CLIP (Cross-Linking and Immunoprecipitation). Cold Spring Harb Protoc **May**: 1146–1160

Das B, Butler JS, Sherman F (2003) Degradation of Normal mRNA in the Nucleus of

Saccharomyces cerevisiae. Mol Cell Biol **23**: 5502–5515

De S, Babu MM (2010) Genomic neighbourhood and the regulation of gene expression. Curr Opin Cell Biol **22**: 326–333

Dedow LK, Bailey-Serres J (2019) Searching for a Match: Structure , Function and Application of Sequence-Specific RNA-Binding Proteins. Plant Cell Physiol **60**: 1927–1938

Djebali S, Davis CA, Merkel A, Dobin A, Lassmann T, Mortazavi A, Tanzer A, Lagarde J, Lin W, Schlesinger F, et al (2012) Landscape of transcription in human cells. Nature **489**: 101–108

Duncan S, Olsson T, Hartley M, Dean C, Rosa S (2017) Single Molecule RNA FISH in Arabidopsis Root Cells. Bio-Protocol **7**: 1–10

Ehrnsberger HF, Grasser KD (2019) Nucleocytosolic mRNA transport in plants : export factors and their influence on growth and development. **70**: 3757–3763

Eser P, Demel C, Maier KC, Schwalb B, Pirkl N, Martin DE, Cramer P, Tresch A (2014) Periodic mRNA synthesis and degradation co-operate during cell cycle gene expression. Mol Syst Biol **10**: 1–15

Forde BG, Walch-liu PIA (2009) Nitrate and glutamate as environmental cues for behavioural responses in plant roots. Plant, Cell Environ **32**: 682–693

Fredes I, Moreno S, Díaz F, Gutierrez RA (2019) Nitrate signaling and the control of Arabidopsis growth and development. Curr Opin Plant Biol **47**: 112–118

Gaudinier A, Rodriguez-Medina J, Zhang L, Olson A, Liseron-Monfils C, Bågman A, Foret J, Abbitt S, Tang M, Li B, et al (2018) Transcriptional regulation of nitrogen-associated metabolism and growth. Nature **563**: 259–264

Gifford ML, Dean A, Gutierrez RA, Coruzzi GM, Birnbaum KD (2008) Cell-specific nitrogen responses mediate developmental plasticity. Proc Natl Acad Sci **105**: 803–808

Gosai SJ, Foley SW, Deal RB, Gregory BD, Gosai SJ, Foley SW, Wang D, Silverman IM, Selamoglu N, Nelson ADL (2015) Global Analysis of the RNA-Protein Interaction and RNA Secondary Structure Landscapes of the Arabidopsis Nucleus Resource Global Analysis of the RNA-Protein Interaction and RNA Secondary Structure Landscapes of the Arabidopsis Nucleus. Mol Cell **57**: 376–388

Grant CE, Bailey TL, Noble WS (2011) FIMO : scanning for occurrences of a given motif. Bioinformatics **27**: 1017–1018

Gras DE, Vidal EA, Undurraga SF, Riveras E, Moreno S, Dominguez-Figueroa J, Alabadi D, Blázquez MA, Medina J, Gutiérrez RA (2018) SMZ/SNZ and gibberellin signaling are required for nitrate- elicited delay of flowering time in Arabidopsis thaliana. J Exp Bot **69**: 619–631

Gruber BD, Giehl RFH, Friedel S, von Wirén N (2013) Plasticity of the Arabidopsis Root

System under Nutrient De fi ciencies 1 [C][W][OPEN]. Plant Physiol **163**: 161–179

Guan P, Ripoll J, Wang R, Vuong L, Bailey-steinitz LJ, Ye D, Crawford NM (2017) Interacting TCP and NLP transcription factors control plant responses to nitrate availability. Proc Natl Acad Sci **114**: 2419–2424

Gutiérrez RA (2013) Systems Biology for Enhanced Plant Nitrogen Nutrition. Science (80-) **336**: 1673–1676

Gutierrez RA, Ewing RM, Cherry JM, Green PJ (2002) Identification of unstable transcripts in Arabidopsis by cDNA microarray analysis: rapid decay is associated with a group of touch- and specific clock-controlled genes. Proc Natl Acad Sci U S A **99**: 11513–8

Gutiérrez RA, Lejay L V, Dean A, Chiaromonte F, Shasha DE, Coruzzi GM (2007) Qualitative network models and genome-wide expression data define carbon/nitrogen-responsive molecular machines in Arabidopsis. Genome Biol **8**: R7

Hansen MMK, Desai R V, Simpson ML, Weinberger LS (2018) Cytoplasmic Amplification of Transcriptional Noise Generates Substantial Cell-to-Cell Variability. Cell Syst **7**: 384–397

Hieronymus H, Silver PA (2003) Genome-wide analysis of RNA – protein interactions illustrates specificity of the mRNA export machinery. Nat Genet **33**: 155–161

Hirel B, Tétu T, Lea PJ, Dubois F (2011) Improving Nitrogen Use Efficiency in Crops for Sustainable Agriculture. Sustainability **3**: 1452–1485

Ho CH, Lin SH, Hu HC, Tsay YF (2009) CHL1 Functions as a Nitrate Sensor in Plants. Cell **138**: 1184–1194

Hogan DJ, Riordan DP, Gerber AP, Herschlag D, Brown PO (2008) Diverse RNA-Binding Proteins Interact with Functionally Related Sets of RNAs, Suggesting an Extensive Regulatory System. PLoS Biol **6**: 2297–2313

Hu H, Wang Y, Tsay Y (2009) AtCIPK8 , a CBL-interacting protein kinase , regulates the low-affinity phase of the primary nitrate response. Plant J **57**: 264–278

Jin J, Tian F, Yang DC, Meng YQ, Kong L, Luo J, Gao G (2017) PlantTFDB 4.0: Toward a central hub for transcription factors and regulatory interactions in plants. Nucleic Acids Res **45**: D1040–D1045

Jovanovic M, Rooney MS, Mertins P, Przybylski D, Chevrier N, Satija R, Rodriguez EH, Fields AP, Schwartz S, Raychowdhury R, et al (2015) Dynamic profiling of the protein life cycle in response to pathogens. Immunogenetics **347**: 1–8

Katari MS, Nowicki SD, Aceituno FF, Nero D, Kelfer J, Thompson LP, Cabello JM, Davidson RS, Goldberg AP, Shasha DE, et al (2010) VirtualPlant: A Software Platform to Support Systems Biology Research. Plant Physiol **152**: 500–515

Keene JD (2007) RNA regulons: coordination of post-transcriptional events. Nat Rev Genet **8**: 533–543

Kim D, Langmead B, Salzberg SL (2015) HISAT: A fast spliced aligner with low memory requirements. Nat Methods **12**: 357–360

Kim E, Magen A, Ast G, Aviv R (2007) Different levels of alternative splicing among eukaryotes. Nucleic Acids Res **35**: 125–131

Kim J-E, Hong YH, Kim JY, Jeon GS, Jung JH, Yoon B-N, Son S-Y, Lee K, Kim J-I, Sung J-J (2017) Altered nucleocytoplasmic proteome and transcriptome distributions in an in vitro model of amyotrophic lateral sclerosis. PLoS One **12**: 1–23

King GJ, Chanson AH, Mccallum EJ, Ohme-takagi M, Byriel K, Hill JM, Martin JL, Mylne JS (2013) The Arabidopsis B3 Domain Protein VERNALIZATION1 (VRN1) Is Involved in Processes Essential for Development, with Structural and Mutational Studies Revealing Its DNA-binding. J Biol Chem **288**: 3198–3207

Köster T, Marondedze C, Meyer K, Staiger D (2017) RNA-Binding Proteins Revisited – The Emerging Arabidopsis mRNA Interactome. Trends Plant Sci **22**: 512–526

Krouk G, Mirowski P, LeCun Y, Shasha DE, Coruzzi GM (2010) Predictive network modeling of the high-resolution dynamic plant transcriptome in response to nitrate. Genome Biol **11**: 1–19

Krouk G, Tranchina D, Lejay L, Cruikshank AA, Shasha D, Coruzzi GM, Gutiérrez RA (2009) A systems approach uncovers restrictions for signal interactions regulating genome-wide responses to nutritional cues in Arabidopsis. PLoS Comput Biol **5**: 1–12

Łabno A, Tomecki R, Dziembowski A (2016) Cytoplasmic RNA decay pathways - Enzymes and mechanisms. Biochim Biophys Acta **1863**: 3125–3147

Landrein B, Formosa-jordan P, Malivert A, Schuster C, Melnyk CW, Yang W, Turnbull C, Meyerowitz EM, Locke JCW, Jönsson H (2018) Nitrate modulates stem cell dynamics in Arabidopsis shoot meristems through cytokinins. Proc Natl Acad Sci **115**: 1382–1387

Lee ES, Akef A, Mahadevan K, Palazzo AF (2015) The Consensus 5 ' Splice Site Motif Inhibits mRNA Nuclear Export. PLoS One **10**: 1–21

Lee TA, Bailey-Serres J (2019) Integrative Analysis from the Epigenome to Translatome Uncovers Patterns of Dominant Nuclear Regulation during Transient Stress. Plant Cell **31**: 2573–2595

Lei H, Dias AP, Reed R (2011) Export and stability of naturally intronless mRNAs require speci fi c coding region sequences and the TREX mRNA export complex. Proc Natl Acad Sci **108**: 17985–17990

Levy YY, Mesnage S, Mylne JS, Gendall AR, Dean C (2002) Multiple Roles of Arabidopsis VRN1 in Vernalization and Flowering Time Control. Science (80-) **297**: 243–246

Liao Y, Smyth GK, Shi W (2013) The Subread aligner: Fast, accurate and scalable read mapping by seed-and-vote. Nucleic Acids Res **41**: 1–17

Liu KH, Tsay YF (2003) Switching between the two action modes of the dual-affinity nitrate transporter CHL1 by phosphorylation. EMBO J **22**: 1005–1013

Lorenz R, Bernhart SH, Höner C, Tafer H, Flamm C, Stadler PF, Hofacker IL (2011) ViennaRNA Package 2.0. Algorithms Mol Biol **6**: 1–14

Love MI, Huber W, Anders S (2014) Moderated estimation of fold change and dispersion for RNA-seq data with DESeq2. Genome Biol **15**: 1–21

Ma W, Li J, Qu B, He X, Zhao X, Li B, Fu X, Tong Y (2014) Auxin biosynthetic gene TAR2 is involved in low nitrogen-mediated reprogramming of root architecture in Arabidopsis. Plant J **78**: 70–79

Macrae E (2007) Extraction of Plant RNA. Methods Mol Biol **353**: 15–24

Maeda Y, Konishi M, Kiba T, Sakuraba Y, Sawaki N, Kurai T, Ueda Y, Sakakibara H, Yanagisawa S (2018) A NIGT1-centred transcriptional cascade regulates nitrate signalling and incorporates phosphorus starvation signals in Arabidopsis. Nat Commun. doi: 10.1038/s41467-018-03832-6

Maere S, Heymans K, Kuiper M (2005) BiNGO: A Cytoscape plugin to assess overrepresentation of Gene Ontology categories in Biological Networks. Bioinformatics **21**: 3448–3449

Mancini A, Niemann-seyde SC, Pankow R, Bounkari O El, Klebba-färber S, Koch A, Jaworska E, Spooncer E, Gruber AD, Whetton AD, et al (2010) THOC5/FMIP, an mRNA export TREX complex protein, is essential for hematopoietic primitive cell survival in vivo. BMC Biol **17**: 1–17

Marchive C, Roudier F, Castaings L, Bréhaut V, Blondet E, Colot V, Meyer C, Krapp A (2013) Nuclear retention of the transcription factor NLP7 orchestrates the early response to nitrate in plants. Nat Commun **4**: 1713

Marondedze C, Thomas L, Serrano NL, Lilley KS, Gehring C (2016) The RNA-binding protein repertoire of Arabidopsis thaliana. Nat Publ Gr 1–13

Martin W, Koonin E V (2006) Introns and the origin of nucleus–cytosol compartmentalization. Nature **440**: 41–45

Masclaux-Daubresse C, Daniel-Vedele F, Dechorgnat J, Chardon F, Gaufichon L, Suzuki A (2010) Nitrogen uptake, assimilation and remobilization in plants: Challenges for sustainable and productive agriculture. Ann Bot **105**: 1141–1157

Matiolli CC, Tomaz JP, Duarte GT, Prado FM, Viana C, Mascio P Di, Meyer C, Drumond RD, Vincentz M (2011) The Arabidopsis bZIP Gene AtbZIP63 Is a Sensitive Integrator of Transient Abscisic Acid. Plant Physiol **157**: 692–705

Mauger O, Lemoine F, Scheiffele P (2016) Targeted Intron Retention and Excision for Rapid Gene Regulation in Response to Neuronal Activity Article Targeted Intron Retention and Excision for Rapid Gene Regulation in Response to Neuronal Activity. Neuron **92**: 1266–1278

McGuirre AM, Pearson MD, Neafsey DE, Galagan JE (2008) Cross-kingdom patterns of alternative splicing and splice recognition. Genome Biol **9**: 1–19

Medici A, Marshall-Colon A, Ronzier E, Szponarski W, Wang R, Gojon A, Crawford NM, Ruffel S, Coruzzi GM, Krouk G (2015) AtNIGT1/HRS1 integrates nitrate and phosphate signals at the Arabidopsis root tip. Nat Commun. doi: 10.1038/ncomms7274

Miller C, Schwalb B, Maier K, Schulz D, Dümcke S, Zacher B, Mayer A, Sydow J, Marcinowski L, Dölken L, et al (2011) Dynamic transcriptome analysis measures rates of mRNA synthesis and decay in yeast. Mol Syst Biol **7**: 1–13

Monteuuis G, Wong JJL, Bailey CG, Schmitz U, Rasko EJ (2019) The changing paradigm of intron retention : regulation , ramifications and recipes. **47**: 11497–11513

Mordstein C, Savisaar R, Young RS, Taylor MS, Hurst LD, Kudla G, Mordstein C, Savisaar R, Young RS, Bazile J, et al (2020) Article Codon Usage and Splicing Jointly Influence mRNA Localization ll Codon Usage and Splicing Jointly Influence mRNA Localization. Cell Syst **10**: 351-362.e8

Moreno S, Canales J, Hong L, Robinson D, Roeder AHK, Gutiérrez RA (2020) Nitrate Defines Shoot Size through Compensatory Roles for Endoreplication and Cell Division in Arabidopsis thaliana. Curr Biol **30**: 1–13

Mueller F, Senecal A, Tantale K, Marie-nelly H, Ly N, Collin O, Basyuk E, Bertrand E, Darzacq X, Zimmer C (2013) FISH-quant : automatic counting of transcripts in 3D FISH images. Nat Methods **10**: 277–278

Mylne JS, Barrett L, Tessadori F, Mesnage S, Johnson L, Bernatavichute Y V, Jacobsen SE, Fransz P, Dean C (2006) LHP1, the Arabidopsis homologue of HETEROCHROMATIN PROTEIN1, is required for epigenetic silencing of FLC. Proc Natl Acad Sci **103**: 5012–5017

Narsai R, Howell KA, Millar AH, O'Toole N, Small I, Whelan J (2007) Genome-Wide Analysis of mRNA Decay Rates and Their Determinants in Arabidopsis thaliana. Plant Cell **19**: 3418–3436

O'Brien JA, Vega A, Bouguyon E, Krouk G, Gojon A, Coruzzi G, Gutiérrez RA (2016) Nitrate transport, sensing and responses in plants. Mol Plant 837–856

O'Malley RCO, Carol S, Song L, Galli M, Ecker JR, Malley RCO, Huang SC, Song L, Lewsey MG, Bartlett A, et al (2016) Cistrome and Epicistrome Features Shape the Regulatory DNA Landscape Resource Cistrome and Epicistrome Features Shape the Regulatory DNA Landscape. Cell **165**: 1280–1292

Okamura M, Inose H, Masuda S (2015) RNA Export through the NPC in Eukaryotes. Genes (Basel) **6**: 124–149

Owen AG, Jones DL (2001) Competition for amino acids between wheat roots and rhizosphere microorganisms and the role of amino acids in plant N acquisition. Soil Biol Biochem **33**: 651–657

Palazzo AF, Lee ES (2018) Sequence determinants for nuclear retention and cytoplasmic export of mRNAs and lncRNAs. Front Genet **9**: 1–16

Palovaara J, Weijers D (2019) Adapting INTACT to analyse cell - type - specific transcriptomes and nucleocytoplasmic mRNA dynamics in the Arabidopsis embryo. Plant Reprod **32**: 113–121

Parry G (2015) The plant nuclear envelope and regulation of gene expression. J Exp Bot **66**: 1673–1685

Pastro L, Smircich P, Di Paolo A, Becco L, Duhagon MA, Sotelo-Silveira J, Garat B (2017) Nuclear Compartmentalization Contributes to Stage-Specific Gene Expression Control in Trypanosoma cruzi. Front Cell Dev Biol **5**: 1–14

Patterson K, Cakmak T, Cooper A, Lager IDA, Rasmusson AG, Escobar MA (2010) Distinct signalling pathways and transcriptome response signatures differentiate ammonium- and nitrate-supplied plants. Plant Cell Environ **33**: 1486–1501

Pfaff C, Ehrnsberger HF, Flores-tornero M, Sørensen BB, Schubert T, Längst G, Griesenbeck J, Sprunck S, Grasser M, Grasser KD (2018) ALY RNA-Binding Proteins Are Required for Nucleocytosolic mRNA Transport and Modulate Plant Growth and Development. Plant Physiol **177**: 226–240

Poitout A, Crabos A, Novák O, Krouk G, Lacombe B (2018) Responses to Systemic Nitrogen Signaling in Arabidopsis Roots Involve trans -Zeatin in Shoots. Plant Cell **30**: 1243–1257

Poultney CS, Gutiérrez RA, Katari MS, Gifford ML, Paley WB, Coruzzi GM, Shasha DE (2007) Sungear: Interactive visualization and functional analysis of genomic datasets. Bioinformatics **23**: 259–261

Rabani M, Raychowdhury R, Jovanovic M, Rooney M, Stumpo DJ, Hacohen N, Schier AF, Blackshear PJ, Friedman N, Amit I, et al (2014) High resolution sequencing and modeling identifies distinct dynamic RNA regulatory strategies. Cell **159**: 1698–1710

Rahayu YS, Walch-liu P, Nuemann G, Römheld V, von Wirén N, Bangerth F (2005) Root-derived cytokinins as long-distance signals for -induced stimulation of leaf growth. J Exp Bot **56**: 1143–1152

Ramakers C, Ruijter JM, Lekanne RH, Moorman AFM (2003) Assumption-free analysis of quantitative real-time polymerase chain reaction (PCR) data. Neurosci Lett **339**: 62–66

Raza A, Farwa A, Zou X, Zhang X, Tosif H (2020) Plant Adaptation and Tolerance to Environmental Stresses : Mechanisms and Perspectives. Plant Ecophysiol Adapt under Clim Chang Mech Perspect I **Chapter 5**: 117–145

Reynoso MA, Kajala K, Bajic M, West DA, Woodhouse M, Rodriguez-medina J, Sinha N, Brady SM, Deal RB, Bailey-Serres J (2019) Evolutionary flexibility in flooding response circuitry in angiosperms. Science (80-) **1295**: 1291–1295

Reynoso MA, Pauluzzi GC, Kajala K, Cabanlit S, Velasco J, Bazin J, Deal R, Sinha NR, Brady SM, Bailey-Serres J (2018) Nuclear Transcriptomes at High Resolution Using

Retooled. Plant Physiol **176**: 270–281

Riveras E, Alvarez JM, Vidal EA, Oses C, Vega A, Gutiérrez RA (2015) The Calcium Ion Is a Second Messenger in the Nitrate Signaling Pathway of Arabidopsis. Plant Physiol **169**: 1397–1404

Ruffel S, Krouk G, Ristova D, Shasha D, Birnbaum KD, Coruzzi GM (2011) Nitrogen economics of root foraging : Transitive closure of the nitrate – cytokinin relay and distinct systemic signaling for N supply vs . demand. Proc Natl Acad Sci **108**: 18524–18529

Saavedra C, Kuei-shu T, A C, Cole CN (1996) Regulation of mRNA export in response to stress in Saccharomyces cerevisiae. Genes Dev **10**: 1608–1620

Saeed AI, Sharov V, White J, Li J, Liang W, Bhagabati N, Braisted J, Klapa M, Currier T, Thiagarajan M, et al (2003) TM4: A Free, Open-Source System for Microarray Data Management and Analysis. Biotechniques **34**: 374–378

Sakakibara H, Kyoko Kobayashi, Sugiyama T (1997) Partial characterization of the signaling pathway for the nitrate-dependent expression of genes for nitrogen-assimilatory enzymes using detached maize leaves. Plant Cell Physiol **38**: 837–843

Sanagi M, Lu Y, Aoyama S, Morita Y, Mitsuda N, Ikeda M, Ohme-takagi M, Sato T, Yamaguchi J (2018) Sugar-responsive transcription factor bZIP3 affects leaf shape in Arabidopsis plants. Plant Biotechnol **35**: 167–170

Santos-Filho PR, Saviani EE, Salgado I, Oliveira HC (2014) The effect of nitrate assimilation deficiency on the carbon and nitrogen status of Arabidopsis thaliana plants. Amono Acids **46**: 1121–1129

Schachtman DP, Shin R (2007) Nutrient Sensing and Signaling : NPKS. Annu Rev Plant Biol **58**: 47–69

Scheible W-R, González-Fontes A, Lauerer M, Müller-Röber B, Caboche M, Stitt M (1997) Nitrate Acts as a Signal to lnduce Organic Acid Metabolism and Repress Starch Metabolism in Tobacco. Plant Cell **9**: 783–798

Schwanhäusser B, Busse D, Li N, Dittmar G, Schuchhardt J, Wolf J, Chen W, Selbach M (2011) Global quantification of mammalian gene expression control. Nature **473**: 338–342

Shannon P, Markiel A, Ozier O, Baliga N, Wang J, Ramage D, Amin N, Schwikowski B, Ideker T (2003) Cytoscape: A Software Environment for Integrated Models of Biomolecular Interaction Networks. Genome Res **13**: 2498–2504

Silverman IM, Li F, Gregory BD (2013) Plant Science Genomic era analyses of RNA secondary structure and RNA-binding proteins reveal their significance to post-transcriptional regulation in plants. Plant Sci **205**–**206**: 55–62

Smyth GK (2005) limma: Linear Models for Microarray Data. Stat Biol Heal Bioinforma Comput Biol Solut Using R Bioconductor **1st Editio**: 397–420

Solnestam BW, Stranneheim H, Hällman J, Käller M, Lundberg E (2012) Comparison of

total and cytoplasmic mRNA reveals global regulation by nuclear retention and miRNAs. BMC Genomics **13**: 1–9

Sorenson RS, Deshotel MJ, Johnson K, Adler FR, Sieburth LE (2018) Arabidopsis mRNA decay landscape arises from specialized RNA decay substrates, decapping-mediated feedback, and redundancy. Proc Natl Acad Sci **115**: 1485–1494

Stewart M (2019) Polyadenylation and nuclear export of mRNAs. JBC Rev **294**: 2977–2987

Su G, Kuchinsky A, Morris JH, States DJ, Meng F (2010) GLay : community structure analysis of biological networks. Bioinformatics **26**: 3135–3137

Sun M, Schulz D, Pirkl N, Etzold S, Larivie L, Maier KC, Seizl M, Tresch A, Cramer P (2012) Comparative dynamic transcriptome analysis (cDTA) reveals mutual feedback between mRNA synthesis and degradation. Genome Res **22**: 1350–1359

Supek F, Bosnjak M, Skunca N, Smuc T (2011) REVIGO Summarizes and Visualizes Long Lists of Gene Ontology Terms. PLoS One **6**: 1–9

Swift J, Alvarez JM, Araus V, Gutiérrez RA, Coruzzi GM (2020) Nutrient dose-responsive transcriptome changes driven by Michaelis – Menten kinetics underlie plant growth rates. **117**: 12531–12540

Takata MA, Gonçalves-Carneiro D, Zang T, Soll SJ, York A, Blanco-Melo D, Bieniasz PD (2017) CG-dinucleotide suppression enables antiviral defense targeting non-self RNA. Nature **550**: 124–127

Tamura K (2020) Nuclear pore complex - mediated gene expression in Arabidopsis thaliana. J Plant Res. doi: 10.1007/s10265-020-01177-0

Tamura K, Fukao Y, Iwamoto M, Haraguchi T, Hara-nishimura I (2010) Identification and Characterization of Nuclear Pore Complex Components in Arabidopsis thaliana. Plant Cell **22**: 4084–4097

Thieme CJ, Rojas-triana M, Stecyk E, Schudoma C, Zhang W, Yang L, Miñambres M, Walther D, Schulze WX, Paz-ares J, et al (2015) Endogenous Arabidopsis messenger RNAs transported to distant tissues. Nat Plants **1**: 1–8

Tippmann SC, Ivanek R, Gaidatzis D, Schöler A, Hoerner L, Van Nimwegen E, Stadler MB, Schübeler D (2012) Chromatin measurements reveal contributions of synthesis and decay to steady-state mRNA levels. Mol Syst Biol 1–11

Tudek A, Schmid M, Heick T (2019) Escaping nuclear decay : the significance of mRNA export for gene expression. Curr Genet **65**: 473–476

Undurraga SF, Ibarra-Henríquez C, Fredes I, Álvarez JM, Gutiérrez RA (2017) Nitrate signaling and early responses in Arabidopsis roots. J Exp Bot **68**: 2541–2551

Varala K, Marshall-Colón A, Cirrone J, Brooks MD, Pasquino A V., Léran S, Mittal S, Rock TM, Edwards MB, Kim GJ, et al (2018) Temporal transcriptional logic of dynamic regulatory networks underlying nitrogen signaling and use in plants. Proc Natl Acad Sci

115: 6494–6499

Vidal EA, Álvarez JM, Araus V, Riveras E, Matthew D, Gutiérrez RA (2020) Nitrate in 2020: Thirty years from transport to signaling networks. Plant Cell **32**: 2094–2119

Vidal EA, Álvarez JM, Moyano TC, Gutiérrez RA (2015) Transcriptional networks in the nitrate response of Arabidopsis thaliana. Curr Opin Plant Biol **27**: 125–132

Vidal EA, Araus V, Lu C, Parry G, Green PJ, Coruzzi GM, Gutiérrez RA (2010) Nitrate-responsive miR393/AFB3 regulatory module controls root system architecture in Arabidopsis thaliana. Proc Natl Acad Sci **107**: 4477–4482

Vidal EA, Gutierrez RA (2008) A systems view of nitrogen nutrient and metabolite responses in Arabidopsis. Curr Opin Plant Biol **11**: 521–529

Vidal EA, Moyano TC, Krouk G, Katari MS, Tanurdzic M, Mccombie WR, Coruzzi GM, Gutiérrez RA (2013a) Integrated RNA-seq and sRNA-seq analysis identifies novel nitrate-responsive genes in Arabidopsis thaliana roots. BMC Genomics **14**: 1–15

Vidal EA, Moyano TC, Riveras E, Contreras-López O, Gutiérrez RA (2013b) Systems approaches map regulatory networks downstream of the auxin receptor AFB3 in the nitrate response of Arabidopsis thaliana roots. Proc Natl Acad Sci **110**: 12840–12845

Walker L, Boddington C, Jenkins D, Wang Y, Grønlund JT, Hulsmans J, Kumar S, Patel D, Moore JD, Carter A, et al (2017) Changes in Gene Expression in Space and Time Orchestrate Environmentally Mediated Shaping of Root Architecture. Plant Cell **29**: 2393–2412

Wang K, Wang L, Wang J, Chen S, Shi M, Cheng H (2018) Intronless mRNAs transit through nuclear speckles to gain export competence. J Cell Biol **217**: 3912–3929

Wang L, Miao Y, Zheng X, Lackford B, Zhou B, Han L, Yao C, Ward JM, Burkholder A, Lipchina I, et al (2013) The THO Complex Regulates Pluripotency Gene mRNA Export and Controls Embryonic Stem Cell Self-Renewal and Somatic Cell Reprogramming. Stem Cell **13**: 676–690

Wang R, Okamoto M, Xing X, Crawford NM (2003) Microarray Analysis of the Nitrate Response in Arabidopsis Roots and Shoots Reveals over 1000 Rapidly Responding Genes and New Linkages to Glucose, Trehalose-6-Phosphate, Iron, and Sulfate Metabolism. Plant Physiol **132**: 556–567

Wang R, Tischner R, Gutiérrez RA, Hoffman M, Xing X, Chen M, Coruzzi G, Crawford NM (2004) Genomic analysis of the nitrate response using a nitrate reductase-null mutant of Arabidopsis. Plant Physiol **136**: 2512–2522

Wang R, Xing X, Crawford N (2007) Nitrite Acts as a Transcriptome Signal at Micromolar Concentrations in Arabidopsis Roots. Plant Physiol **145**: 1735–1745

Weirauch MT, Yang A, Albu M, Cote AG, Montenegro-Montero A, Drewe P, Najafabadi HS, Lambert SA, Mann I, Cook K, et al (2014) Determination and Inference of Eukaryotic Transcription Factor Sequence Specificity. Cell **158**: 1431–1443

Wickramasinghe VO, Andrews R, Ellis P, Langford C, Gurdon JB, Stewart M, Venkitaraman AR, Laskey RA (2014) Selective nuclear export of specific classes of mRNA from mammalian nuclei is promoted by GANP. Nucleic Acids Res **42**: 5059–5071

Wickramasinghe VO, Laskey RA (2015) Control of mammalian gene expression by selective mRNA export. Nat Rev Mol Cell Biol **16**: 431–442

Wickramasinghe VO, Savill JM, Chavali S, Jonsdottir AB, Rajendra E, Laskey RA, Babu MM, Venkitaraman AR (2013) Human Inositol Polyphosphate Multikinase Regulates Transcript-Selective Nuclear mRNA Export to Preserve Genome Integrity. Mol Cell **51**: 737–750

Wu H, Li B, Iwakawa H, Pan Y, Tang X, Ling-hu Q, Liu Y, Sheng S, Feng L, Zhang H, et al (2020) Plant 22-nt siRNAs mediate translational repression and stress adaptation. Nature **581**: 89–93

Xu F, Copeland C (2012) Nuclear Extraction from Arabidopsis thaliana. Bio-protocol **2**: 18–21

Xu N, Wang R, Zhao L, Zhang C, Li Z, Lei Z, Liu F, Guan P, Chu Z, Crawford NM, et al (2016) The Arabidopsis NRG2 Protein Mediates Nitrate Signaling and Interacts with and Regulates Key Nitrate Regulators. Plant Cell **28**: 485–504

Yamada T, Akimitsu N (2018) Contributions of regulated transcription and mRNA decay to the dynamics of gene expression. WIREs RNA **10**: 1–18

Yan D, Easwaran V, Chau V, Okamoto M, Ierullo M, Kimura M, Endo A, Yano R, Pasha A, Gong Y, et al (2016) NIN-like protein 8 is a master regulator of nitrate-promoted seed germination in Arabidopsis. Nat Commun **7**: 1–11

Yang W, Wightman R, Meyerowitz EM (2017a) Cell Cycle Control by Nuclear Sequestration of Article Cell Cycle Control by Nuclear Sequestration of CDC20 and CDH1 mRNA in Plant Stem Cells. Mol Cell **68**: 1–12

Yang Y, Wang W, Chu Z, Zhu J, Zhang H (2017b) Roles of Nuclear Pores and Nucleo-cytoplasmic Trafficking in Plant Stress Responses. Front Plant Sci **8**: 1–8

Yeap W-C, Namasivayam P, Keong Ooi TE, Kulaveerasingam H, Ho C-L (2019) EgRBP42 from oil palm enhances adaptation to stress in Arabidopsis through regulation of nucleocytoplasmic transport of stress - responsive mRNAs. Plant, Cell Environ **42**: 1657–1673

Yelina NE, Smith LM, Jones AME, Patel K, Kelly KA (2010) Putative Arabidopsis THO / TREX mRNA export complex is involved in transgene and endogenous siRNA biosynthesis. Proc Natl Acad Sci **107**: 13948–13953

Zander G, Hackmann A, Bender L, Becker D, Lingner T, Salinas G, Krebber H (2016) mRNA quality control is bypassed for immediate export of stress-responsive transcripts. Nat Lett **540**: 593–596

Zhang H, Forde BG (1998) An Arabidopsis MADS Box Gene That Controls Nutrient-Induced

Changes in Root Architecture. Science (80-) **279**: 407–409

Zhao R, Bodnar MS, Spector DL (2009) Nuclear neighborhoods and gene expression. Curr Opin Genet Dev **19**: 172–179

Zhou H, Song Z, Zhong S, Zuo L, Qi Z, Qu L, Lai L (2019) Mechanism of DNA-Induced Phase Separation for Transcriptional Repressor VRN1. Angew Chemie Int Ed **58**: 4858–4862